

ENHANCED STRUCTURAL ORGANIZATION AND SORPTION PROPERTIES OF
COVALENT ORGANIC FRAMEWORKS THROUGH RATIONAL MONOMER DESIGN

by

Sampath Bandara Alahakoon



APPROVED BY SUPERVISORY COMMITTEE:

Dr. Ronald A. Smaldone, Chair

Dr. Michael C. Biewer

Dr. Jeremiah J. Gassensmith

Dr. John P. Ferraris

Copyright 2018

Sampath Bandara Alahakoon

All Rights Reserved

*Dedicated to my loving parents, Sarath Alahakoon, Chandralekha Alahakoon, sister, Sandhuni
Alahakoon and beloved wife, Ishanka for their endless love and encouragement*

ENHANCED STRUCTURAL ORGANIZATION AND SORPTION PROPERTIES OF
COVALENT ORGANIC FRAMEWORKS THROUGH RATIONAL MONOMER DESIGN

by

SAMPATH BANDARA ALAHAKOON, BS

DISSERTATION

Presented to the Faculty of

The University of Texas at Dallas

in Partial Fulfillment

of the Requirements

for the Degree of

DOCTOR OF PHILOSOPHY IN

CHEMISTRY

THE UNIVERSITY OF TEXAS AT DALLAS

August 2018

ACKNOWLEDGMENTS

First of all, I would like to express my sincere gratitude to my research advisor, Dr. Ronald A. Smaldone, for his invaluable guidance, support, and encouragement through my successful graduate career. It is a great privilege for me to be a Smaldone Lab member and it will be an unforgettable experience in my life. I also pass my sincere thanks to Dr. Michael C. Biewer, Dr. Jeremiah J. Gassensmith, and Dr. John P. Ferraris for serving on my committee and providing me valuable suggestions, guidance, and comments throughout the past years.

I would like to express my special thanks to present and past Smaldone lab members, especially Dr. Christina Thompson, Dr. Arosha Karunathilake, Dr. Sumudu Wijenayake, Dr. Gayan Adhikari, Gino Occhialini, Amy Nguyen, Daniel Berry, Alejandra Durand, Whitney Ong, and Shashini Diwakara for their support and encouragement. Many thanks to Dr. Gregory McCandless for his valuable contribution in all my projects and being supportive throughout the years. I would like to acknowledge all the past and present members of the Chemistry and Biochemistry department, Dr. Hein Nguyen, Dr. Pathum Panapitiya, Dr. George McDonald, Betty Maldonado, Linda Heard, Kelli Lewis, and, Lydia Selvidge who helped me throughout the past years. I would like to thank all the past and present Sri Lankan friends and their families at UTD who helped me in numerous ways. My sincere thank goes to the Sri Lankan community outside UTD for their endless support in many ways. I am grateful to all my Sri Lankan friends across the US and back in Sri Lanka for their support. I am thankful for my past teachers at Kingswood College, Kandy and University of Peradeniya, Peradeniya for their valuable advice and guidance provided me throughout the journey in my life.

Finally, I would like to express loving gratitude to my mother Chandralekha Alahakoon, my father Sarath Alahakoon, my sister Sandhuni Alahakoon and my beloved wife Ishanka Hemachandra, for their endless love, support and encouragement offered every day. You are my heroes and without you, I would not have been able to get this far.

June 2018

ENHANCED STRUCTURAL ORGANIZATION AND SORPTION PROPERTIES OF
COVALENT ORGANIC FRAMEWORKS THROUGH RATIONAL MONOMER DESIGN

Sampath Bandara Alahakoon, PhD
The University of Texas at Dallas, 2018

Supervising Professor: Dr. Ronald A. Smaldone

Covalent Organic Frameworks (COFs) are a class of crystalline porous polymer networks which have attracted much attention over the past decade due to their unique properties. COFs consist of lightweight elements (C, N, H, O, B, *etc.*) and have a higher surface area, crystallinity, permanent porosity and low density. The formation of these materials primarily depends on the interplay between dynamic covalent bond formation and supramolecular interactions between the monomer units. Over the past decade, boron ester, imine, azine, and hydrazone formation reactions have been intensively utilized as dynamic covalent reactions to overcome the crystallization problem with the aid of dipolar and π - π stacking interactions in the synthesis of crystalline COFs. Depending on the geometry of the starting monomers these materials can be divided into 2D- and 3D-COFs. Even though the 3D-COFs exhibit higher degree of order, most 2D-COFs show moderate crystallinity. So developing strategies to improve the long-range order, surface area, and sorption capabilities are of prime importance to make the COFs promising candidates in gas storage and separation, electrical energy storage, heterogeneous catalysis, sensing, drug delivery, *etc.* Thus, the overall goal of this research effort is to improve the

material properties of 2D-COFs aiming at developing general synthetic rules to support future materials development.

The first chapter of the dissertation provides a literature review of efforts to develop 2D-COFs in gas and electrical energy storage. Some of the design strategies for developing the gas sorption properties of COFs and mechanistic studies of their formation are also discussed.

In the second chapter, the use of a six-fold symmetric hexaphenylbenzene based aldehyde (HEX) in the synthesis of an azine-linked COF with triangular micropores and excellent sorption capability for CO₂ (20 wt%) and CH₄ (2.3 wt%) is discussed. This is the first report of the study of sorption capability of a hexaphenylbenzene based COF in literature.

In the third chapter, the use of fluorines in the COF monomers to improve the structural organization of COFs is discussed. Furthermore, a detailed synthesis and an intensive characterization of a series of fluorine-containing COFs are also discussed with their mechanism of formation.

Further insight into the effect of fluorines in the COF synthesis through mixed linker studies and computational calculations is discussed in the fourth chapter.

TABLE OF CONTENTS

ACKNOWLEDGMENTS	v
ABSTRACT	vii
LIST OF FIGURES	xi
LIST OF TABLES	xvi
CHAPTER 1 DESIGN PRINCIPLES FOR COVALENT ORGANIC FRAMEWORKS IN ENERGY STORAGE APPLICATIONS	1
1.1 Abstract	2
1.2 Introduction	2
1.3 Gas storage in COFs	8
1.4 COFs for electrical energy storage	19
1.5 Capacitive storage in COFs	27
1.6 COFs for fuel cell membranes	30
1.7 Conclusion	32
1.8 References	33
CHAPTER 2 AN AZINE-LINKED HEXAPHENYLBENZENE BASED COVALENT ORGANIC FRAMEWORK	41
2.1 Abstract	42
2.2 Introduction	42
2.3 Experimental	44
2.4 Results and discussion	48
2.5 Conclusion	54
2.6 Acknowledgements	54
2.7 References	55
CHAPTER 3 ENHANCED STRUCTURAL ORGANIZATION IN COVALENT ORGANIC FRAMEWORKS THROUGH FLUORINATION	58
3.1 Abstract	59
3.2 Introduction	59
3.3 Experimental	60

3.4 Results and discussion	70
3.5 Conclusion.....	74
3.6 Acknowledgement	75
3.7 Appendix – Supporting information	76
3.8 References.....	87
CHAPTER 4 EXPERIMENTAL AND THEORETICAL INSIGHT INTO THE EFFECT OF FLUORINE SUBSTITUENTS ON THE PROPERTIES OF AZINE LINKED COVALENT ORGANIC FRAMEWORKS.....	89
4.1 Abstract.....	90
4.2 Introduction.....	90
4.3 Experimental.....	91
4.4 Results and discussion	93
4.5 Conclusion.....	98
4.6 Acknowledgement	98
4.7 Appendix – Supporting information	99
4.8 References.....	110
BIOGRAPHICAL SKETCH	112
CURRICULUM VITAE.....	113

LIST OF FIGURES

Figure 1.1. (A) Illustration of a hexagonal 2D COF demonstrating the forces involved in their assembly (B) Examples of the reticular design strategies used to make COFs. (C) Common dynamic covalent bond types that have been used to make COFs.	4
Figure 1.2. Mechanistic steps possible during the formation of a 2D COF.....	6
Figure 1.3. Relative rates of formation for boronate ester COFs, related to their π -surface area....	7
Figure 1.4. Computed CH ₄ adsorption isotherms in (A) COFs; (B) Li-doped COFs at T=298 K. Figure taken with permission from reference 15.	11
Figure 1.5. Illustration of the types of interactions that can be incorporated into COFs to enhance CO ₂ gas adsorption and examples of COF design that incorporate these types of functionality resulting in strong CO ₂ adsorption. The channel-wall functionalized COFs shown represent those with the highest CO ₂ adsorption capacity out of this series of COFs.	16
Figure 1.6. Illustration of the evolution of solar cell design from a bilayer approach to a bulk heterojunction approach to precise molecular architecture designs made possible with COFs. (Top) Examples of COFs that have shown photo-responsive charge separation. (Bottom).....	20
Figure 1.7. (A) Illustration of a method to electropolymerize EDOT into the pores of a pre-formed conductive COF network resulting in a synergistically conductive and stable capacitive material (B). Figure taken with permission from reference 121.	29
Figure 2.1. (A) Synthesis of a COF using a six fold symmetric HEX monomer containing aldehyde groups and hydrazine. (B) HEX-based monomers are non-planar as a result of the steric hindrance between the phenyl rings. Resultant COFs have topologically planar 2D structures despite the lack of planarity in the monomers.....	43
Figure 2.2. Synthesis of HEX and HEX-COF 1	45
Figure 2.3. ¹ H NMR (400 MHz) of HEX in DMSO-d ₆	46
Figure 2.4. ¹³ C NMR (400 MHz) of HEX in DMSO-d ₆	47
Figure 2.5. FT-IR spectra of HEX-COF 1 (Blue) and HEX (Red).....	48
Figure 2.6. Zoomed in image of FT-IR spectra of HEX-COF 1 (Blue) and HEX (Red).	48
Figure 2.7. TGA of HEX-COF 1 under a nitrogen atmosphere.....	49

Figure 2.8. (A) N ₂ isotherm at 77 K. The BET surface area of HEX-COF 1 was measured to be 1214 m ² /g. (B) NLDFT pore size distribution obtained from the N ₂ isotherm.	50
Figure 2.9. (A) The powder X-ray diffraction pattern of HEX-COF 1 (black line) and the simulated diffraction pattern from the model (red line). (B) A view of the interlayer spacing of the model showing the lack of face-to-face π stacking interactions. (C) Molecular model of HEX-COF 1 showing the pores measuring 11 Å in diameter.....	52
Figure 2.10. (A) CO ₂ isotherms at 273 K (filled circles) and 298 K (open circles). (B) CH ₄ isotherms at 273 K (filled circles) and 298 K (open circles). (c) Enthalpy of adsorption measurements for CO ₂ (black line) and CH ₄ (red line).....	53
Figure 3.1. Synthesis of 1,3,5- <i>tris</i> (4-formylphenyl)benzene (NF).....	62
Figure 3.2. Synthesis of 1,3,5- <i>tris</i> (3-fluoro-4-formylphenyl)benzene (TF-1).....	62
Figure 3.3. ¹ H NMR (600 MHz) of 1,3,5- <i>tris</i> (3-fluoro-4-formylphenyl)benzene (TF-1) in.....	63
Figure 3.4. ¹⁹ F NMR (600 MHz) of 1,3,5- <i>tris</i> (3-fluoro-4-formylphenyl)benzene (TF-1) in	63
Figure 3.5. ¹³ C NMR (600 MHz) of 1,3,5- <i>tris</i> (3-fluoro-4-formylphenyl)benzene (TF-1) in.....	64
Figure 3.6. Synthesis of 1,3,5-trifluoro-2,4,6- <i>tris</i> (4-formylphenyl)benzene (TF-2)	64
Figure 3.7. ¹ H NMR (600 MHz) of 1,3,5-trifluoro-2,4,6- <i>tris</i> (4-formylphenyl)benzene (TF-2)...	65
Figure 3.8. ¹⁹ F NMR (600 MHz) of 1,3,5-trifluoro-2,4,6- <i>tris</i> (4-formylphenyl)benzene (TF-2) ..	66
Figure 3.9 ¹³ C NMR (600 MHz) of 1,3,5-trifluoro-2,4,6- <i>tris</i> (4-formylphenyl)benzene (TF-2) ...	66
Figure 3.10. Synthesis of NF-COF	67
Figure 3.11. Synthesis of TF-COF 1.....	68
Figure 3.12. Synthesis of TF-COF 2.....	69
Figure 3.13. Experimental PXRDs of (A) NF-COF (black), (B) TF-COF 1 (red), (C) and TF-COF 2 (blue) with Pawley refined spectra, simulated eclipsed models and difference spectra (purple, green and orange respectively). Insets: Modeled eclipsed structures of COFs (C, grey; O, red; N, blue; F, light green. (H atoms are omitted for clarity). (D), (E) and (F) are SEM images of NF-COF, TF-COF 1 and TF-COF 2, respectively.	71
Figure 3.14. (A), (C) and (E) N ₂ adsorption (solid circles) and desorption (open circles) isotherms (77 K) of 1 d RT, 1 d 120 °C and 3 d 120 °C COFs, respectively. (B), (D) and	

(F) PSD plots of 1 d RT, 1 d 120 °C and 3 d 120 °C COFs, respectively. (G) BET surface areas and (H) and mass recovery (%) of COFs.	72
Figure S3.1. Experimental powder X-ray diffraction patterns of (A) NF-COF, (B) TF-COF 1 and (C) TF-COF 2 prepared at 3d, 120 °C (black), at 1d, 120 °C, (yellow), at 1d, r.t. (green).....	76
Figure S3.2. FT-IR spectra of (A) NF-COF, (B) TF-COF 1 and (C) TF-COF 2 synthesized at 1d, rt (green), at 1d, 120 °C (yellow) and at 3d, 120 °C (black) compared with the corresponding aldehyde (red)	77
Figure S3.3. Experimental powder X-ray diffraction pattern of NF-COF (black), compared with simulated PXRD patterns of eclipsed layers of COF (green) considering $P3$ symmetry and staggered layers of COF (purple) considering $P6_3/m$ symmetry.	78
Figure S3.4. View of the simulated structure of the eclipsed NF-COF along c axis.....	79
Figure S3.5. View of the simulated structure of the eclipsed NF-COF along a axis.....	79
Figure S3.6. View of the simulated structure of the staggered NF-COF along c axis.....	79
Figure S3.7. View of the simulated structure of the staggered NF-COF along a axis	79
Figure S3.8. Experimental powder X-ray diffraction pattern of TF-COF 1 (red), compared with simulated PXRD patterns of eclipsed layers of COF (green) considering $P3$ symmetry and staggered layers of COF (purple) considering $P6_3/m$ symmetry.	80
Figure S3.9. View of the simulated structure of the eclipsed TF-COF 1 along c axis	81
Figure S3.10. View of the simulated structure of the eclipsed TF-COF 1 along a axis.....	81
Figure S3.11. View of the simulated structure of the staggered TF-COF 1 along c axis.....	81
Figure S3.12. View of the simulated structure of the staggered TF-COF 1 along a axis.....	81
Figure S3.13. Experimental powder X-ray diffraction pattern of TF-COF 2 (blue), compared with simulated PXRD patterns of eclipsed layers of COF (green) considering $P3$ symmetry and staggered layers of COF (purple) considering $P6_3/m$ symmetry.	82
Figure S3.14. View of the simulated structure of the eclipsed TF-COF 2 along c axis	83
Figure S3.15. View of the simulated structure of the eclipsed TF-COF 2 along a axis.....	83
Figure S3.16. View of the simulated structure of the staggered TF-COF 2 along c axis.....	83

Figure S3.17. View of the simulated structure of the staggered TF-COF 2 along <i>a</i> axis.....	84
Figure S3.18. TGA curves of NF-COF 3d, 120 °C (black), TF-COF 1 3d, 120 °C (red) and TF-COF 2 3d, 120 °C (blue).....	84
Figure S3.19. SEM images of (A) TF-COF 1 1d, 120 °C and (B) TF-COF 2 1d, 120 °C	85
Figure S3.20. Geometry optimized structures of the aldehydes used in the COF synthesis (A) 1,3,5- <i>tris</i> (4-formylphenyl)benzene (B) 1,3,5- <i>tris</i> (3-fluoro-4-formylphenyl)benzene (C) 1,3,5-trifluoro-2,4,6- <i>tris</i> (4-formylphenyl)benzene (D) Calculated torsion angles of the precursor aldehydes. Calculation of the torsion angle of the aldehydes was carried out using Materials Studio Visualizer. Universal Force Field (UFF) was utilized for the geometry optimization of the aldehyde precursors.	86
Figure 4.1. Synthesis of the TFX-COF series by varying the mole % of the TF monomer with the remaining monomers represented by NF.....	92
Figure 4.2. (A) Eclipsed layers of COFs. (B) PXRD spectra of the series of COFs. Black, Green, Purple, Blue and Red lines represent the TF ₀ -COF, TF ₂₅ -COF, TF ₅₀ -COF, TF ₇₅ -COF and TF ₁₀₀ -COF, respectively. (C) H ¹ -NMR spectra of digested mixed COFs and the interaction of each aldehyde peaks in the mixed COFs.	93
Figure 4.3. Morphological change in the SEM images with the variation of TF content in the COFs.	94
Figure 4.4. (A) Nitrogen isotherms (77 K), (B) NLDFT pore size distributions and (C) BET surface areas of the TFX-COFs.	95
Figure 4.5. Computational models of the energy minimized stacked dimers (top, hydrogen atoms omitted for clarity). Interaction energies of the face-to-face stacking arrangements possible in each of the representative mixed COFs (bottom). The energies are measured relative to the highest energy NF/NF dimer.	97
Figure S4.1. FT-IR spectra of TF ₀ -COF (black), TF ₂₅ -COF (green), TF ₅₀ -COF (purple), TF ₇₅ -COF (blue) and TF ₁₀₀ -COF (red) compared with TF aldehyde monomer (orange).....	99
Figure S4.2. Experimental powder X-ray diffraction pattern of TF ₁₀₀ -COF (red), compared with simulated PXRD patterns of eclipsed layers of COF (green) considering P3 symmetry and staggered layers of COF (purple) considering P6 ₃ /m symmetry.	100
Figure S4.3. View of the simulated structure of the eclipsed TF ₁₀₀ -COF along <i>c</i> axis	101
Figure S4.4. View of the simulated structure of the eclipsed TF ₁₀₀ -COF along <i>a</i> axis	101
Figure S4.5. View of the simulated structure of the staggered TF ₁₀₀ -COF along <i>c</i> axis	101

Figure S4.6. View of the simulated structure of the staggered TF₁₀₀-COF along *a* axis.....101

LIST OF TABLES

Table S3.1. EDX data of TF-COF 1 3d, 120 °C and TF-COF 2 3d, 120 °C.....	85
Table S4.1. Atom Coordinates for TF/TF Dimer.....	102
Table S4.2. Atom Coordinates for TF/NF Dimer.....	104
Table S4.3. Atom Coordinates for NF/NF Dimer.....	107

CHAPTER 1
DESIGN PRINCIPLES FOR COVALENT ORGANIC FRAMEWORKS IN ENERGY
STORAGE APPLICATIONS

Authors: Sampath B. Alahakoon, Christina M. Thompson, Gino Occhialini, and
Ronald A. Smaldone

Department of Chemistry and Biochemistry, BSB13

The University of Texas at Dallas

800 West Campbell Road

Richardson, Texas 75080-3021

Alahakoon, S. B.; Thompson, C. M.; Occhialini, G.; Smaldone, R. A. Design Principles for Covalent Organic Frameworks in Energy Storage Applications. *ChemSusChem* **2017**, *10*, 2116-2129. Copyright (2017) Wiley-VCH Verlag GmbH & Co. KGaA, Weinheim.

1.1 Abstract

Covalent organic frameworks (COFs) are an exciting class of porous materials that have been explored as energy storage materials for more than a decade. This review will discuss the efforts to develop these materials for applications in gas and electrical power storage. This review will also discuss some of the design strategies for developing the gas sorption properties of COFs and mechanistic studies on their formation.

1.2 Introduction

In the changing energy landscape of the 21st century, the need for cheaper, smaller, more efficient, and more environmentally friendly energy harvesting and storage technologies has never been greater. Energy demands are constantly increasing as more people carry batteries in their pockets that must last longer while powering more complex devices, new car technologies require better supercapacitors to run efficiently, and biomedical applications seek miniaturized powered devices to implant into biological systems. To meet these demands, it is not only technology that must progress, but also the exploration and development of new materials to be used by those technologies. One of the more promising classes of materials being developed for use in energy harvesting and storage are covalent organic frameworks, or COFs. COFs are a class of crystalline, porous, polymers whose structure is controlled by interplay between non-covalent aromatic interactions (π -stacking, in the case of 2D COFs) and dynamic covalent bond formation. This interplay forms characteristic one-dimensional channels along the c-crystallographic axis, the size, shape, and chemical environment of which can be very specifically tuned through the modular design of COF building blocks. The ability to design

COFs with such a wide variety of functionality has made COFs a rapidly growing part of micro and mesoporous materials discovery¹⁻³ for use as components for electronic and conductive materials,³⁻⁸ catalysis,⁹⁻¹¹ and for clean energy applications in gas storage and separations. This minireview will discuss the state of the field in terms of COF synthesis and efforts that have been made to use them as materials for gaseous and electrical energy storage. We will also highlight some of the fundamental efforts toward a better understanding of the design rules for making new COFs and improving their properties.

1.2.1 Principles of design and synthesis of COFs

To design reliable materials for any part of the energy sector, a thorough understanding of the underlying principles controlling those materials is paramount. 2D COFs and their applications will be the primary focus of this minireview, although there are a few examples of 3D COFs.¹²⁻²² The difference between these two classes lies in the design of their monomers and the type of bonds that connect them in three dimensions. 3D COF monomers are designed such that they are polymerized through the formation of covalent bonds in all directions. In contrast, the growth of 2D COFs is controlled by two orthogonal processes: polymerization in two dimensions through the use of thermodynamically controlled covalent bond formation (i.e., dynamic covalent chemistry), and crystallization of these layers via non-covalent forces such as aromatic stacking or dipolar forces. The eclipsed arrangements of the aromatic units makes 2D COFs ideally suited for applications where electronic communication between π -conjugated functional groups (e.g., conductance, charge transfer, redox coupling) are important properties.

The modular design principles used to make COFs are shared in many ways with the reticular design concepts of other classes of porous materials such as metal-organic frameworks

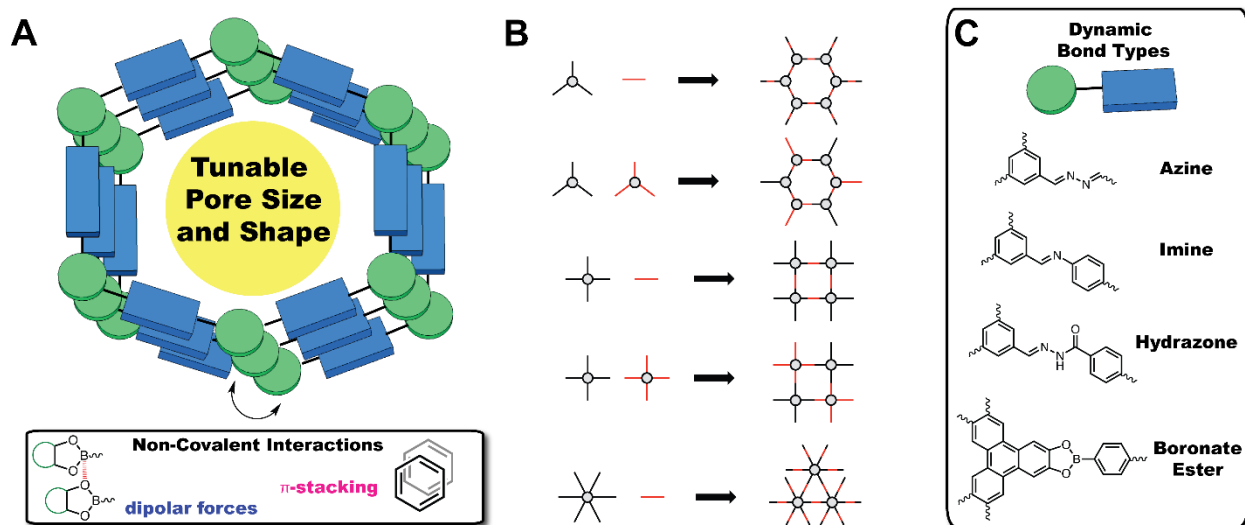


Figure 1.1. (A) Illustration of a hexagonal 2D COF demonstrating the forces involved in their assembly (B) Examples of the reticular design strategies used to make COFs. (C) Common dynamic covalent bond types that have been used to make COFs.

(MOFs).^{23,24} Since COFs are crystalline materials, microscopic structural attributes such as pore size and shape (Figure 1.1a) can be controlled by the shape of the chosen monomer. There have been many examples of 2D COFs that use the conventional net topologies shown in Figure 1.1b (e.g., trigonal, tetragonal, hexagonal), although in recent years there have been many variations on these designs that use linkers with asymmetric structures and mixtures of linkers with like topologies but different sizes.²⁵⁻²⁸ The most common types of covalent bonds used to make 2D COFs are azines,^{6,25,29-31} imines,^{11,32} hydrazones, or boronic ester linkages^{1,7,8,33-38} (Figure 1.1c). Each of these bond types offers varying advantages from high crystallinity (boronate esters), to superior resistance to hydrolysis (hydrazones) and each of these classes of COFs form under different conditions and mechanisms, requiring different design rules. This section will discuss those efforts to date.

1.2.2 Mechanistic studies

While COFs have been at the forefront of porous materials development for a decade, only recently have researchers attempted to better understand the mechanistic forces that dictate the overall formation of 2D COFs. The first COFs, reported by Yaghi and Côté in 2005, utilized boronate ester and boroxine linkages which resulted in microporous materials with excellent crystallinity.¹ Later, work by Dichtel and co-workers³⁹ attributed this to interactions between the lone pairs of the oxygen atoms and the empty p-orbitals of the boron atoms in the adjacent COF layers (Figure 1.1a, bottom). This has proven to be a powerful and general strategy for synthesizing crystalline COFs as there have been dozens of examples of boronate ester COFs since the first report with a diverse set of monomer structures. In most other COF types, however, the 2D layers are primarily held together through aromatic stacking forces.

In recent years there have been several studies reported that attempt to elucidate the mechanism of COF formation in greater detail.^{40,41} Shown in Figure 1.2 are several possible processes responsible for the polymerization and crystallization of 2D COFs. Some of these mechanistic steps are more prominent depending on the class of COF, and some are likely endpoints for COFs that do not form well (i.e., kinetic trapping points). Previous studies of dynamic imine directed assembly have characterized the nature of these kinetic traps and, given their similarity to COF polymers, they are likely analogous.⁴²

One of the first efforts to elucidate the mechanism of COF formation was reported by Dichtel, *et al.*, on the synthesis of boronate ester COFs. Most COFs are synthesized using solvent conditions that result in a suspension or slurry.⁴⁰ By designing solvent conditions that resulted in a homogeneous solution, the rates of COF formation could be determined through turbidity

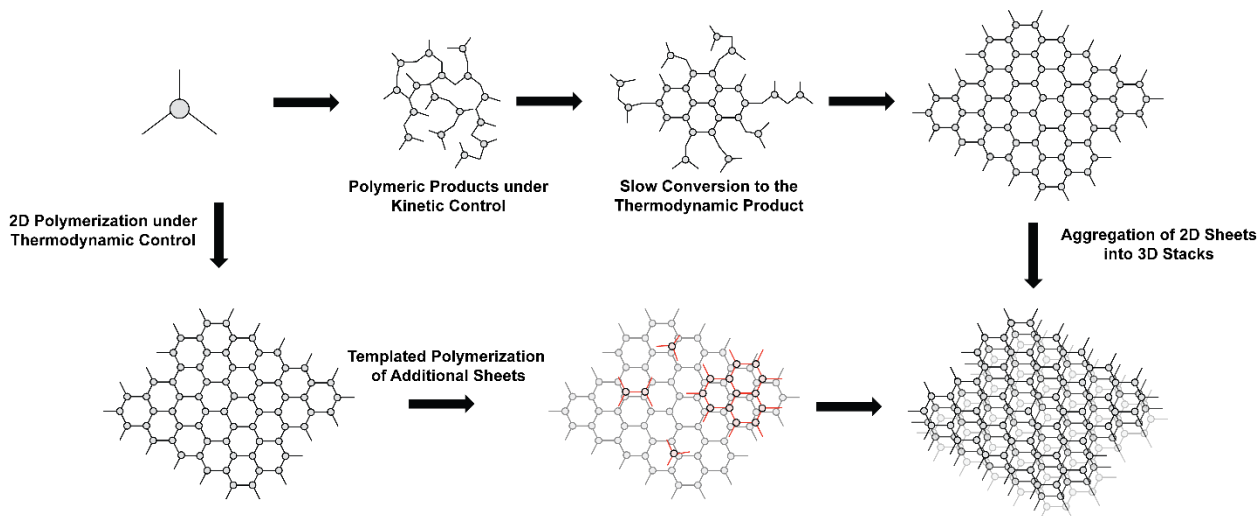


Figure 1.2. Mechanistic steps possible during the formation of a 2D COF.

measurements. This study found that the rate of COF formation was qualitatively related to the aromatic stacking capability of the monomer (Figure 1.3), in other words, larger aromatic monomers formed COFs at a faster rate, and resisted hydrolysis better than their smaller counterparts.

Another report established that structural characteristics, in this case the dihedral angles^{9,43} between aromatic rings within the monomers, can influence both crystallinity and porosity in COFs. Lötsch, and co-workers⁴³ planarized a 1,3,5-triphenylbenzene-based COF monomer through the introduction of nitrogen atoms to the central ring. This alleviated the steric hindrance between the central and peripheral rings resulting in a coplanar arrangement between the phenyl rings. Modifying this dihedral angle resulted in a substantial improvement in both the surface area and crystallinity of the resultant COFs. These improved COFs were used as effective scaffolds for photocatalytic hydrogen generation. Seemingly in contrast, a report by Bein and co-workers used a non-planar tetraphenylethylene linker⁴⁴ to show that, if properly

designed, non-planar aromatic systems can “lock” COF layers into place resulting in improved long-range crystallinity. Building on this work, a pyrene based COF with peripheral phenylene rings showed that this principle could be extended to other structural cores.⁴⁵ Electronic effects can also play a role, as demonstrated by Jiang, *et al.* through the use of electronically complementary monomers.⁴⁶ Salonen, *et al.* showed that the cancellation of dipole moments in COF monomers could also be used with success to improve the microscopic structure.⁴⁷ Our group recently demonstrated that the use of electron-poor fluorinated monomers can also improve both surface area, crystallinity, and pore fidelity.⁴⁸

While it appears that there are contradictory design rules for COFs, these reports demonstrate that the design rules for COFs are complex and deserving of more study. Furthermore, this work serves to tighten the link between supramolecular chemistry and the study of COFs as many of the concepts of self-assembly appear to be highly important for understanding the nature of COF polymerization.

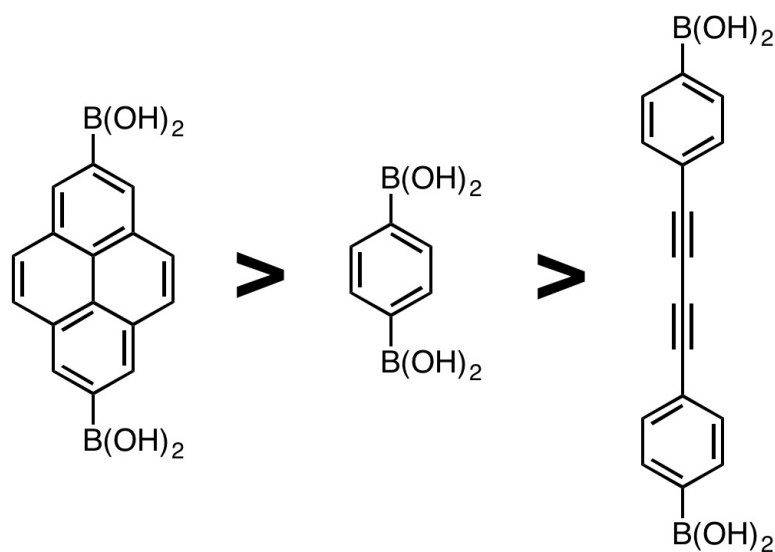


Figure 1.3. Relative rates of formation for boronate ester COFs, related to their π -surface area

1.3 Gas storage in COFs

Analogous to other classes of micro- and mesoporous materials, COFs have been studied over the past decade for use in sorption and separation of energy relevant gases including H₂, CH₄, CO₂, and others. The major bottleneck for the use of H₂ and CH₄ as clean fuel substitutes for petroleum in automobiles is the lack of suitable storage materials.² This section will discuss efforts to develop COFs as storage materials for gases relevant to clean energy.⁴⁹

1.3.1 COFs for hydrogen storage

The search for clean energy sources as alternatives to fossil fuels is critical to finding a solution for green house gas emission, air pollution, and the increasing need for energy. The ideal substitute for traditional carbon based resources is H₂, due to its high thermal energy content and clean combustion for automobile applications.^{50,51} In practice, a minimum of 4 kg of H₂ must be stored to drive several hundred kilometers before refueling.^{49,52} Two basic approaches have been identified to store practical amounts of hydrogen for automobile use. One is to chemisorb H₂ as metal hydrides⁵³ while the other is to physisorb H₂ in porous materials such as porous polymers,^{54,55} zeolites,⁵⁶ MOFs,^{57,58} and COFs.⁵⁹

The use of COFs as hydrogen storage materials has attracted much attention owing to several theoretical⁵⁹⁻⁶² and experimental studies^{13,49,63,64} that have demonstrated that COFs have comparable or better hydrogen storage capabilities than other materials such as MOFs. Since the first report of H₂ sorption in COFs in 2008 numerous attempts have been made to improve the H₂ sorption properties of COFs. For example, 3D COF-102 (BET surface area, 3620 m² g⁻¹) displays the highest observed excess hydrogen uptake reported to date of 7.24 wt% at 35 bar and

77 K.⁴⁹ This is slightly higher than that of the comparable porous polymer PAF-1 (7.0 wt%, BET surface area of 5600 m² g⁻¹).⁶⁵

In general, the ability of COFs to store H₂ gas correlates to their surface area.^{49,66} For instance, COF-1, COF-8, and COF-5, which have BET surface areas of 750, 1350, and 1670 m² g⁻¹ respectively, have H₂ excess uptake capacities of 1.48, 3.50, and 3.58 wt% at 35 bar and 77 K, respectively.⁴⁹ Though these values are promising, it should be pointed out that these H₂ sorption experiments have been carried out at 77 K, an exceptionally cold temperature for practical use. Significant uptake at room temperature or higher remains a challenge. The US Department of Energy (DOE) has set the target H₂ storage to be 5.5 wt% at -40 to 60 °C under a maximum pressure of 100 atm for 2017.²

Nonetheless, computational studies and experimental attempts indicate that good H₂ storage can be made possible at practical temperature ranges (273-298 K), in particular for metal-doped COF materials.^{61,63} Numerous simulation and experimental studies^{13,59-63,67} have been performed to study the improved H₂ uptake capabilities of Li, Sc, Pd, and Ca doped COFs under practical conditions. For example, gravimetric adsorption capacities of hydrogen for Li-doped COF-105 and COF-108 reach 6.84 and 6.73 wt% at 298 K and 100 bar.¹³ The authors of this study noted that positively charged Li atoms make dative bonds with H₂ which improve the uptake. Neutral Li atoms or anions have no such effect. Gao and co-workers showed in a theoretical study that a Ca intercalated COF containing diphenylethyne units, reached an H₂ sorption of 5 wt% at near-ambient conditions (300 K, 20 bar).^{26a} In this case the metal atom is adsorbed on to the center of the organic unit rather than the boronic ester or boroxine rings. The neutral Ca atom is intercalated between the π -systems of the phenyl rings. Another excellent study demonstrated

the use of a 3D-COF, COF-102, for the stabilization of Pd nanoparticles and shows that the excess H₂ storage capacities were improved by a factor of 2–3 *via* Pd impregnation at room temperature and 20 bar. This remarkable enhancement can be attributed to not only the Pd hydride formation, but also hydrogenation of residual organic compounds.⁶³ Apart from the metal-doped COFs, a simulation was carried out on four 3D-COFs which substitute the phenylene moieties of COF-102 with diphenyl, triphenyl, naphthalene, and pyrene units to produce the theoretical COF-102-2, COF-102-3, COF-102-4, and COF-102-5, respectively. Of these materials, COF-102-3 demonstrated the best total uptake performance and reached 26.7 and 6.5 wt% at 77 and 300 K, respectively at 100 bar. This improvement can be attributed to the enhancement of surface area, pore volume, and the enthalpy of adsorption, all of which facilitate physisorption.⁵⁹

1.3.2 COFs for methane storage

Natural gas is another alternative to traditional fossil fuels, and has attracted much attention due to its relatively low impact on the environment.⁶⁸ Methane is the major component of natural gas, which is cleaner, more abundant, and less expensive than gasoline or diesel. However, the same problems that plague hydrogen also exist for methane. To use methane as a fuel in automobiles, effective and safe storage systems are needed given the dangers of using a flammable gas as a fuel.⁴⁹ The current DOE methane storage target is 350 cm³ (STP) cm⁻³ (STP = standard temperature and pressure) at 35 bar and ambient temperature.⁶⁹ In order to achieve the DOE target a porous framework must be designed to have a high sorption capacity, a good adsorption enthalpy, and an efficient charge-discharge rate.⁷⁰

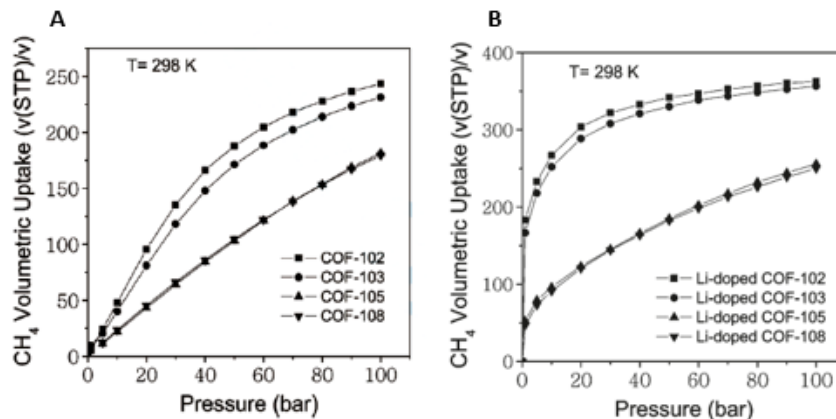


Figure 1.4. Computed CH₄ adsorption isotherms in (A) COFs; (B) Li-doped COFs at T=298 K. Figure taken with permission from reference 15.

Methane storage capabilities of COFs have been evaluated both experimentally^{49,71} and theoretically.^[4d, 35-36] Like hydrogen, the amount of methane uptake is correlated to surface area, with higher surface area COFs typically adsorbing more than lower surface area analogues. For example, the gravimetric excess uptake of methane in 3D COF-102 (187 mg g⁻¹) and COF-103 (175 mg g⁻¹) is higher than that of 2D COF-5 (89 mg g⁻¹) at 298K and 35 bar.^[19] Goddard and co-workers have performed a simulation study using 14 COFs to explore their methane storage ability. They have shown two fundamental ways to improve methane storage in COFs, a) by using ligands with low steric encumbrance to minimize the methane-COF interaction at low pressure and b) by improving the heat of adsorption.^[36] Another theoretical study by Wang and co-workers^[4d] studied the excess storage capacities of methane in 3D COFs and their Li-doped counterparts at 243 and 298 K and 35 bar. This study indicates that the gravimetric capacities of Li-doped COF-102 and COF-103 reach 303 and 290 cm³ (STP) cm⁻³, respectively, which is more than double those in the parent COFs (127 and 108 cm³ (STP) cm⁻³) at 298 K and 35 bar (Figure

4). This improvement was attributed to increased London-dispersion forces and induced dipole interactions between methane and the adsorbed Li cations.

1.3.3 COFs for carbon dioxide capture and separation

Carbon dioxide is the main byproduct of fossil fuel combustion and is a major contributor to global warming. To help combat this global threat, there is a massive demand for green, cost effective strategies for carbon capture and sequestration (CCS).⁷² Several classes of porous materials have been identified as suitable candidates⁷³ for CCS due to the drawbacks⁷⁴ of other methods.⁷⁵ Among zeolites, porous carbons, and metal-organic frameworks (MOFs), COFs have been posited as a superior candidate for CO₂ capture.¹ The first examples of CO₂ sorption in boronate ester COFs were reported in 2009.⁴⁹ Each of these reported examples were 2D-COFs having eclipsed layered structures with pores in the form of 1D channels.^{1,76} 3D COFs-102 and 103 were evaluated for their CO₂ capture capability in addition to their hydrogen storage properties previously discussed in section 2.1.¹² These studies generally demonstrated that COFs with small pores were better at adsorbing CO₂ than those with very large surface areas and larger pore sizes. However, owing to the poor hydrolytic stability of boronate esters they likely are not useful for practical applications in gas sequestration.

Other COF designs aimed to bind CO₂ molecules more effectively by incorporating a higher density of polar functional groups. Triazine-based COFs were first developed by Thomas and co-workers in 2008 through ionothermal synthesis and have demonstrated good properties for CO₂ adsorption.⁷⁷ Triazine COFs are formed under often harsh conditions (strongly acidic, or at temperatures >300 °C) which enable dynamic reversibility in the triazine functional groups. The first triazine-based COF (CTF-1) was made from terephthalonitrile, and has a BET surface area

of $791 \text{ m}^2 \text{ g}^{-1}$. In 2013, Han *et al.* reported a perfluorinated variant of CTF-1 (named FCTF-1) and compared its CO_2 sorption with CTF-1.⁷⁸ FCTF-1 exhibited a higher Q_{st} value (35.0 kJ mol^{-1}), indicating a stronger affinity to CO_2 when compared to the non fluorinated CTF-1. It is hypothesized that the incorporation of fluorine substituents enhances the interaction between the COF structure and CO_2 in two ways, 1) through increased electrostatic interactions between the electronegative fluorine and the electron poor carbon atom of carbon dioxide, and 2) by reducing the size of the micropores to less than 0.5 nm , which facilitates CO_2 uptake and CO_2/N_2 separation through kinetic selectivity.

The CO_2/N_2 selectivity of these COFs was studied using the ideal adsorption solution theory (IAST) which is based on single-gas adsorption isotherms at 298 K and 1 bar .⁷⁹ These measurements showed that the fluorinated FCTF-1 had an improved IAST selectivity of 31 while the selectivity for the non-fluorinated CTF was 20. In addition to this, column breakthrough experiments were also performed under kinetic flow conditions at 298 K and 1 bar with 10:90 v/v mixtures of CO_2 and N_2 . These experiments showed even greater improvements in selectivity between FCTF-1 (77) and CTF-1 (18). Moreover, FCTF-1 showed only a 12% decrease in CO_2 uptake when using wet CO_2 . These results validate the benefit of FCTF-1 over conventional sorbents, which generally lose more than 50% of original CO_2 adsorption capacity when used under practical conditions that simulate ambient moisture, or the water found in the exhaust streams of combustion reactors.⁸⁰

In a recent report,⁸¹ two CTFs, CTF-FUM made from fumaronitrile, and CTF-DCN made from 1,4 dicyanonaphthalene were synthesized exhibiting ultramicropores of less than 7 \AA . These COFs were made through ionothermal synthesis at 350 , 400 and $500 \text{ }^\circ\text{C}$. Among all CTF-FUM

and CTF-DCN frameworks, the CTF-FUM-350 had the highest CO₂ adsorption capacity of 57.2 cm³ g⁻¹ (112 mg g⁻¹), and selectivities for CO₂ over N₂ and CH₄ of 102.4 and 20.5 at 298 K, respectively. This performance was attributed to the ultramicroporous nature and the high nitrogen content (27.64%) in CTF-FUM-350.

One of the most common classes of COFs are imine COFs, which rely on the effective use of dynamic imine chemistry to form their primary structure.¹⁴ The first CO₂ sorption measurements of an imine COF were reported in 2012 by Banerjee *et.al.*⁸² They reported the synthesis of TpPa-1 and TpPa-2 using 1,3,5-triformylphloroglucinol (Tp) with *p*-phenylenediamine (Pa-1) and 2,5-dimethyl *p*-phenylenediamine (Pa-2), respectively, which were highly chemically stable 2D-COFs. The BET surface areas of TpPa-1 and TpPa-2 were reported as 535 m² g⁻¹ and 339 m² g⁻¹, respectively. The CO₂ uptake of TpPa-1 and TpPa-2 was measured to be 78.0 (153) and 64.0 (126) cm³ g⁻¹ (mg g⁻¹) at 273 K and 1 bar, respectively.

A room temperature, solvent-free, mechanochemical grinding approach was introduced to make these imine COFs (TpPa-1 and TpPa-2) along with new TpBD COFs utilizing benzidine (BD) monomer as the diamine component.⁸³ Although these COFs seem to have lower crystallinity, they exhibited higher chemical stability. The CO₂ uptake of TpBD using this method was 40.0 cm³ g⁻¹ (78.6 mg g⁻¹) at 273 K and 1 bar.

Lin Wang *et al.* introduced a microwave-aided methodology to synthesize TpPa-1 (TpPa-COF (MW)) with high crystallinity and a BET surface area of 724.6 m² g⁻¹, a 35% improvement compared to the 52.6 m² g⁻¹ found for traditionally produced TpPa-1.⁸⁴ The CO₂ uptake of TpPa-COF (MW) was 111 cm³ g⁻¹ (218 mg g⁻¹) with a Q_{st} of 34.1 kJ mol⁻¹ at 273 K and 1 bar. The selectivity of CO₂/N₂ was calculated to be 32 at 273K. The comparatively higher CO₂ sorption

can be attributed to the microporous nature of the material, high surface area, and the numerous N-H sites on the pores that have favorable interactions with polarizable CO₂ molecules through hydrogen bonding.

While imine-based COFs exhibit high crystallinity, they suffer from poor or moderate chemical stability, which limits the application of imine COFs in gas storage under normal environmental conditions. To overcome this limitation, a new strategy was developed to introduce –OH functionality, and therefore intramolecular hydrogen bonding, near the Schiff base –C=N– centers in 2D-COFs. This COF, DhaTph, showed both improved chemical stability and surface area, as the basic imine nitrogen is protected from hydrolysis by intramolecular hydrogen bonds.⁸⁵ DhTph and its analogue without the pendent –OH groups, DmaTph, show CO₂ uptakes of 65.0 (128) and 37 (73) cm³ g⁻¹ (mg g⁻¹), respectively. CO₂ adsorption can be improved further in these materials by assembling these COFs into vesicles with spherical morphology that retains their microscopic crystallinity.⁸⁶

Another report demonstrated the use of pyrene cores to synthesize a highly crystalline mesoporous imine-based COF (ILCOF-1). The reversible condensation between 1, 3, 6, 8-tetrakis (4'- formylphenyl)-pyrene and *p*-phenylenediamine, in the presence of acid catalyst, yielded ILCOF-1, which exhibited a high BET surface area of 2723 m² g⁻¹.⁸⁷ The excess CO₂ sorption capability was measured to be 31 cm³ g⁻¹ (61 mg g⁻¹) at 273 K and 1 bar with a *Q*_{st} value of 18.3 kJ mol⁻¹. The high pressure (40 bar) CO₂ sorption of ILCOF-1 was 656 cm³/g at 298 K. This CO₂ sorption capability of ILCOF-1 outperforms most of the 2D and 3D COFs in the literature to date. The high CO₂ sorption was attributed to an enhanced CO₂ binding ability of the COF's nitrogen-rich pore-walls.

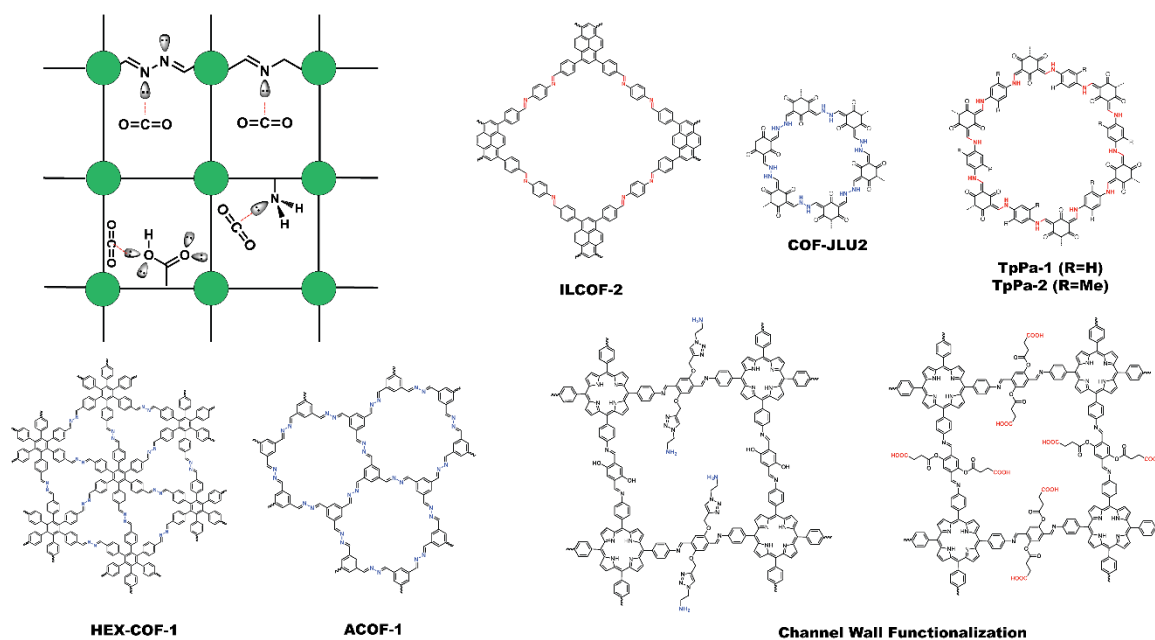


Figure 1.5. Illustration of the types of interactions that can be incorporated into COFs to enhance CO₂ gas adsorption and examples of COF design that incorporate these types of functionality resulting in strong CO₂ adsorption. The channel-wall functionalized COFs shown represent those with the highest CO₂ adsorption capacity out of this series of COFs.

Azine-linked COFs are another popular class of COFs where the dynamic reaction between an aldehyde and hydrazine is utilized in the synthesis. Jiang *et al.* first reported the synthesis of an azine-linked COF (Py-Azine COF) in 2013, synthesized by condensation between hydrazine and 1,3,6,8-tetrakis(4-formylphenyl)pyrene.²⁹ The first CO₂ sorption of an azine COF was reported for ACOF-1, which was synthesized by the condensation between hydrazine hydrate and 1,3,5-triformylbenzene.⁸⁸ This had a BET surface area of 1176 m² g⁻¹ with a CO₂ uptake of 90.0 cm³ g⁻¹ (177 mg g⁻¹) at 273 K and 1 bar. The Q_{st} for CO₂ sorption was 27.6 kJ mol⁻¹ and the selectivity of CO₂ /N₂ was 40 at 273 K.

Smaldone and co-workers reported an azine COF (HEX-COF-1) based on a six-fold symmetric hexaphenylbenzene (HEX) monomer functionalized with aldehyde groups.⁸⁹ The BET

surface area of HEX-COF 1 was $1214 \text{ m}^2 \text{ g}^{-1}$ with an average pore size of 1 nm. It showed an excellent sorption capability for carbon dioxide of $102.0 \text{ cm}^3 \text{ g}^{-1}$ (200.0 mg g^{-1}) at 273 K and 1 bar with a Q_{st} of 42 kJ mol^{-1} . These measurements indicate a strong affinity between the HEX-COF 1 and CO_2 gas molecules due to a high content of nitrogen atoms and small pore size (Figure 1.5).

COF-JLU2, another 2D azine COF synthesized by condensation of hydrazine hydrate and 1,3,5-triformylphloroglucinol,⁹⁰ shows high crystallinity, a surface area of $410 \text{ m}^2 \text{ g}^{-1}$, and a pore diameter of 0.96 nm. The CO_2 sorption capacity was reported as $110.0 \text{ cm}^3 \text{ g}^{-1}$ (216.1 mg g^{-1}) at 273 K and 1 bar, which is remarkably high among reported COFs.^{14,88} The Q_{st} of COF-JLU2 for CO_2 at low coverage was 31 kJ mol^{-1} . The high CO_2 uptake capacity and heat of adsorption was attributed to the nitrogen and oxygen rich micropore walls of the framework. The CO_2/N_2 selectivity of 77 is also quite high.^{90,91}

With so many successful examples of CO_2 storage in nitrogen and oxygen rich COFs, strategies have been developed to post-synthetically incorporate functional groups into the pores of 2D COFs. In 2015, Jiang *et al.* decorated the interior pore channels of a conventional 2D-COF containing hydroxyl groups (termed $[\text{HO}]_{\text{x}\%}\text{-H}_2\text{P-COFs}$) with carboxylic acid groups through the use of a ring opening reaction to form a new material named $[\text{HO}_2\text{C}]_{\text{x}\%}\text{-H}_2\text{P-COF}$.⁹² This modification lead to a CO_2 storage capacity of $23\text{-}32 \text{ cm}^3 \text{ g}^{-1}$ ($45\text{-}63 \text{ mg g}^{-1}$) at 273 K and 1 bar, almost three times that of the unmodified COF. However, due to the steric pore filling from the postsynthetically added side chains, the shape of the isotherm was changed to a type I from a type IV. In addition to this, the BET surface area was reduced by approximately half, for the modified COF. The $[\text{HO}_2\text{C}]_{100\%}\text{-H}_2\text{P-COF}$ (Figure 1.5) showed the highest CO_2 sorption of

89.0 cm³ g⁻¹ (175 mg g⁻¹) at 273 K and 1 bar. The enhancement in the sorption properties was attributed to the higher content of carboxylate groups, which can form a dipolar interaction with CO₂. The selectivity of adsorption for CO₂ over N₂ was calculated for these COFs using the IAST method. [HO₂C]_{100%}-H₂P-COF showed a selectivity of 323 for a 15/85 CO₂/N₂ mixture at 298 K and 0.1 kPa, while [HO]_{100%}-H₂P-COF showed a selectivity of only 18 under the same conditions. This work was followed up by the Jiang and co-workers⁹² using a click chemistry approach to modify the channel walls of a COF with a variety of different functional groups, including Et (ethyl), COOMe (ester), EtOH (hydroxyl), AcOH (carboxylic acid) and EtNH₂ (amino). Though the pore functionalization negatively effects the BET surface area, in all cases except for Et incorporation, the CO₂ uptake capacity has been enhanced. The CO₂ sorption capacities and the Q_{st} values of these COFs increased with increasing functional group polarity. When the molar ratio (x) = 50, the [EtNH₂]_x-H₂P-COFs, [EtOH]_x-H₂P-COFs, [AcOH]_x-H₂P-COFs, and [MeOAc]_x-H₂P-COFs showed the greatest CO₂ adsorption. Of these, [EtNH₂]₅₀-H₂P-COF (Figure 1.5) exhibited the highest adsorption capacity of 80.0 cm³ g⁻¹ (157 mg g⁻¹) at 273 K and 1 bar.

Of the different classes of COFs discussed, the triazine, imine, and azine-based COFs exhibit some of the highest chemical stability and high CO₂ adsorption profiles that would be required for use in CO₂ storage applications. The high CO₂ sorption capability of these COFs can be attributed to favorable interactions between CO₂ molecules and the polar functional groups in the frameworks. Further investigation of new COFs that exploit the use of pore wall functionalization could help create viable materials for future clean energy applications.

1.4 COFs for electrical energy storage

The role for COFs in the field of sustainable energy doesn't end with gas separation and storage. Among all classes of porous materials, 2D COFs are unique in being able to orient building blocks in crystalline, closely spaced, eclipsed formations. Early computational models indicated that this structural characteristic of COFs, coupled with building blocks designed to carry charge, would allow for charge transfer not only through the covalent bonds forming the two-dimensional sheets of COFs, but also along the c-axis of the final crystalline solid.⁹³ This fundamental property has led to an explosion of interest in developing and understanding the electrochemical properties of COFs.⁴ Several excellent electroactive COFs have since been produced,^{7,94-98} showing the promise of COFs for a variety of sustainable energy applications where conductivity and charge transfer are required, including photovoltaic technologies and batteries.

1.4.1 COFs for photovoltaic applications

Capturing the energy of the sun has long been a clean energy goal, with vast amounts of research effort being directed towards both inorganic and organic photovoltaic materials. Solar cells made from fully organic materials are generally made from conductive polymers, and have lower efficiencies and lifetimes than their inorganic counterparts, though they benefit from being lighter weight and more easily processed than inorganic analogues.⁹⁹ It is known that the decreased efficiency of organic solar cells can be countered by controlling the way donor and acceptor molecules are assembled within the conducting material. Solar cells with a bulk heterojunction design are superior as the interface between the donor and acceptor components is

increased compared to a cell with a bilayer arrangement of these components. If individual donor and acceptor molecules can be arrayed in space in a controlled, alternating fashion, then the interface between donors and acceptors could be organized at the molecular level (Figure 1.6). COFs, with their high surface area and ordered pore structures could host such donor acceptor arrangements.

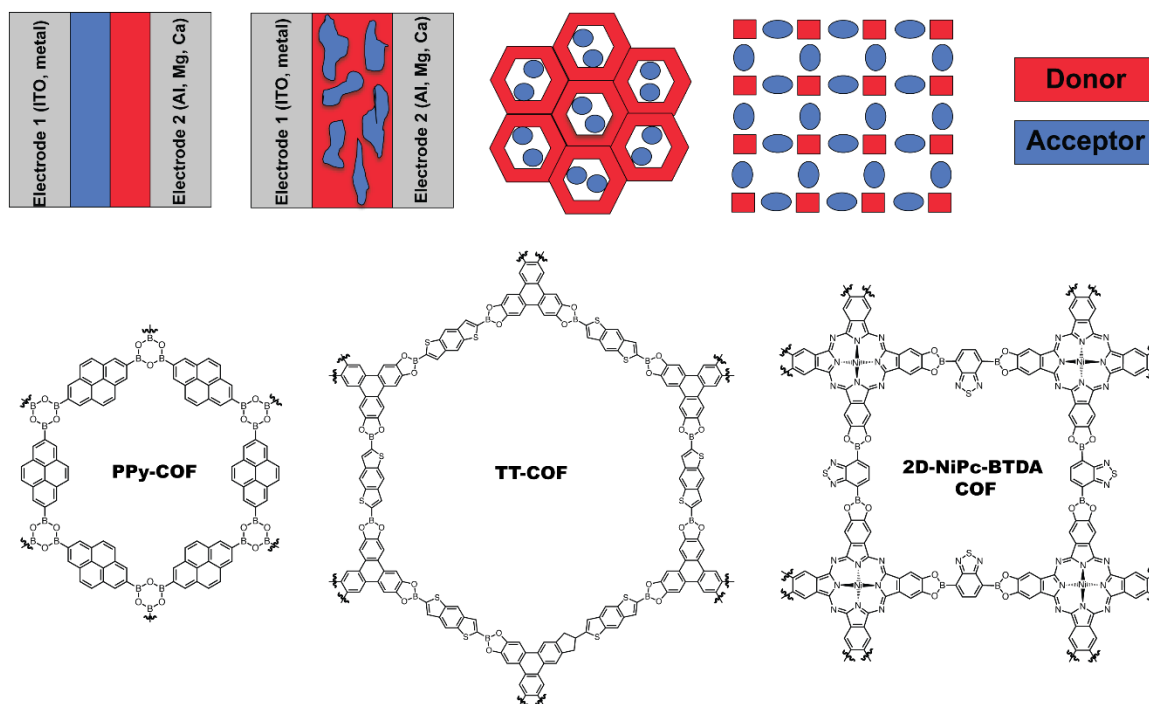


Figure 1.6. Illustration of the evolution of solar cell design from a bilayer approach to a bulk heterojunction approach to precise molecular architecture designs made possible with COFs. (Top) Examples of COFs that have shown photo-responsive charge separation. (Bottom)

Jiang *et al.* produced the first example of a photoconductive COF with the publication of a PPy-COF, made through the self condensation of pyrene diboronic acid to form a boroxine linked COF.⁹⁴ PPy-COF is an exceptionally crystalline COF, growing cube-shaped crystals on the micrometer scale. Jiang measured the photoconductivity of PPy-COF by evaporating a thin film of COF onto an Al electrode. They then deposited a 30 nm layer of Au onto the film using vapor

deposition, and irradiated the resulting electrode with visible light from a xenon lamp. The result was a linear I - V response at 25 °C, and they were able to show that the material could be switched multiple times without deterioration of the on-off ratio. This remarkable photo response is attributed by the authors to the perfect eclipsed stacking of PPy-COF, allowing exciton migration through the framework. As low off-set in the COF network seems to be a general property of highly conductive COFs, the available computational models to predict *a priori* the amount of off-set expected in COF formation could be useful in designing other conductive COFs.¹⁰⁰

Subsequent photoactive COFs was published by Ding and co-workers with a Ni phthalocyanine based COF they created by co-condensing Ni phthalocyanine with 1,4-benzenediboronic acid (BDBA). This COF was able to produce a photocurrent of 3 μ A when processed into an electrode and irradiated with a xenon lamp by the same procedure used for PPy-COF.¹⁰¹ Ding also showed that the identity of the metal bound to the phthalocyanine was able to tune the electronic character.¹⁰² By exchanging the BDBA component with benzodiathiazole (BTDA), the resulting COF was improved and was able to generate a photocurrent of 15 μ A under the same conditions.¹⁰¹ Replacing the phthalocyanine with porphyrin and condensing that with BDBA allowed for the production of a series of photoactive COFs with different electron and hole mobility based on the metal in the porphyrin building block.⁹⁵ Jiang and co-workers then reported CS-COF, a conductive and chemically stable COF produced by the co-condensation of triphenylene hexamine (TPHA) and *tert*-butylpyrene tetraone (PT).¹⁰³ Initial measurements for conductivity using flash photolysis time-resolved microwave conductivity (FP-TRMC) method showed CS-COF to have a hole-conducting mobility of 4.2 cm² V⁻¹ s⁻¹, making it one of the best

hole-transporting organic semi-conductors reported at that time. By soaking C₆₀ into the CS-COF framework, and adding 50 wt% of an organic semi-conductor, [6,6]-phenyl-C₆₁-butyric acid methyl ester (PCBM), and poly(methyl methacrylate) to act as a glue, they were able to fabricate an electrode sandwich of tin oxide (ITO)/spin coated active layer/Al to test for photoactive properties. This device showed a power conversion efficiency of 0.9%, a large open-circuit voltage of 0.98 V, and the ability to switch multiple times without degradation of the device. Partnering electron donating COF frameworks with electron accepting C₆₀ was further explored by Chen and co-workers. By condensing (2,3,9,10,16,17,23,24-(octahydroxyphthalocyanato) zinc (ZnPc[OH]₈) with a mixture of BDBA and a derivative of BDBA that contained a pendent azide (N₃-BDBA), they were able to covalently link C₆₀ to the inside of the COF pores¹⁰⁴ and showed that charge was efficiently transferred.

Several efforts incorporating thiophene based monomers into COFs have been reported.^{7,105,106} Bein and co-workers have reported a thiophene based COF that was successfully used to fabricate a photovoltaic device. By co-condensing thieno-[3,2-b]-thiophene-2,5-diyldiboronic acid (TTBA) and hexahydroxytriphenylene (HHTP), they produced TT-COF.⁹⁶ As thiophene based polymers show excellent photoinduced charge transfer in the presence of PCBM, Bein and co-workers soaked TT-COF in a solution of PCBM, and showed by decrease in BET surface area that the COF was taking it up into the framework, which was then confirmed through photoluminescence quenching of the 487 nm emission of pristine TT-COF. When a thin film of this COF was used to produce a photovoltaic cell using ITO/TT-COF:PCBM/Al, the efficiency was reported as 0.053, with an open-circuit voltage of 0.62 V. A Monte Carlo simulation was performed to study how the PCBM packs into the COF pores. This simulation suggested that

designing a COF with larger pores could potentially increase the observed efficiency by allowing for better packing of PCBM, and therefore better charge transfer.¹⁰⁷

While the previous examples have demonstrated the effectiveness of COFs to work with dopants such as C₆₀ to separate and conduct charge, one could also envision creating a COF in which the donor and the acceptor molecules are part of the COF framework itself. This concept was realized by Jiang and co-workers with their integrated donor-acceptor COF, 2D D-A COF.⁹⁵ Typically, when donor and acceptor molecules are co-crystallized they stack on top of each other, causing rapid combination of charge carriers and very low efficiencies. However, by using donor and acceptor building blocks to produce a COF, the directed self-assembly of COF formation over-rides the propensity of donors and acceptors to stack together and instead forms periodic and columnar arrays of donor and acceptor molecules. This creates vertically ordered p-n heterojunctions and a very large D-A interface, which should significantly increase the photoconductivity of the material, without the need for an added dopant. A co-condensation of 2,1,3-benzothiadiazole-4,7-diboronic acid (BTDADA) and hexahydroxyterphenylene (HHTP) was used to create 2D-D-A COF as orange crystals. Again using FP-TRMC, this material was shown to conduct both electrons and holes with a mobility of 0.01 and 0.04 cm² V⁻¹ S⁻¹ respectively.¹⁰¹ Computational modeling was performed on this COF by Er *et al.*, using density functional theory to further explore the conductive nature of this COF. Their calculations support a hypothesis that it is the vertically stacked donors and acceptors that are responsible for the high charge mobility.¹⁰⁸ Another reported donor-acceptor COF, D_{ZnPc}-ANDI-COF, which is composed of zinc phthalocyanine as the donor molecule and naphthaline diimide as the acceptor¹⁰⁹ was studied using time resolved spectroscopy. These measurements showed that charge separation

occurs in just 1.4 ps, with the lifetimes of the charge separated states lasting as long as 10 μ s. A recent publication expanded upon this study further by exchanging the Zn metal in the electron donor to Cu or Ni, and then paired each metal with three different diimide acceptors to compare their physical properties.¹⁰⁹ This study found that when the acceptor was held constant and the metal changed, the charge separation lifetimes were similar, however, given a single acceptor, the identity of the metal did affect the charge lifetimes. D_{CuPc}-A_{PryDI}-COF achieved the longest lifetimes of 33 μ s, and shows that optimization between acceptors and donors is an important part of D-A COF design.

Metal free D-A COF systems have also been explored. Jin *et al.* synthesized two COFs using triphenylene as the donor component, and either naphthalene diimide (D_{TP}-A_{NDI}-COF) or pyrromellitic diimide (D_{TP}-A_{PyrDI}-COF) as the acceptor components. Though no direct photoinduced current was measured, the observed fluorescence lifetimes for D_{TP}-A_{NDI}-COF and D_{TP}-A_{PyrDI}-COF of 0.92 and 1.0 ns respectively confirmed that charge transfer is occurring between adjacent donor and acceptor molecules.¹⁰⁹

Though there are many excellent examples of conductive and photoactive COFs, a major drawback to their incorporation into devices is their propensity to form interpenetrated, cross-linked, insoluble powders. To fully explore the electronic properties of COFs in a device such as an electrode, the COFs need to be produced in ordered arrays, without grain boundaries that lower efficiencies. Drop casting membranes or incorporating other conductive polymers to serve as supports does work, but the major breakthrough required for device fabrication came in 2011, when Dichtel and co-workers found that by incorporating single-layer graphene (SLG) on Cu substrates into the solvothermal conditions used for generating COFs, they could grow oriented

COF thin films.³³ Using 1,4-phenylenebis(boronic acid) (PBBA) with HHTP, to produce what is known as COF-5, the surface of the graphene could be coated in a layer of COF after just 30 minutes of reaction time. Synchrotron X-ray diffraction showed the characteristic peaks associated with bulk COF-5 were present, confirming that an ordered crystalline network of COF-5 is being produced. SEM images of an SLG substrate that was covered in a protective Pt layer before being subjected to the COF forming conditions for 30 minutes showed a 200 nm thick layer of COF covering the substrate. They further demonstrated that COF films formed on other SLG substrates, with SLG/SiO₂ growing 100 nm thick COF sheets after a thirty minute reaction time with a more uniform film-substrate interface than the corresponding SLG/Cu substrate. The films were further enhanced when grown on SLG/SiC substrates. With these they found that a longer reaction time of 8 hours was required, but the films produced contained no visible grain boundaries. With this proof of principle in hand, two other COFs with known conductivity properties were grown on transparent SLG/SiO₂ substrates. The first of these was TP-COF, produced through a co-condensation of pyrene-2,7-diboronic acid and HHTP.¹¹⁰ The diffraction data for the COF films grown with these building blocks matched powdered TP-COF samples, and the photoluminescence of the films showed the strong pyrene excimer emission that is seen in TP-COF powders. The second conductive polymer that was grown was a square lattice COF produced from Ni phthalocyanine and PBBA. This example shows that non-hexagonal COFs can also be grown on these substrates, making the method remarkably general.

Bein and co-workers recently reported the first synthesis of an oriented thin film of a benzodithiophene containing COF interpenetrated with C₆₀, forming for the first time a periodic D-A system as a thin film on a variety of device relevant substrates.¹¹¹ This was achieved by co-

condensing benzo[1,2-b:4,5-b']dithiophene-2,6-diyl diboronic acid (BDTBA) and HHTP under solvothermal conditions in the presence of an ITO coated glass substrate. These conditions produced uniform, crack-free COF films of 150 nm with the c axis of the COF perpendicular to the substrate surface. The thin films were then spin coated with either [60]PCBM or [70]PCBM, and fluorescence quenching studies showed both acceptors were able to quench the fluorescence of the BDTBA COF with approximately 60% efficiency, confirming that charge transfer is occurring from the donor COF to the infiltrating acceptors.

Spitler *et al.* reported¹¹² the growth of oriented thin films of a series of lattice expanded ZnPC COFs on SLG, creating COF films with diagonal pore widths ranging from 2.7 to 4.4 nm. While these COFs have not been investigated for photoconductive properties, the ZnPC COF they are based on is photoactive, and the larger pores are expected to allow for more versatility in the choice of acceptor molecule partners.

Finally, Calik and co-workers have now incorporated a new D-A COF into the first photovoltaic device that uses only a COF as the photoactive layer.¹¹³ By co-condensing bis(boronphenyl)porphyrin and HHTP they produced TP-Por COF with segregated donor and acceptor columns in which electrons can flow through the columns of porphyrins and holes flow through the columns of HHTP. A thin film of TP-Por COF was grown on a patterned ITO substrate that had been pre-coated with a 10 nm MoO_x layer as a hole extraction layer. The COF was then spin coated with a 20 nm thick coating of ZnO nanoparticles followed by thermal evaporation onto Al electrodes. This device was then illuminated with simulated solar light, producing an open-circuit voltage of 312 mV. Though the device suffered from low power conversion, it shows conclusively that with more development and a deeper understanding of

their design rules, COFs have exciting promise as component materials for the photovoltaics of the future.

1.5 Capacitive storage in COFs

With the modern world's rapidly expanding technology and energy demands, it's not just harvesting energy that is important, the ability to store and access energy is increasingly important as well. Batteries have long been the traditional choice for energy storage due to their large energy capacity, and there have been reports of COFs as useful scaffolding materials for lithium ion^{98,114} and lithium sulfur batteries¹¹⁵. However, the rate to store and access energy (power) in batteries is often limited by a low power density.¹¹⁶ Recently, supercapacitors have emerged as a higher power density solution with long cycle life,¹¹⁶ and there is expanding demand to increase the energy density of supercapacitors even further. One type of supercapacitor, pseudocapacitors, also referred to as electrochemical capacitors, represent a middle ground between capacitors and batteries, utilizing both chemical reactions (such as reversible oxidation/reduction reactions) and electrostatic interactions to store energy. This hybrid type of capacitor is able to provide high power and energy densities.^{116,117} The demand for electric cars has driven a large part of the push for supercapacitive devices. When accelerating, a car needs rapid access to large amounts of energy; in other words, a high power density is required. Supercapacitors are uniquely positioned to fill this need by providing both high energy and power densities. Electric cars could then utilize battery power while maintaining speed since immediate access to large energy reserves is not required.¹¹⁶ Recent research has sought to apply COFs as components for the electrodes of electrochemical capacitors in order to optimize energy storage.

Since the energy storage for supercapacitors occurs at the electrolyte-electrode interface, high surface area materials are often utilized to maximize the formation of double layer charge separation, maximizing the ability to store electrostatic energy.¹¹⁷ It has been found that optimizing surface area and pore structure can have a large affect on energy storage potential.¹¹⁶ Chmiola et al.¹¹⁸ demonstrated that pore size has a significant effect on capacitance, demonstrating a sharp increase in capacitance below 1 nm. For pseudocapacitors, the electrode material must also be able to utilize rapid, reversible chemical reactions notably oxidation/reduction reactions. Typical materials used in pseudocapacitors include transition metal oxides, conducting polymers, and carbon materials doped with electrochemically active material.^{116,117} COFs offer many advantages over typical materials for electrochemical capacitor electrodes. Notably, COFs allow well-defined control over pore size, shape, and surface area, as well as over the placement and character of redox active groups.¹¹⁹ In this way, COFs offer design potential and flexibility such that capacitive energy storage processes can be studied and optimized.

DeBlase et al.¹²⁰ utilized the hydrolysis resistant β -ketoenamine linkage to create redox active COFs using DAAQ and TFP monomers. These COFs were capable of specific capacitance of 48 F g⁻¹. With these COFs there was poor accessibility of the redox active anthraquinone groups, approximately 2.5%, which they attributed to random alignment of the COF particles.¹²⁰ In another report by DeBlase et al.⁶ improvements in the capacitive properties of this COF were obtained by synthesizing oriented thin films on a gold electrode, which yielded much higher accessibility of the anthraquinone groups (80-99%) and a specific capacitance of 3 mF cm⁻², a 400% improvement compared to the randomly oriented powder. Zha et al.⁸ have synthesized

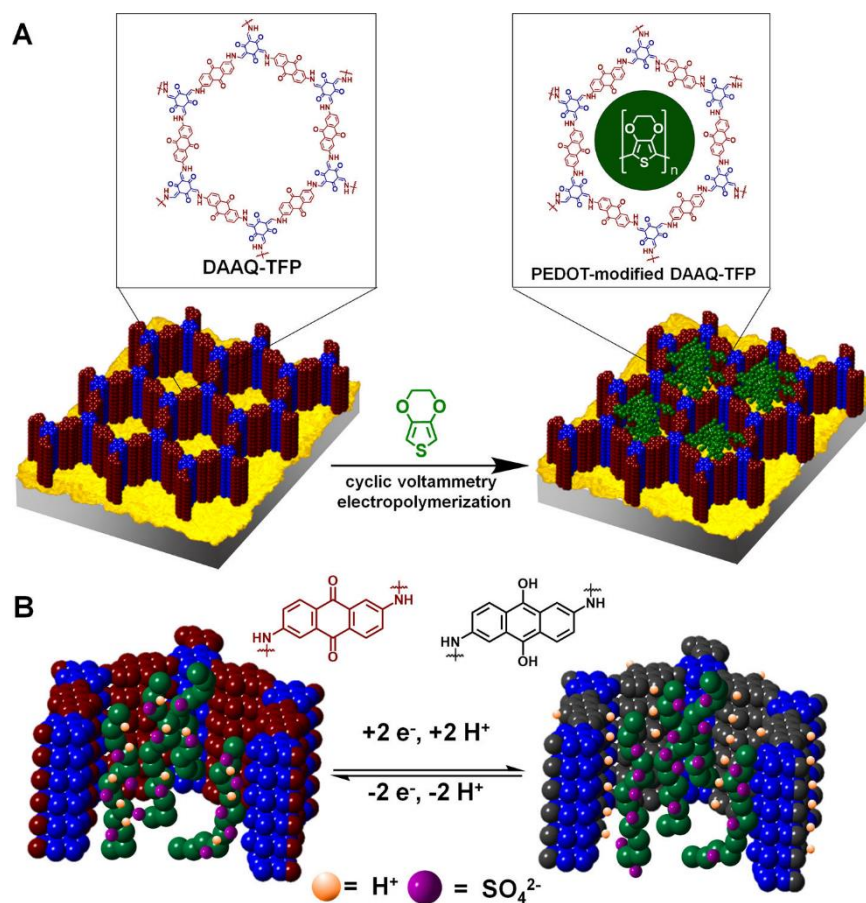


Figure 1.7. (A) Illustration of a method to electropolymerize EDOT into the pores of a pre-formed conductive COF network resulting in a synergistically conductive and stable capacitive material (B). Figure taken with permission from reference 121.

a similar DAAQ based COF thin film on graphene with a specific capacitance of 7.6 mF cm^{-2} . Khattak et al.¹¹⁹ produced a redox active pyridine based COF by condensing diaminopyridine (DAP) with triformylphloroglucinol (TFP). This COF demonstrated a specific capacitance of 209 F g^{-1} and had high (92%) cycle stability after 6000 charge-discharge cycles. Redox active units can also be incorporated into the pores of COFs, thereby taking advantage of their ordered structure to arrange charge carriers in space. Xu et al.¹¹ demonstrated a general strategy for post-synthetically modifying COFs to functionalize them with redox active organic radicals. This was

accomplished through a copper-catalyzed azide-alkyne click reaction between 4-azido-2,2,6,6-tetramethyl-1-piperidinyloxy (TEMPO) groups and the alkyne functionalized COF. This allows the reversible redox process of switching between oxidation states of a neutral radical and an oxoammonium cation. This post-synthetically functionalized COF exhibited a specific capacitance of 167 F g^{-1} .

Recently, Mulzer *et al.*¹²¹ were able to electropolymerize EDOT inside the pores of DAAQ-TFP COF (Figure 1.7). They demonstrated that there is a synergistic effect between the conductive PEDOT polymer and the redox active COF, overcoming the low conductivity of the COF, and low cycle stability of the polymer thereby achieving overall improved capacitive properties. The PEDOT enhanced COF had a very high volumetric capacity of 350 F cm^{-3} and showed stable performance over 10,000 charge cycles.

1.6 COFs for fuel cell membranes

Proton transport is another potential area for COFs to contribute to energy applications. A critical component of hydrogen fuel cells is a proton conducting membrane that transports protons away from the anode, allowing them to recombine with oxygen at the cathode to form water. Many porous materials including MOFs have already shown great promise as proton conducting media,^{122,123} and recent reports suggest that COFs could as well, while exhibiting advantages over MOFs such as lower density and higher stability to acidic and basic conditions.

The first report of proton conduction in COFs came in 2014 from Banerjee *et al.*¹²⁴ Their approach was to exploit the highly ordered channels formed in COF frameworks to organize proton transporting materials. To this end, they synthesized an azo-containing COF using triformylphloroglucinol and 4,4'-azodianiline that was then treated with phosphoric acid. The

authors hypothesized that the azo groups would increase proton conductivity by serving as anchoring points for the phosphoric acid, and indeed, the resulting PA@Tp-Azo COF showed proton conduction in humid and anhydrous environments of 9.9×10^{-4} and 6.7×10^{-5} S cm⁻¹ respectively.

The Jiang lab employed a similar strategy by soaking N-heterocycle proton carriers into the imine linked TPB-DMTP-COF.¹²⁵ The highly ordered, 3.26 nm channels present in this COF allowed for extremely high loading of the proton transporting material, up to 180 wt% for triazole. The resulting trz@TPB-DMTP-COF had a proton conductivity of 1.1×10^{-3} S cm⁻¹ at 130 °C. A similar procedure was used to load the COF channels with imidazole, which showed a similar conductance of 4.37×10^{-3} S cm⁻¹ at 130 °C, showing the generality of this process.

Another strategy for designing COFs for proton transport is to develop COFs with an intrinsic ability to transport charge. Ma and co-workers synthesized a cationic COF linker containing a positively charged ethidium bromide substrate.^[91] Interesting, while the as-synthesized ED-COF:Br with bromine as the counter ion showed a proton conductance of 2.82×10^{-6} S cm⁻¹, exchanging the bromine for the polyoxometalate Pw₁₂O₄₀³⁻ greatly enhanced the proton transport properties, reaching 3.32×10^{-3} S cm⁻¹ at room temperature and 97% relative humidity.

Chandra and co-workers combined the intrinsic and extrinsic strategies, publishing a COF that contained both a pendant sulfonic acid group for intrinsic proton transport, as well as a basic nitrogen that could interact with acidic proton carriers for extrinsic transport.¹²⁶ They showed that TpPa-SO₃H COF decorated with just the intrinsic sulfonic acid groups along the 1D channels had a proton conductivity of 1.7×10^{-5} S cm⁻¹ at 120 °C in an anhydrous media. When the pyridine containing COF was loaded with phytic acid, it had a proton conductivity of $7.5 \times$

$10^{-4} \text{ S cm}^{-1}$. However, when the COF containing both the sulfonic acid and pyridine nitrogen was loaded with phytic acid to make Phytic@TpPa-(SO₃H-Py), the proton transport was improved by an order of magnitude to $5 \times 10^{-4} \text{ S cm}^{-1}$, showing a clear synergy between the proton conducting mechanisms.

Just last year, Banerjee *et al.* were able to successfully demonstrate the use of a COF as the solid electrolyte in a proton exchange membrane fuel (PEMF) Cells.¹²⁷ They did this using TpBpy-Me,¹²⁸ a mechanochemically synthesized bipyridine containing imine COF loaded with phosphoric acid. The PA@TpBpy-Me COF showed an impressive proton conduction of $1.4 \times 10^{-2} \text{ S cm}^{-1}$ at 120 °C. Importantly, the COF material procured by mechanochemically grinding the two substrates together out-performed the traditional solvothermally produced COF in the membrane electrode assembly device. The authors attribute this to the lower porosity of the mechanochemically produced material, which does a superior job keeping the fuel gasses within the cell separate. The fabricated device showed an open circuit potential of 0.93 V, a clear indication of the potential for COFs as solid electrolytes in hydrogen fuel cells.

1.7 Conclusion

Covalent organic frameworks are a promising class of materials for energy storage applications however there are still many challenges that need to be met. Using any new material in our expansive energy infrastructure first requires that it be available in large quantities. In most of the reports cited in this review, the COF materials are synthesized on a research scale, often as little as 10-20 milligrams, which is of course far from the quantities needed to capture CO₂ or make batteries that could power automobiles or homes. Several attempts have been made to remedy this situation through the use of high-efficiency synthetic techniques that allow for scale-

up production without excessive solvent and starting material waste. Continuous flow methods^{128,129} and mechanochemical solid-state syntheses^{127,128,130} have recently been reported for several types of COFs. Colloidal synthesis methods have also now been developed allowing COFs to be conveniently formed into films and sheets through solution processing.¹³¹ Despite the challenges, these advancements are encouraging for the eventual development of COFs into practical, commercially produced materials and devices.

1.8 References

1. Cote, A. P.; Benin, A. I.; Ockwig, N. W.; O'Keeffe, M.; Matzger, A. J.; Yaghi, O. M. *Science* **2005**, *310*, 1166.
2. Ding, S.; Wang, W. *Chem. Soc. Rev.* **2013**, *42*, 548-568.
3. Colson, J. W.; Dichtel, W. R. *Nat. Chem.* **2013**, *5*, 453.
4. Dogru, M.; Bein, T. *Chem. Commun.* **2014**, *50*, 5531-5546.
5. Dalapati, S.; Addicoat, M.; Jin, S.; Sakurai, T.; Gao, J.; Xu, H.; Irle, S.; Seki, S.; Jiang, D. *Nat. Commun.* **2015**, *6*, 7786.
6. DeBlase, C. R.; Hernandez-Burgos, K.; Silberstein, K. E.; Rodriguez-Calero, G. G.; Bisbey, R. P.; Abruna, H. D.; Dichtel, W. R. *ACS Nano* **2015**, *9*, 3178-3183.
7. Duhovic, S.; Dinca, M. *Chem. Mater.* **2015**, *27*, 5487-5490.
8. Zha, Z.; Xu, L.; Wang, Z.; Li, X.; Pan, Q.; Hu, P.; Lei, S. *ACS Appl. Mater. Interfaces* **2015**, *7*, 17837-17843.
9. Stegbauer, L.; Schwinghammer, K.; Lotsch, B. V. *Chem. Sci.* **2014**, *5*, 2789-2793.
10. Lin, S.; Diercks, C. S.; Zhang, Y.; Kornienko, N.; Nichols, E. M.; Zhao, Y.; Paris, A. R.; Kim, D.; Yang, P.; Yaghi, O. M.; Chang, C. J. *Science* **2015**, *349*, 1208.
11. Chen, X.; Addicoat, M.; Jin, E.; Zhai, L.; Xu, H.; Huang, N.; Guo, Z.; Liu, L.; Irle, S.; Jiang, D. *J. Am. Chem. Soc.* **2015**, *137*, 3241-3247.
12. El-Kaderi, H.; Hunt, J. R.; Mendoza-Cortes, J. L.; Cote, A. P.; Taylor, R. E.; O'Keeffe, M.; Yaghi, O. M. *Science* **2007**, *316*, 268.
13. Cao, D.; Lan, J.; Wang, W.; Smit, B. *Angew. Chem. Int. Ed.* **2009**, *48*, 4730-4733.

14. Uribe-Romo, F.; Hunt, J. R.; Furukawa, H.; Klock, C.; O'Keeffe, M.; Yaghi, O. M. *J. Am. Chem. Soc.* **2009**, *131*, 4570-4571.
15. Lan, J.; Cao, D.; Wang, W. *Langmuir* **2010**, *26*, 220-226.
16. Ma, H.; Ren, H.; Meng, S.; Yan, Z.; Zhao, H.; Sun, F.; Zhu, G. *Chem. Commun.* **2013**, *49*, 9773-9775.
17. Zhang, Y.; Su, J.; Furukawa, H.; Yun, Y.; Gandara, F.; Duong, A.; Zou, X.; Yaghi, O. M. *J. Am. Chem. Soc.* **2013**, *135*, 16336-16339.
18. Fang, Q.; Gu, S.; Zheng, J.; Zhuang, Z.; Qiu, S.; Yan, Y. *Angew. Chem. Int. Ed.* **2014**, *53*, 2878-2882.
19. Li, X.; Guo, J.; Zhang, H.; Cheng, X.; Liu, X. *RSC Adv.* **2014**, *4*, 24526-24532.
20. Fang, Q.; Wang, J.; Gu, S.; Kaspar, R. B.; Zhuang, Z.; Zheng, J.; Guo, H.; Qiu, S.; Yan, Y. *J. Am. Chem. Soc.* **2015**, *137*, 8352-8355.
21. Baldwin, L. A.; Crowe, J. W.; Pyles, D. A.; McGrier, P. L. *J. Am. Chem. Soc.* **2016**, *138*, 15134-15137.
22. Lin, G.; Ding, H.; Yuan, D.; Wang, B.; Wang, C. *J. Am. Chem. Soc.* **2016**, *138*, 3302-3305.
23. Yaghi, O. M.; Li, H.; Davis, C.; Richardson, D.; Groy, T. L. *Acc. Chem. Res.* **1998**, *31*, 474-484.
24. Tranchemontagne, D. J.; Mendoza-Cortes, J.; O'Keeffe, M.; Yaghi, O. M. *Chem. Soc. Rev.* **2009**, *38*, 1257-1283.
25. Zhu, Y.; Wan, S.; Jin, Y.; Zhang, W. *J. Am. Chem. Soc.* **2015**, *137*, 13772-13775.
26. Cai, S.; Zhang, K.; Tan, J.; Wang, S.; Zheng, S.; Fan, J.; Yu, Y.; Zhang, W.; Liu, Y. *ACS Macro Lett.* **2016**, *5*, 1348-1352.
27. Dalapati, S.; Jin, E.; Addicoat, M.; Heine, T.; Jiang, D. *J. Am. Chem. Soc.* **2016**, *138*, 5797-5800.
28. Huang, N.; Zhai, L.; Couprie, D. E.; Addicoat, M. A.; Okushita, K.; Nishimura, K.; Heine, T.; Jiang, D. *Nat. Commun.* **2016**, *7*, 12325.
29. Dalapati, S.; Jin, S.; Gao, J.; Xu, Y.; Nagai, A.; Jiang, D. *J. Am. Chem. Soc.* **2013**, *135*, 17310-17313.
30. Stegbauer, L.; Hahn, M. W.; Jentys, A.; Savasci, G.; Ochsenfeld, C.; Lercher, J. A.; Lotsch, B. V. *Chem. Mater.* **2015**, *27*, 7874-7881.
31. Yue, J.; Liu, X.; Sun, B.; Wang, D. *Chem. Commun.* **2015**, *51*, 14318-14321.

32. Chen, X.; Huang, N.; Gao, J.; Xu, H.; Xu, F.; Jiang, D. *Chem. Commun.* **2014**, *50*, 6161-6163.
33. Colson, J. W.; Woll, A. R.; Mukherjee, A.; Levendorf, M. P.; Spitler, E. L.; Shields, V. B.; Spencer, M. G.; Park, J.; Dichtel, W. R. *Science* **2011**, *332*, 228.
34. Smith, B. J.; Dichtel, W. R. *J. Am. Chem. Soc.* **2014**, *136*, 8783-8789.
35. Baldwin, L. A.; Crowe, J. W.; Shannon, M. D.; Jaroniec, C. P.; McGrier, P. L. *Chem. Mater.* **2015**, *27*, 6169-6172.
36. Colson, J. W.; Mann, J. A.; DeBlase, C. R.; Dichtel, W. R. *J. Polym. Sci. Part A J. Polym. Sci. A* **2015**, *53*, 378-384.
37. Cui, D.; MacLeod, J. M.; Ebrahimi, M.; Perepichka, D. F.; Rosei, F. *Chem. Commun.* **2015**, *51*, 16510-16513.
38. Lu, H.; Wang, C.; Chen, J.; Ge, R.; Leng, W.; Dong, B.; Huang, J.; Gao, Y. *Chem. Commun.* **2015**, *51*, 15562-15565.
39. Spitler, E. L.; Koo, B. T.; Novotney, J. L.; Colson, J. W.; Uribe-Romo, F.; Gutierrez, G. D.; Clancy, P.; Dichtel, W. R. *J. Am. Chem. Soc.* **2011**, *133*, 19416-19421.
40. Smith, B. J.; Hwang, N.; Chavez, A. D.; Novotney, J. L.; Dichtel, W. R. *Chem. Commun.* **2015**, *51*, 7532-7535.
41. Smith, B. J.; Overholts, A. C.; Hwang, N.; Dichtel, W. R. *Chem. Commun.* **2016**, *52*, 3690-3693.
42. Elliott, E. L.; Hartley, C. S.; Moore, J. S. *Chem. Commun.* **2011**, *47*, 5028-5030.
43. Vyas, V. S.; Haase, F.; Stegbauer, L.; Savasci, G.; Podjaski, F.; Ochsenfeld, C.; Lotsch, B. V. *Nat. Commun.* **2015**, *6*, 8508.
44. Ascherl, L.; Sick, T.; Margraf, J. T.; Lapidus, S. H.; Calik, M.; Hettstedt, C.; Karaghiosoff, K.; Doblinger, M.; Clark, T.; Chapman, K. W.; Auras, F.; Bein, T. *Nat. Chem.* **2016**, *8*, 310-316.
45. Auras, F.; Ascherl, L.; Hakimioun, A. H.; Margraf, J. T.; Hanusch, F. C.; Reuter, S.; Bessinger, D.; Doblinger, M.; Hettstedt, C.; Karaghiosoff, K.; Herbert, S.; Knochel, P.; Clark, T.; Bein, T. *J. Am. Chem. Soc.* **2016**, *138*, 16703-16710.
46. Chen, X.; Addicoat, M.; Irle, S.; Nagai, A.; Jiang, D. *J. Am. Chem. Soc.* **2013**, *135*, 546-549.
47. Salonen, L. M.; Medina, D. D.; Carbo-Argibay, E.; Goesten, M. G.; Mafra, L.; Guldris, N.; Rotter, J. M.; Stroppa, D. G.; Rodriguez-Abreu, C. *Chem. Commun.* **2016**, *52*, 7986-7989.

48. Alahakoon, S. B.; McCandless, G. T.; Karunathilake, A. A. K.; Thompson, C. M.; Smaldone, R. A. *Chem. Eur. J.* **2017**, *23*, 4255-4259.
49. Furukawa, H.; Yaghi, O. M. *J. Am. Chem. Soc.* **2009**, *131*, 8875-8883.
50. Schlapbach, L.; Züttel, A. *Nature* **2001**, *414*, 353.
51. Graetz, J. *Chem. Soc. Rev.* **2009**, *38*, 73-82.
52. Felderhoff, M.; Weidenthaler, C.; von Helmolt, R.; Eberle, U. *Phys. Chem. Chem. Phys.* **2007**, *9*, 2643-2653.
53. Orimo, S.; Nakamori, Y.; Eliseo, J. R.; Züttel, A.; Jensen, C. M. *Chem. Rev.* **2007**, *107*, 4111-4132.
54. Wood, C. D.; Tan, B.; Trewin, A.; Niu, H.; Bradshaw, D.; Rosseinsky, M. J.; Khimyak, Y. Z.; Campbell, N. L.; Kirk, R.; Stockel, E.; Cooper, A. I. *Chem. Mater.* **2007**, *19*, 2034-2048.
55. Germain, J.; Fréchet, J. M. J.; Svec, F. *Small* **2009**, *5*, 1098-1111.
56. Weitkamp, J.; Fritz, M.; Ernst, S. *Int. J. Hydrogen Energy* **1995**, *20*, 967-970.
57. Sun, Y.; Wang, L.; Amer, W. A.; Yu, H.; Ji, J.; Huang, L.; Shan, J.; Tong, R. *Journal of Inorg. Organomet. Polym. Mater* **2013**, *23*, 270-285.
58. Ren, J.; Musyoka, N. M.; Annamalai, P.; Langmi, H. W.; North, B. C.; Mathe, M. *Int. J. Hydrogen Energy* **2015**, *40*, 9382-9387.
59. Klontzas, E.; Tylianakis, E.; Froudakis, G. E. *Nano Lett.* **2010**, *10*, 452-454.
60. Gao, T.; Zhang, H. *Struct. Chem.* **2014**, *25*, 503-513.
61. Tylianakis, E.; Klontzas, E.; Froudakis, G. E. *Nanoscale* **2011**, *3*, 856-869.
62. Pramudya, Y.; Mendoza-Cortes, J. *J. Am. Chem. Soc.* **2016**, *138*, 15204-15213.
63. Kalidindi, S. B.; Oh, H.; Hirscher, M.; Esken, D.; Wiktor, C.; Turner, S.; Van Tendeloo, G.; Fischer, R. A. *Chem. Eur. J.* **2012**, *18*, 10848-10856.
64. Jackson, K. T.; Reich, T. E.; El-Kaderi, H. *Chem. Commun.* **2012**, *48*, 8823-8825.
65. Ben, T.; Ren, H.; Ma, S.; Cao, D.; Lan, J.; Jing, X.; Wang, W.; Xu, J.; Deng, F.; Simmons, J.; Qiu, S.; Zhu, G. *Angew. Chem. Int. Ed.* **2009**, *48*, 9457-9460.
66. Tilford, R. W.; Mugavero, S. J.; Pellechia, P. J.; Lavigne, J. J. *Adv. Mater.* **2008**, *20*, 2741-2746.
67. Mendoza-Cortes, J. L.; Han, S. S.; Goddard, W. A. *J. Phys. Chem. A* **2012**, *116*, 1621-1631.

68. Menon, V. C.; Komarneni, S. *J. Porous Mater.* **1998**, *5*, 43-58.
69. Mason, J. A.; Veenstra, M.; Long, J. R. *Chem. Sci.* **2014**, *5*, 32-51.
70. Lozano-Castelló, D.; Alcañiz-Monge, J.; de la Casa-Lillo, M. A.; Cazorla-Amorós, D.; Linares-Solano, A. *Fuel* **2002**, *81*, 1777-1803.
71. Mendoza-Cortes, J. L.; Han, S. S.; Furukawa, H.; Yaghi, O. M.; Goddard, W. A. *J. Phys. Chem. A* **2010**, *114*, 10824-10833.
72. Haszeldine, R. S. *Science* **2009**, *325*, 1647.
73. D'Alessandro, D.; Smit, B.; Long, J. *Angew. Chem. Int. Ed.* **2010**, *49*, 6058-6082.
74. Rochelle, G. T. *Science* **2009**, *325*, 1652.
75. Weiland, R. H.; Dingman, J. C.; Cronin, D. B. *J. Chem. Eng. Data* **1997**, *42*, 1004-1006.
76. Tilford, R. W.; Gemmill, W. R.; zur Loye, H.; Lavigne, J. J. *Chem. Mater.* **2006**, *18*, 5296-5301.
77. Kuhn, P.; Antonietti, M.; Thomas, A. *Angew. Chem.* **2008**, *120*, 3499-3502.
78. Zhao, Y.; Yao, K. X.; Teng, B.; Zhang, T.; Han, Y. *Energy Environ. Sci.* **2013**, *6*, 3684-3692.
79. Baticle, P.; Kiefer, C.; Lakhchaf, N.; Leclerc, O.; Persin, M.; Sarrazin, J. *Sep. Purif. Technol.* **2000**, *18*, 195-207.
80. Dawson, R.; Stevens, L. A.; Drage, T. C.; Snape, C. E.; Smith, M. W.; Adams, D. J.; Cooper, A. I. *J. Am. Chem. Soc.* **2012**, *134*, 10741-10744.
81. Wang, K.; Huang, H.; Liu, D.; Wang, C.; Li, J.; Zhong, C. *Environ. Sci. Technol.* **2016**, *50*, 4869-4876.
82. Kandambeth, S.; Mallick, A.; Lukose, B.; Mane, M. V.; Heine, T.; Banerjee, R. *J. Am. Chem. Soc.* **2012**, *134*, 19524-19527.
83. Biswal, B. P.; Chandra, S.; Kandambeth, S.; Lukose, B.; Heine, T.; Banerjee, R. *J. Am. Chem. Soc.* **2013**, *135*, 5328-5331.
84. Wei, H.; Chai, S.; Hu, N.; Yang, Z.; Wei, L.; Wang, L. *Chem. Commun.* **2015**, *51*, 12178-12181.
85. Kandambeth, S.; Shinde, D. B.; Panda, M. K.; Lukose, B.; Heine, T.; Banerjee, R. *Angew. Chem. Int. Ed.* **2013**, *52*, 13052-13056.
86. Kandambeth, S.; Venkatesh, V.; Shinde, D. B.; Kumari, S.; Halder, A.; Verma, S.; Banerjee, R. *Nat. Commun.* **2015**, *6*, 6786.

87. Rabbani, M. G.; Sekizkardes, A. K.; Kahveci, Z.; Reich, T. E.; Ding, R.; El-Kaderi, H. M. *Chem. Eur. J.* **2013**, *19*, 3324-3328.
88. Li, Z.; Feng, X.; Zou, Y.; Zhang, Y.; Xia, H.; Liu, X.; Mu, Y. *Chem. Commun.* **2014**, *50*, 13825-13828.
89. Alahakoon, S. B.; Thompson, C. M.; Nguyen, A. X.; Occhialini, G.; McCandless, G. T.; Smaldone, R. A. *Chem. Commun.* **2016**, *52*, 2843-2845.
90. Li, Z.; Zhi, Y.; Feng, X.; Ding, X.; Zou, Y.; Liu, X.; Mu, Y. *Chem. Eur. J.* **2015**, *21*, 12079-12084.
91. Zhu, Y.; Long, H.; Zhang, W. *Chem. Mater.* **2013**, *25*, 1630-1635.
92. Huang, N.; Krishna, R.; Jiang, D. *J. Am. Chem. Soc.* **2015**, *137*, 7079-7082.
93. Patwardhan, S.; Kocherzhenko, A. A.; Grozema, F. C.; Siebbeles, L. D. A. *J. Phys. Chem. C* **2011**, *115*, 11768-11772.
94. Wan, S.; Guo, J.; Kim, J.; Ihee, H.; Jiang, D. *Angew. Chem. Int. Ed.* **2009**, *48*, 5439-5442.
95. Feng, X.; Chen, L.; Honsho, Y.; Saengsawang, O.; Liu, L.; Wang, L.; Saeki, A.; Irle, S.; Seki, S.; Dong, Y.; Jiang, D. *Adv. Mater.* **2012**, *24*, 3026-3031.
96. Dogru, M.; Handloser, M.; Auras, F.; Kunz, T.; Medina, D.; Hartschuh, A.; Knochel, P.; Bein, T. *Angew. Chem. Inter. Ed.* **2013**, *52*, 2920-2924.
97. Jin, S.; Sakurai, T.; Kowalczyk, T.; Dalapati, S.; Xu, F.; Wei, H.; Chen, X.; Gao, J.; Seki, S.; Irle, S.; Jiang, D. *Chem. Eur. J.* **2014**, *20*, 14608-14613.
98. Yang, H.; Zhang, S.; Han, L.; Zhang, Z.; Xue, Z.; Gao, J.; Li, Y.; Huang, C.; Yi, Y.; Liu, H.; Li, Y. *ACS Appl. Mater. Interfaces* **2016**, *8*, 5366-5375.
99. Coropceanu, V.; Cornil, J.; da, S. F.; Olivier, Y.; Silbey, R.; Bredas, J. *Chem. Rev.* **2007**, *107*, 926-952.
100. Koo, B. T.; Dichtel, W. R.; Clancy, P. *J. Mater. Chem.* **2012**, *22*, 17460-17469.
101. Ding, X.; Chen, L.; Honsho, Y.; Feng, X.; Saengsawang, O.; Guo, J.; Saeki, A.; Seki, S.; Irle, S.; Nagase, S.; Parasuk, V.; Jiang, D. *J. Am. Chem. Soc.* **2011**, *133*, 14510-14513.
102. Ding, X.; Feng, X.; Saeki, A.; Seki, S.; Nagai, A.; Jiang, D. *Chem. Commun.* **2012**, *48*, 8952-8954.
103. Guo, J.; Xu, Y.; Jin, S.; Chen, L.; Kaji, T.; Honsho, Y.; Addicoat, M. A.; Kim, J.; Saeki, A.; Ihee, H.; Seki, S.; Irle, S.; Hiramoto, M.; Gao, J.; Jiang, D. *Nat. Commun.* **2013**, *4*, 2736.
104. Chen, L.; Furukawa, K.; Gao, J.; Nagai, A.; Nakamura, T.; Dong, Y.; Jiang, D. *J. Am. Chem. Soc.* **2014**, *136*, 9806-9809.

105. Bertrand, G. H. V.; Michaelis, V. K.; Ong, T.; Griffin, R. G.; Dinca, M. *Proc. Natl. Acad. Sci.* **2013**, *110*, 4923-4928.
106. Lohse, M. S.; Rotter, J. M.; Margraf, J. T.; Werner, V.; Becker, M.; Herbert, S.; Knochel, P.; Clark, T.; Bein, T.; Medina, D. D. *CrystEngComm* **2016**, *18*, 4295-4302.
107. Koo, B. T.; Berard, P. G.; Clancy, P. J. *Chem. Theory Comput.* **2015**, *11*, 1172-1180.
108. Er, D.; Dong, L.; Shenoy, V. B. *J. Phys. Chem. C* **2016**, *120*, 174-178.
109. Jin, S.; Ding, X.; Feng, X.; Supur, M.; Furukawa, K.; Takahashi, S.; Addicoat, M.; El-Khouly, M. E.; Nakamura, T.; Irle, S.; Fukuzumi, S.; Nagai, A.; Jiang, D. *Angew. Chem. Int. Ed.* **2013**, *52*, 2017-2021.
110. Wan, S.; Guo, J.; Kim, J.; Ihee, H.; Jiang, D. *Angew. Chem.* **2008**, *120*, 8958-8962.
111. Medina, D. D.; Werner, V.; Auras, F.; Tautz, R.; Dogru, M.; Schuster, J.; Linke, S.; Doblinger, M.; Feldmann, J.; Knochel, P.; Bein, T. *ACS Nano* **2014**, *8*, 4042-4052.
112. Spitler, E. L.; Colson, J. W.; Uribe-Romo, F. J.; Woll, A. R.; Giovino, M. R.; Saldivar, A.; Dichtel, W. R. *Angew. Chem.* **2012**, *124*, 2677-2681.
113. Calik, M.; Auras, F.; Salonen, L. M.; Bader, K.; Grill, I.; Handloser, M.; Medina, D. D.; Dogru, M.; Lobermann, F.; Trauner, D.; Hartschuh, A.; Bein, T. *J. Am. Chem. Soc.* **2014**, *136*, 17802-17807.
114. Bai, L.; Gao, Q.; Zhao, Y. *J. Mater. Chem. A* **2016**, *4*, 14106-14110.
115. Liao, H.; Ding, H.; Li, B.; Ai, X.; Wang, C. *J. Mater. Chem. A* **2014**, *2*, 8854-8858.
116. Zhai, Y.; Dou, Y.; Zhao, D.; Fulvio, P. F.; Mayes, R. T.; Dai, S. *Adv. Mater.* **2011**, *23*, 4828-4850.
117. Wang, G.; Zhang, L.; Zhang, J. *Chem. Soc. Rev.* **2012**, *41*, 797-828.
118. Chmiola, J.; Yushin, G.; Gogotsi, Y.; Portet, C.; Simon, P.; Taberna, P. L. *Science* **2006**, *313*, 1760.
119. Khattak, A. M.; Ghazi, Z. A.; Liang, B.; Khan, N. A.; Iqbal, A.; Li, L.; Tang, Z. *J. Mater. Chem. A* **2016**, *4*, 16312-16317.
120. DeBlase, C. R.; Silberstein, K. E.; Truong, T.; Abruna, H. D.; Dichtel, W. R. *J. Am. Chem. Soc.* **2013**, *135*, 16821-16824.
121. Mulzer, C. R.; Shen, L.; Bisbey, R. P.; McKone, J. R.; Zhang, N.; Abruna, H. D.; Dichtel, W. R. *ACS Cent. Sci.* **2016**, *2*, 667-673.
122. Horike, S.; Umeyama, D.; Kitagawa, S. *Acc. Chem. Res.* **2013**, *46*, 2376-2384.

123. Meng, X.; Wang, H.; Song, S.; Zhang, H. *Chem. Soc. Rev.* **2017**, *46*, 464-480.
124. Chandra, S.; Kundu, T.; Kandambeth, S.; BabaRao, R.; Marathe, Y.; Kunjir, S. M.; Banerjee, R. *J. Am. Chem. Soc.* **2014**, *136*, 6570-6573.
125. Xu, H.; Tao, S.; Jiang, D. *Nat. Mater.* **2016**, *15*, 722.
126. Chandra, S.; Kundu, T.; Dey, K.; Addicoat, M.; Heine, T.; Banerjee, R. *Chem. Mater.* **2016**, *28*, 1489-1494.
127. Shinde, D. B.; Aiyappa, H. B.; Bhadra, M.; Biswal, B. P.; Wadge, P.; Kandambeth, S.; Garai, B.; Kundu, T.; Kurungot, S.; Banerjee, R. *J. Mater. Chem. A* **2016**, *4*, 2682-2690.
128. Peng, Y.; Xu, G.; Hu, Z.; Cheng, Y.; Chi, C.; Yuan, D.; Cheng, H.; Zhao, D. *ACS Appl. Mater. Interfaces* **2016**, *8*, 18505-18512.
129. Bisbey, R. P.; DeBlase, C. R.; Smith, B. J.; Dichtel, W. R. *J. Am. Chem. Soc.* **2016**, *138*, 11433-11436.
130. Karak, S.; Kandambeth, S.; Biswal, B. P.; Sasmal, H. S.; Kumar, S.; Pachfule, P.; Banerjee, R. *J. Am. Chem. Soc.* **2017**, *139*, 1856-1862.
131. Smith, B. J.; Parent, L. R.; Overholts, A. C.; Beaucage, P. A.; Bisbey, R. P.; Chavez, A. D.; Hwang, N.; Park, C.; Evans, A. M.; Gianneschi, N. C.; Dichtel, W. R. *ACS Cent. Sci.* **2017**, *3*, 58-65.

CHAPTER 2
AN AZINE-LINKED HEXAPHENYLBENZENE BASED COVALENT ORGANIC
FRAMEWORK

Authors: Sampath B. Alahakoon,[†] Christina M. Thompson,[†] Amy X. Nguyen, Gino Occhialini,
Gregory T. McCandless and Ronald A. Smaldone

Department of Chemistry and Biochemistry, BSB13

The University of Texas at Dallas

800 West Campbell Road

Richardson, Texas 75080-3021

[†] These authors contributed equally.

Alahakoon, S. B.; Thompson, C. M.; Nguyen, A. X.; Occhialini, G.; McCandless, G. T.; Smaldone, R. A. An Azine-Linked Hexaphenylbenzene Based Covalent Organic Framework. *Chem. Commun.* **2016**, 52, 2843-2845. Adapted with permission of The Royal Society of Chemistry.

2.1 Abstract

In this communication, we report an azine linked covalent organic framework based on a six-fold symmetric hexaphenylbenzene (HEX) monomer functionalized with aldehyde groups. HEX-COF 1 has an average pore size of 1 nm, a surface area in excess of 1200 m²/g and shows excellent sorption capability for carbon dioxide (20 wt%) and methane (2.3 wt%) at 273 K and 1 atm.

2.2 Introduction

Covalent organic frameworks¹⁻⁴ (COFs) are a class of porous polymers whose structures are formed under dynamic control in either two or three dimensions. The structure and properties of two-dimensional COFs in particular are controlled by the dynamic interplay between noncovalent aromatic interactions (i.e., π -stacking) and covalent bond formation under thermodynamic control. COFs have become a rapidly growing part of micro and mesoporous materials discovery for gas storage,^{1,5-10} catalysis,¹¹⁻¹⁴ and especially as components for electronic and conductive materials^{2,15-22} The wide range of these potential applications is made possible by the modular design of COFs, enabling one to not only predict with high certainty, but also to tune, the pore size, shape, and symmetry of the resulting 2D COF sheets through careful design of the starting materials. Two and three fold symmetric monomers are commonly used to form materials with lattices that fit into hexagonal space groups. Porous polymers containing HEX units have been previously reported by our group^{23,24} and others.²⁵⁻²⁹ Recently, the first COFs containing six-fold symmetric HEX-based components were reported resulting in materials with triangular shaped micropores and electrically conductive properties.¹⁷

HEX-based COFs with this type of structure are interesting due to their high π -density and extremely small pore size. To date, much of the gas storage behavior (specifically CO₂ and CH₄) for HEX-based COFs has yet to be reported. To accomplish this we have synthesized an aldehyde functionalized HEX monomer (Figure 2.1a-b) with six-fold symmetry. Polymerization with a two-fold symmetric co-monomer, such as hydrazine, will result in a COF containing triangular pores. Since azine linkages^{6,30-33} are among the smallest linkers available for COF synthesis, these pores should be approximately 1 nm, making them interesting for a variety of sorption applications including gas separation *via* sieving.

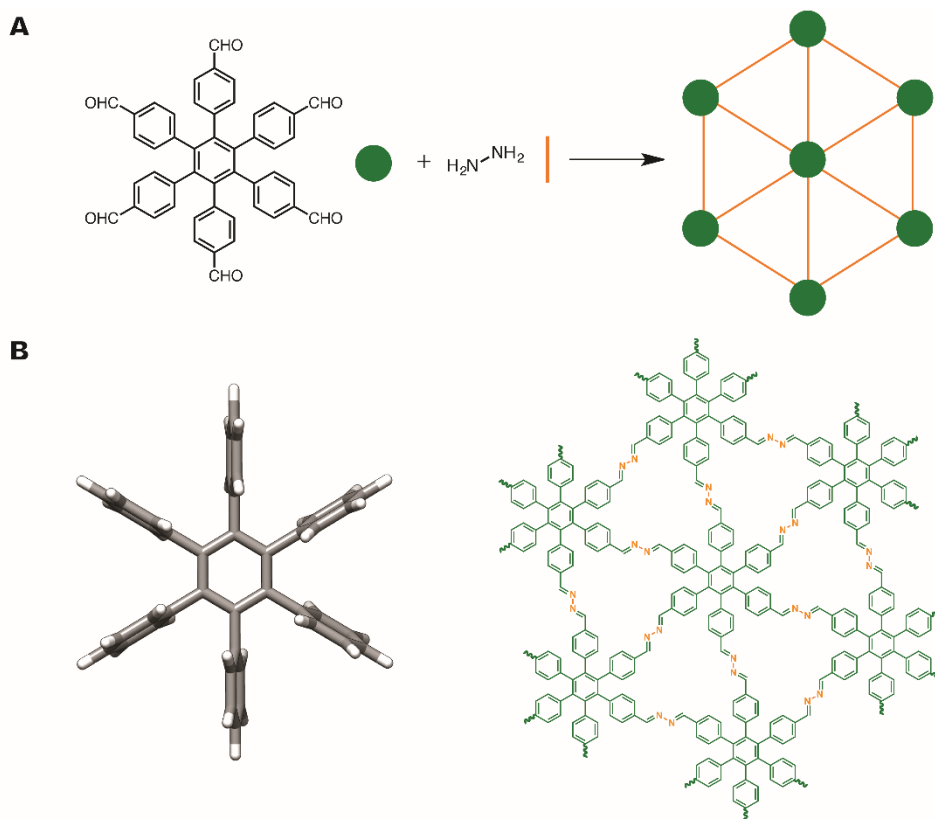


Figure 2.1. (A) Synthesis of a COF using a six fold symmetric HEX monomer containing aldehyde groups and hydrazine. (B) HEX-based monomers are non-planar as a result of the steric hindrance between the phenyl rings. Resultant COFs have topologically planar 2D structures despite the lack of planarity in the monomers.

2.3 Experimental

2.3.1 Materials and methods

All reagents were purchased from commercial suppliers (Sigma-Aldrich and Fisher Scientific) and used as received. Compounds up to **1**³⁴⁻³⁶ (Figure 2.2) were synthesized as previously reported. FT-IR spectra were taken on a Nicolet 360 FT-IR spectrophotometer with a SmartOrbit diamond attenuated total reflectance (ATR) cell. The thermogravimetric analyses were performed using a TA Instruments SDT Q600 Analyzer under nitrogen atmosphere with a heating rate of 10 °C min⁻¹ from 30–1000 °C. Low-pressure gas adsorption experiments (up to 760 torr) were carried out on a Micromeritics ASAP 2020 surface area analyzer. Ultrahigh-purity-grade N₂, H₂, CO₂ and CH₄ gases (obtained from Airgas Corporation) were used in all adsorption measurements. N₂ (77 K) and H₂ (77 K) isotherms were measured using a liquid nitrogen bath. CO₂ and CH₄ isotherms were measured using either a water ice bath (273 K) or in room temperature water bath (298 K) whose temperature was measured prior to use for accuracy. The pore volume of each material was estimated from the Dubinin-Raduskevich (DR) model with the assumption that the adsorbate is in the liquid state and that the adsorption involves a pore-filling process. Pore size distributions were determined using a non-local density functional theory (NLDFT) carbon slit-pore model in the Micromeritics Software Package. Enthalpy of adsorption values were calculated using Van't Hoff plots from CO₂ and CH₄ isotherms at 273 and 298 K. Powder X-ray diffraction of HEX-COF 1 was carried out on a Bruker D8 Advance diffractometer with a sealed tube radiation source (Cu K α , $\lambda = 1.54184 \text{ \AA}$), a low background sample holder, and Lynxeye XE detector. Raw diffraction data was processed using the MDI Jade software package (K α background correction and peak smoothing using the Savitzky-Golay

method). MALDI-ToF measurements were carried out on a Shimadzu Biotech Axima Confidence instrument. All spectra were obtained using tetracyanoquinodimethane (TCNQ) as a matrix. The general procedure for sample preparation was as follows: To a mortar was added TCNQ (10 mg) and the compound of interest (1 mg). This mixture was ground together to form a uniform solid. An aliquot (1 mg) of this solid was then transferred to a separate vial and chloroform (1 mL) was added. The resulting suspension was then spotted onto the MALDI plate and analyzed. ^1H and ^{13}C NMR spectra were carried out on a Bruker 400 or 500 MHz Advance Spectrometer. Microwave reactions were carried out in a CEM Discover reactor. Elemental analyses were performed by Micro-Analysis, Inc. 2038 Telegraph Rd, Wilmington, Delaware 19808.

2.3.2 Monomer and COF synthesis

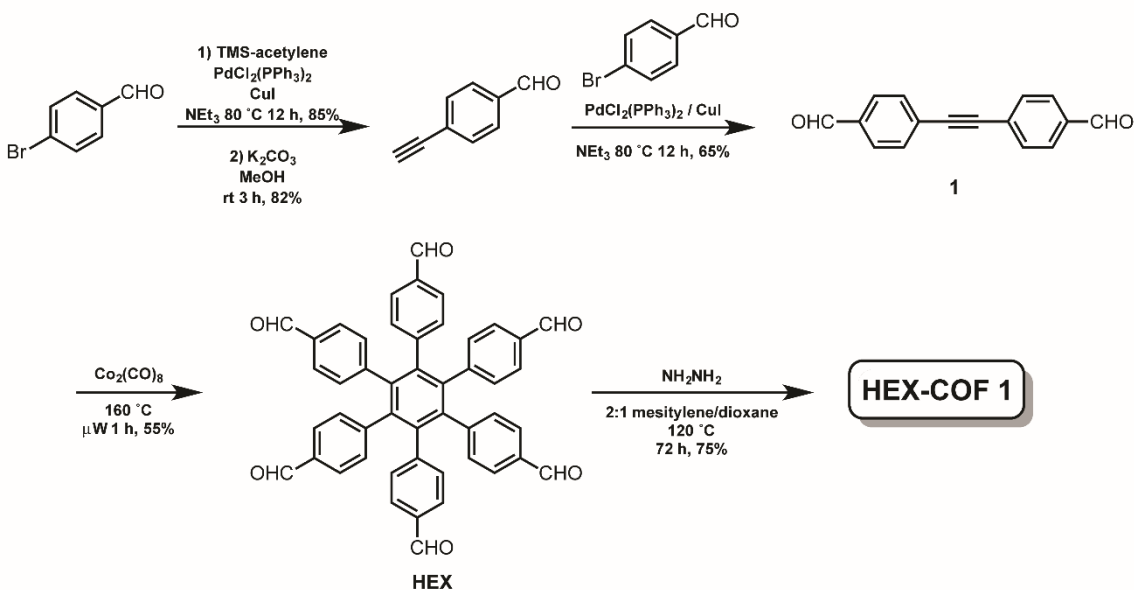


Figure 2.2. Synthesis of HEX and HEX-COF 1

To a microwave tube containing **1** (0.500 g, 2.13 mmol) in dioxane (2 mL) was purged with nitrogen for 15 min before $\text{Co}_2(\text{CO})_8$ (36.5 mg, 0.107 mmol) was added. The reaction was heated at 160 °C at 300 W for 1 h in the microwave reactor. After that time hexane was added in to the tube and the resultant brown precipitate was collected by filtration and washed with hexane until the filtrate was colorless. The collected solid was dissolved in CH_2Cl_2 and filtered through a silica gel plug. Finally, the resultant solution was evaporated to dryness to obtain a brown solid (0.275 g, 55% yield). ^1H NMR (400 MHz, DMSO, δ): 7.20 (d, $J = 8$ Hz, 12H, Ar), 7.46 (d, $J = 8$ Hz, 12H, Ar), 9.73 (s, 6H, ArCHO) (Figure 2.3). ^{13}C NMR (400 MHz, DMSO, δ): 128.63, 132.04, 134.31, 139.63, 145.46, 193.15 (Figure 2.4). MALDI-ToF-MS (m/z) Calculated for $[\text{C}_{48}\text{H}_{30}\text{O}_6]^+$: 702.2. Found: 702.0

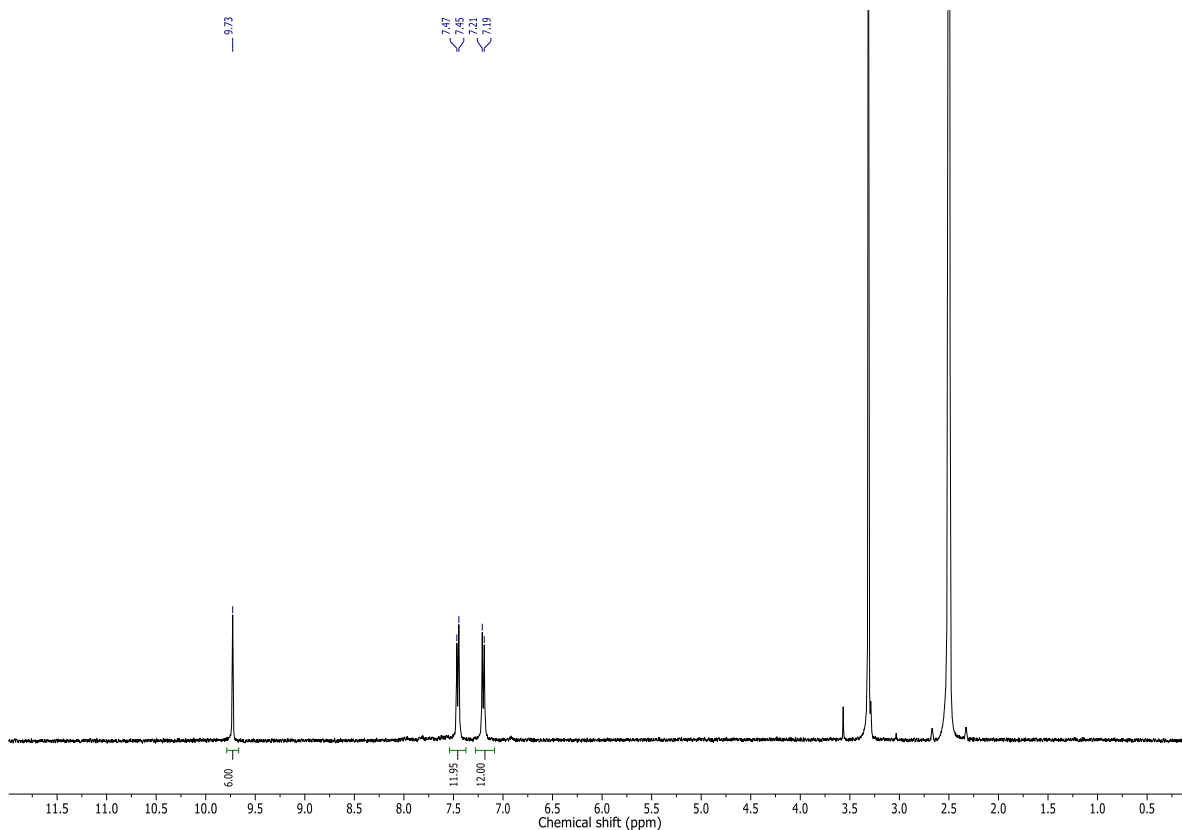


Figure 2.3. ^1H NMR (400 MHz) of HEX in DMSO- d_6

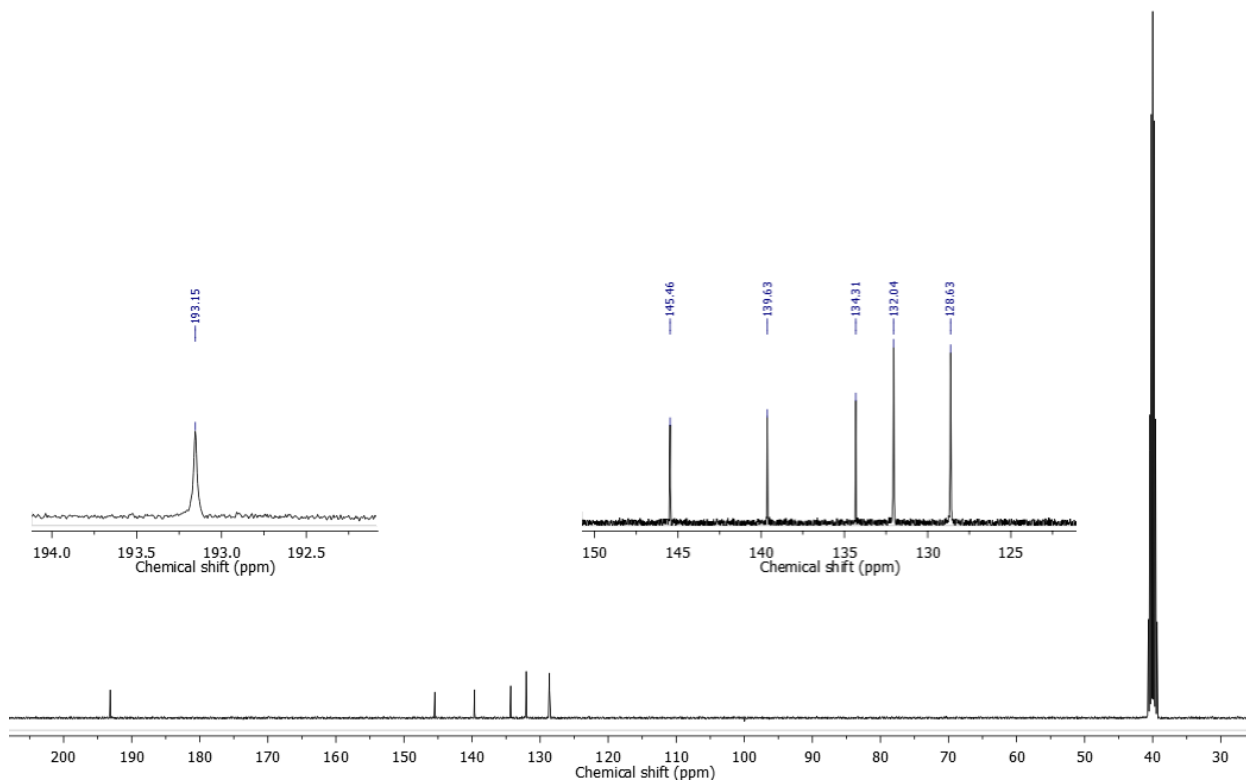


Figure 2.4. ^{13}C NMR (400 MHz) of HEX in DMSO-d_6

HEX-COF 1: A 4 mL ampoule was charged with **HEX** (25.0 mg, 0.0356 mmol), N_2H_4 (3.34 μL , 0.1067 mmol), mesitylene (0.67 mL) and dioxane (0.33 mL). The mixture was sonicated for 10 min and 6M AcOH (0.1 mL) was added. The ampoule was sealed under vacuum after freezing the contents in it with liquid nitrogen. Once it reached RT the ampoule was heated at 120 $^\circ\text{C}$ for 3 d. After that time the mixture was cooled to RT, the obtained light yellow precipitate was soaked in tetrahydrofuran for 2 h and then washed with tetrahydrofuran (20 ml x 3). The remaining yellow solid was dried under vacuum to afford 18.4 mg (75% yield) of HEX-COF 1. Elemental analysis (%) Calcd: C, 83.46; H, 4.38; N, 12.17; Found: C, 75.96; H, 4.35; N,

8.40. The elemental analyses are often reported to be different from the expected values as a result of incomplete combustion, as has also been found in other reports of carbon-rich porous materials^{32,37,38} including our previous work.^{23,24}

2.4 Results and discussion

2.4.1 Characterization of HEX-COF 1

FT-IR spectra (Figure 2.5-2.6) showed the conversion of aldehyde peaks from HEX into azines as demonstrated in previous work.³¹

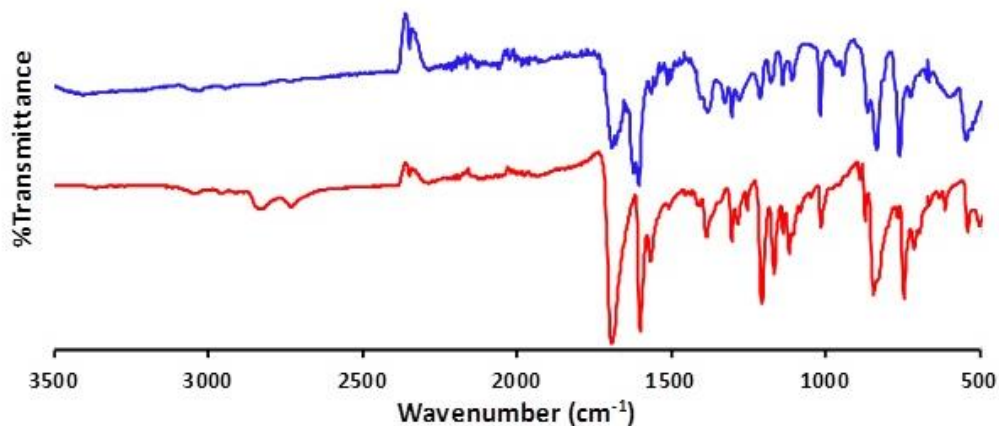


Figure 2.5. FT-IR spectra of HEX-COF 1 (Blue) and HEX (Red)

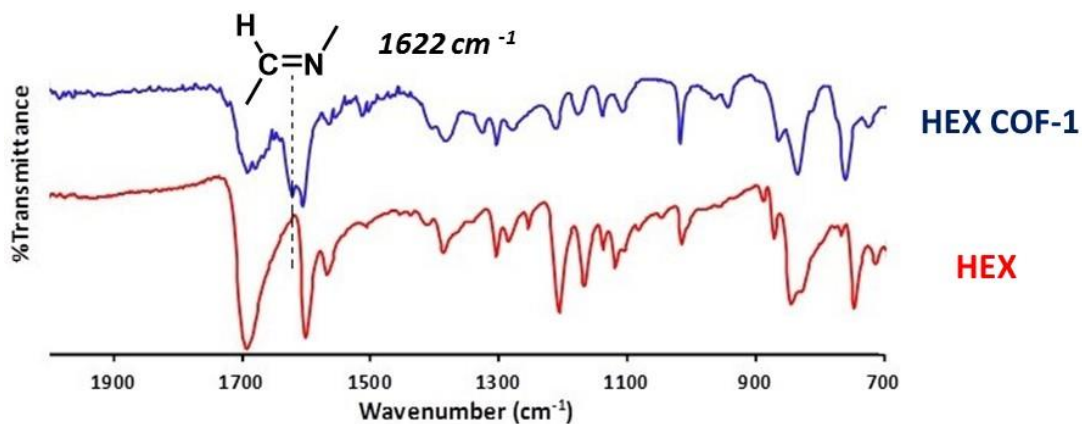


Figure 2.6. Zoomed in image of FT-IR spectra of HEX-COF 1 (Blue) and HEX (Red).

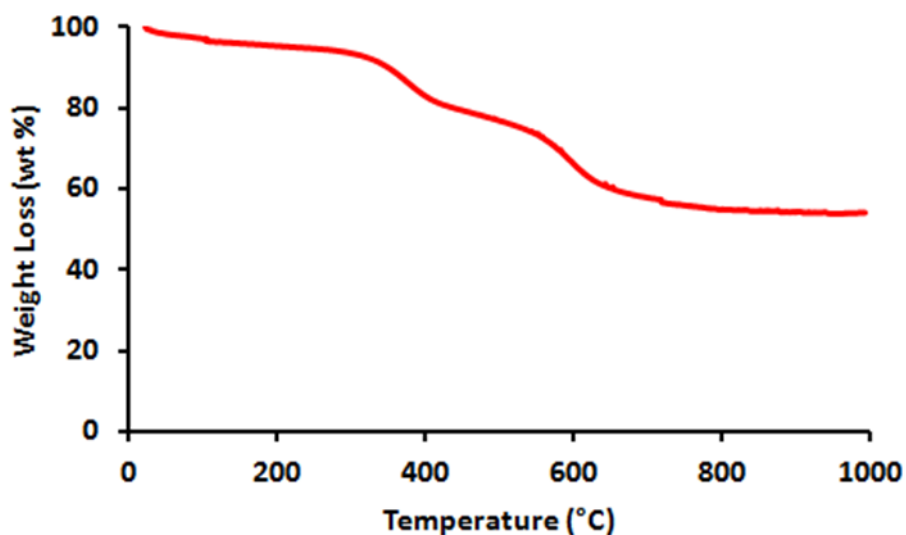


Figure 2.7. TGA of HEX-COF 1 under a nitrogen atmosphere.

2.4.2 Surface area analysis

The surface area and pore size distributions were analysed by nitrogen adsorption measurements at 77 K (Figure 2.8). Using the Brunauer-Emmett-Teller (BET) model the surface area was calculated to be 1214 m²/g. The pore size distribution (Figure 2.8b) was determined using a non-local density functional theory carbon slit pore model showing that the major population of NLDFT pore width resides at ~11 Å.

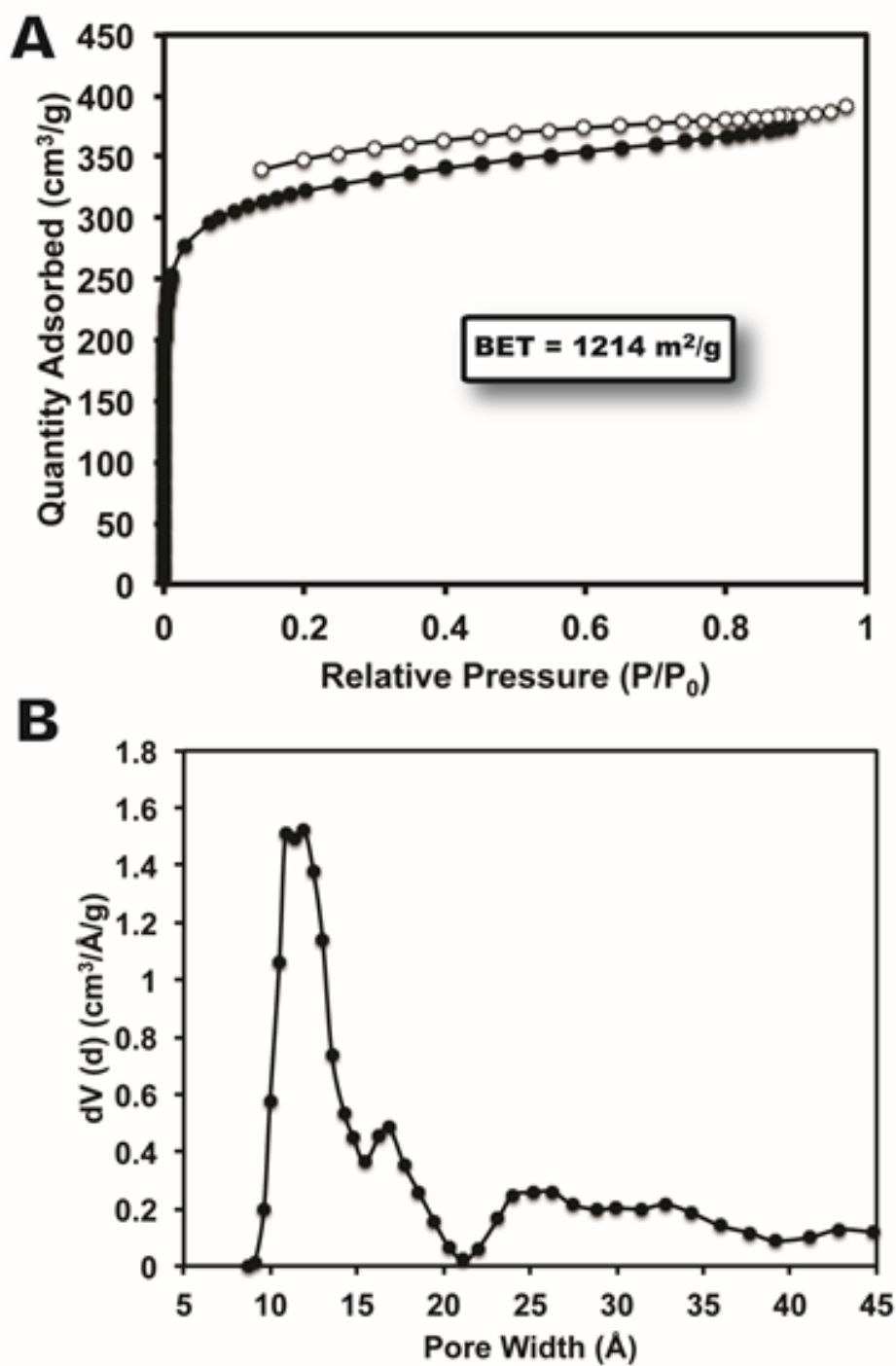


Figure 2.8. (A) N₂ isotherm at 77 K. The BET surface area of HEX-COF 1 was measured to be 1214 m²/g. (B) NLDFT pore size distribution obtained from the N₂ isotherm.

2.4.3 Powder X-ray diffraction and modeling studies

The narrow pore size distribution and high surface area indicate that this is an ordered material. However, powder X-ray diffraction (PXRD) measurements of HEX-COF 1 have low peak intensity ($\sim 10^2$ counts) regardless of the solvent conditions or reaction time used (Figure 2.9a). The poor long-range order may be related to the inherent propeller shape of the HEX monomer. It was recently shown that increasing van der Waals interactions between 2D COF sheets drastically impacts their rate of formation and resulting stability.³⁹ The canonical “face to face” π -stacking found in most COF monomers is lacking in our system, which must instead rely on edge-to-edge interactions for interlayer adhesion.

Weak, or improperly aligned interlayer interactions could result in poor adhesion and reduced long-range crystallinity – something that has also been observed with other COFs that utilize aromatic systems that have non-planar structures.^{11,12} Molecular modeling studies were carried out in Accelrys Materials Studio 7.0. HEX-COF 1 was modeled in the *P6/m* space group and minimized using the universal force field (UFF) in the Forcite module. PXRD patterns were simulated from the model using the Reflex module. PXRD patterns generated from a molecular model of HEX-COF 1 (Figure 2.9a,c) give unit cell parameters of 17.8 Å x 17.8 Å x 5.5 Å. Given the low intensity of the peaks, additional Pawley refinement of the raw data was not possible. The model in Figure 2.9b-c depicts a perfectly eclipsed structure while the real structure is likely slightly offset, these small differences cannot be resolved by PXRD measurements. The modelled pore diameter is in good agreement with the data in Figure 2.8b.

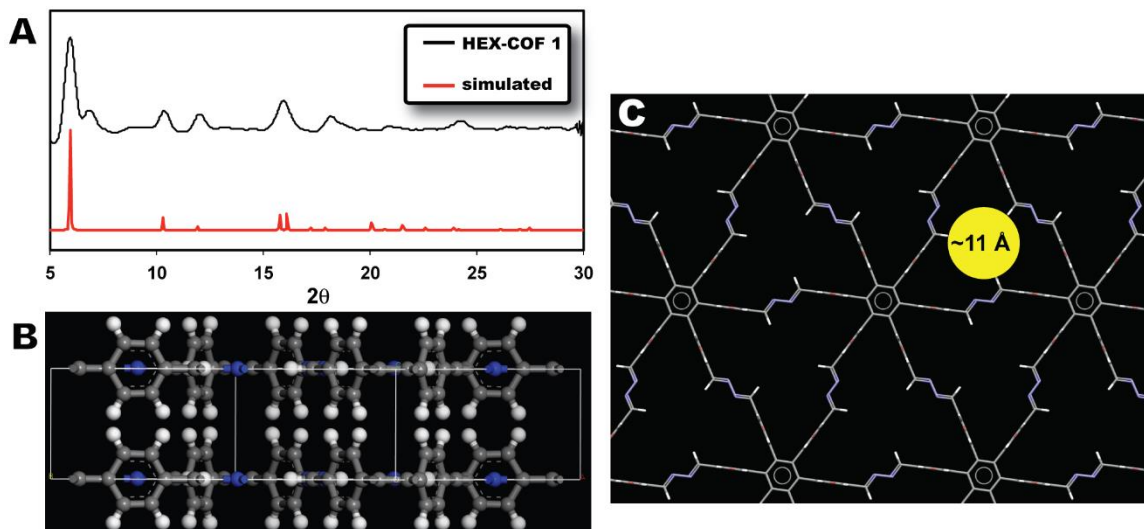


Figure 2.9. (A) The powder X-ray diffraction pattern of HEX-COF 1 (black line) and the simulated diffraction pattern from the model (red line). (B) A view of the interlayer spacing of the model showing the lack of face-to-face π stacking interactions. (C) Molecular model of HEX-COF 1 showing the pores measuring 11 Å in diameter.

2.4.4 Carbon dioxide and methane sorption properties of HEX-COF 1

CO₂ and CH₄ adsorption properties with HEX-COF 1 were also evaluated. CO₂ adsorption studies were performed at both 273 and 298 K (Figure 2.10a) up to 1 atm. These measurements indicate a strong affinity between the HEX-COF 1 and CO₂ gas molecules with nearly 20 wt% adsorbed at 273 K and an enthalpy of adsorption that is 42 kJ/mol (Figure 2.10c). This is an excellent value that ranks among the highest observed in COF-based materials.^{6-8,40,41} In addition to the polar azine functional groups, which no doubt contribute to the strong adsorption, the small pore sizes (~11 Å in diameter) within HEX-based materials could also be a factor. CH₄ adsorption measurements (Figure 2.10b) were also carried out showing that HEX-COF 1 can

store up to 2.3 wt% of CH₄ at 273 K with maximum enthalpies of adsorption around 27 kJ/mol (Figure 2.10c, red line).

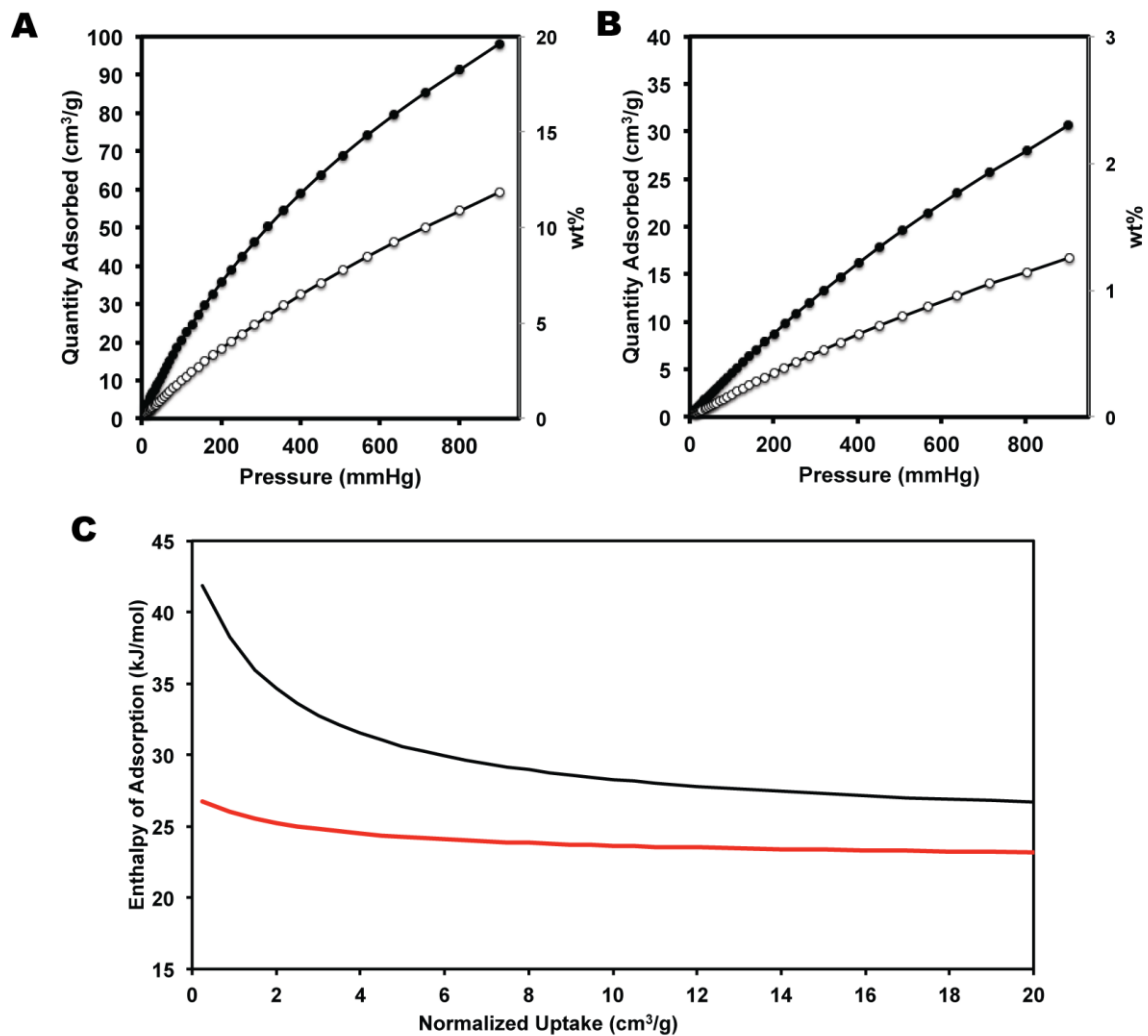


Figure 2.10. (A) CO₂ isotherms at 273 K (filled circles) and 298 K (open circles). (B) CH₄ isotherms at 273 K (filled circles) and 298 K (open circles). (c) Enthalpy of adsorption measurements for CO₂ (black line) and CH₄ (red line)

2.5 Conclusion

In conclusion, we have synthesized a novel azine linked COF based on a six-fold symmetrical aldehyde functionalized hexaphenylbenzene monomer. Interestingly, these COFs display the adsorptions properties of an ordered microporous material with a type I isotherm and a narrow pore size distribution, but with a relatively weak PXRD pattern indicating a low level of long range order, likely owing to the poor interlayer interactions between the propeller-shaped HEX units. Despite the low level of long-range order, HEX-COF 1 exhibits outstanding surface area, CO₂ and CH₄ adsorption capability. We believe the unique triangular shape and very small pore sizes accessible through HEX-based monomers make them an interesting family of COFs to study for insight on how to design new materials for gas storage and sieving. Designing HEX systems with improved interlayer stacking will further improve our understanding of the structure and design rules required to reliably stitch together complex monomers into ordered COFs with designed properties.

2.6 Acknowledgements

This research was carried out with support from The University of Texas, Dallas, and the American Chemical Society Petroleum Research Fund (52906-DNI10). We would like to acknowledge Sahila Peranathan, Wijayantha Perera and Chamaal Karunaweera for assistance with thermal and spectral analysis.

2.7 References

1. Cote, A. P.; Benin, A. I.; Ockwig, N. W.; O'Keeffe, M.; Matzger, A. J.; Yaghi, O. M. *Science* **2005**, *310*, 1166.
2. Colson, J. W.; Dichtel, W. R. *Nat. Chem.* **2013**, *5*, 453.
3. Waller, P. J.; Gandara, F.; Yaghi, O. M. *Acc. Chem. Res.* **2015**, *48*, 3053-3063.
4. El-Kaderi, H.; Hunt, J. R.; Mendoza-Cortes, J. L.; Cote, A. P.; Taylor, R. E.; O'Keeffe, M.; Yaghi, O. M. *Science* **2007**, *316*, 268.
5. Ganz, E.; Dornfeld, M. *J. Phys. Chem. C* **2012**, *116*, 3661-3666.
6. Li, Z.; Feng, X.; Zou, Y.; Zhang, Y.; Xia, H.; Liu, X.; Mu, Y. *Chem. Commun.* **2014**, *50*, 13825-13828.
7. Li, Z.; Zhi, Y.; Feng, X.; Ding, X.; Zou, Y.; Liu, X.; Mu, Y. *Chem. Eur. J.* **2015**, *21*, 12079-12084.
8. Rabbani, M. G.; Sekizkardes, A. K.; Kahveci, Z.; Reich, T. E.; Ding, R.; El-Kaderi, H. M. *Chem. Eur. J.* **2013**, *19*, 3324-3328.
9. Baldwin, L. A.; Crowe, J. W.; Shannon, M. D.; Jaroniec, C. P.; McGrier, P. L. *Chem. Mater.* **2015**, *27*, 6169-6172.
10. Xiang, Z.; Cao, D.; Lan, J.; Wang, W.; Broom, D. P. *Energy Environ. Sci.* **2010**, *3*, 1469-1487.
11. Stegbauer, L.; Schwinghammer, K.; Lotsch, B. V. *Chem. Sci.* **2014**, *5*, 2789-2793.
12. Lin, S.; Diercks, C. S.; Zhang, Y.; Kornienko, N.; Nichols, E. M.; Zhao, Y.; Paris, A. R.; Kim, D.; Yang, P.; Yaghi, O. M.; Chang, C. J. *Science* **2015**, *349*, 1208.
13. Xu, H.; Gao, J.; Jiang, D. *Nat. Chem.* **2015**, *7*, 905-912.
14. Pachfule, P.; Kandambeth, S.; Diaz Diaz, D.; Banerjee, R. *Chem. Commun.* **2014**, *50*, 3169-3172.
15. Dogru, M.; Bein, T. *Chem. Commun.* **2014**, *50*, 5531-5546.
16. Liu, X.; Guan, C.; Wang, D.; Wan, L. *Adv. Mater.* **2014**, *26*, 6912-6920.
17. Dalapati, S.; Addicoat, M.; Jin, S.; Sakurai, T.; Gao, J.; Xu, H.; Irle, S.; Seki, S.; Jiang, D. *Nat. Commun.* **2015**, *6*, 7786.
18. DeBlase, C. R.; Silberstein, K. E.; Truong, T.; Abruna, H. D.; Dichtel, W. R. *J. Am. Chem. Soc.* **2013**, *135*, 16821-16824.

19. DeBlase, C. R.; Hernandez-Burgos, K.; Silberstein, K. E.; Rodriguez-Calero, G. G.; Bisbey, R. P.; Abruna, H. D.; Dichtel, W. R. *ACS Nano* **2015**, *9*, 3178-3183.
20. Duhovic, S.; Dinca, M. *Chem. Mater.* **2015**, *27*, 5487-5490.
21. Zha, Z.; Xu, L.; Wang, Z.; Li, X.; Pan, Q.; Hu, P.; Lei, S. *ACS Appl. Mater. Interfaces* **2015**, *7*, 17837-17843.
22. Du, Y.; Yang, H.; Whiteley, J. M.; Wan, S.; Jin, Y.; Lee, S.; Zhang, W. *Angew. Chem. Int. Ed.* **2016**, *55*, 1737-1741.
23. Thompson, C. M.; McCandless, G. T.; Wijenayake, S. N.; Alfarawati, O.; Jahangiri, M.; Kokash, A.; Tran, Z.; Smaldone, R. A. *Macromolecules* **2014**, *47*, 8645-8652.
24. Thompson, C. M.; Li, F.; Smaldone, R. A. *Chem. Commun.* **2014**, *50*, 6171-6173.
25. Chen, Q.; Luo, M.; Wang, T.; Wang, J.; Zhou, D.; Han, Y.; Zhang, C.; Yan, C.; Han, B. *Macromolecules* **2011**, *44*, 5573-5577.
26. Zhang, C.; Peng, L.; Li, B.; Liu, Y.; Zhu, P.; Wang, Z.; Zhan, D.; Tan, B.; Yang, X.; Xu, H. *Polym. Chem.* **2013**, *4*, 3663-3666.
27. Short, R.; Carta, M.; Bezzu, C. G.; Fritsch, D.; Kariuki, B. M.; McKeown, N. B. *Chem. Commun.* **2011**, *47*, 6822-6824.
28. Carta, M.; Bernardo, P.; Clarizia, G.; Jansen, J. C.; McKeown, N. B. *Macromolecules* **2014**, *47*, 8320-8327.
29. Nguyen, P. T. K.; Nguyen, H. T. D.; Pham, H. Q.; Kim, J.; Cordova, K. E.; Furukawa, H. *Inorg. Chem.* **2015**, *54*, 10065-10072.
30. Stegbauer, L.; Hahn, M. W.; Jentys, A.; Savasci, G.; Ochsenfeld, C.; Lercher, J. A.; Lotsch, B. V. *Chem. Mater.* **2015**, *27*, 7874-7881.
31. Dalapati, S.; Jin, S.; Gao, J.; Xu, Y.; Nagai, A.; Jiang, D. *J. Am. Chem. Soc.* **2013**, *135*, 17310-17313.
32. Zhu, Y.; Wan, S.; Jin, Y.; Zhang, W. *J. Am. Chem. Soc.* **2015**, *137*, 13772-13775.
33. Yue, J.; Liu, X.; Sun, B.; Wang, D. *Chem. Commun.* **2015**, *51*, 14318-14321.
34. Gulia, N.; Pigulski, B.; Szafert, S. *Organometallics* **2015**, *34*, 673-682.
35. de Miguel, G.; Wielopolski, M.; Schuster, D. I.; Fazio, M. A.; Lee, O. P.; Haley, C. K.; Ortiz, A. L.; Echegoyen, L.; Clark, T.; Guldi, D. M. *J. Am. Chem. Soc.* **2011**, *133*, 13036-13054.
36. Borozdina, Y. B.; Mostovich, E.; Enkelmann, V.; Wolf, B.; Cong, P. T.; Tutsch, U.; Lang, M.; Baumgarten, M. *J. Mater. Chem. C* **2014**, *2*, 6618-6629.

37. Lu, W.; Yuan, D.; Zhao, D.; Schilling, C. I.; Plietzsch, O.; Muller, T.; Brase, S.; Guenther, J.; Blumel, J.; Krishna, R.; Li, Z.; Zhou, H. *Chem. Mater.* **2010**, *22*, 5964-5972.
38. Jiang, J.; Su, F.; Trewin, A.; Wood, C.; Campbell, N.; Niu, H.; Dickinson, C.; Ganin, A.; Rosseinsky, M.; Khimyak, Y.; Cooper, A. *Angew. Chem. Int. Ed.* **2007**, *46*, 8574-8578.
39. Smith, B. J.; Dichtel, W. R. *J. Am. Chem. Soc.* **2014**, *136*, 8783-8789.
40. Kahveci, Z.; Islamoglu, T.; Shar, G. A.; Ding, R.; El-Kaderi, H. *CrystEngComm* **2013**, *15*, 1524-1527.
41. Huang, N.; Zhai, L.; Coupry, D. E.; Addicoat, M. A.; Okushita, K.; Nishimura, K.; Heine, T.; Jiang, D. *Nat. Commun.* **2016**, *7*, 12325.

CHAPTER 3
ENHANCED STRUCTURAL ORGANIZATION IN COVALENT ORGANIC
FRAMEWORKS THROUGH FLUORINATION

Authors: Sampath B. Alahakoon, Gregory T. McCandless, Arosha A.K. Karunathilake,
Christina M. Thompson and Ronald A. Smaldone

Department of Chemistry and Biochemistry, BSB13

The University of Texas at Dallas

800 West Campbell Road

Richardson, Texas 75080-3021

Alahakoon, S. B.; McCandless, G. T.; Karunathilake, A. A. K.; Thompson, C. M.; Smaldone, R. A. Enhanced Structural Organization in Covalent Organic Frameworks Through Fluorination. *Chem. Eur. J.* **2017**, *23*, 4255-4259. Copyright (2017) Wiley-VCH Verlag GmbH & Co. KGaA, Weinheim.

3.1 Abstract

Herein we report a structure-function study of imine COFs comparing a series of novel fluorine containing monomers to their non-fluorinated analogue. We found that the fluorine containing monomers produced 2D-COFs with not only greatly improved surface areas (over 2000 m²/g compared to 760 m²/g for the non-fluorinated analogue), but also with improved crystallinity and larger, better defined pore diameters. We then studied the formation of these COFs under varying reaction times and temperatures to obtain a greater insight into their mechanism of formation.

3.2 Introduction

Covalent organic frameworks (COFs)¹⁻⁴ are a class of crystalline porous polymers synthesized utilizing dynamic covalent bonds⁵ such as boronate esters,^{1,2} imines,^{6,7} hydrazones,^{3,8} triazines,⁹ and azines.¹⁰⁻¹⁴ These materials have attracted remarkable attention due to their well-defined structures, high porosity, and potential applications in gas storage,^{1,15,16} catalysis,^{8,17-19} and as materials for electrical energy storage.^{7,20-25} In 2D-COFs, the structure and properties are dictated by both covalent bond formation under thermodynamic control, and by non-covalent interactions between aromatic rings that enables the formation of periodically aligned molecular columns.¹⁴ There have been a number of excellent studies²⁶⁻²⁹ that attribute the efficiency of non-covalent packing in COF formation to forces as wide ranging as monomer planarity,¹³ and molecular recognition through templated docking.^{20,30,31} Given that each of these hypotheses have proven to be successful in making specific types of COFs, it is clear that more studies into the role of non-covalent packing are imperative for the development of general design rules.

The purpose of the work reported here is to further elucidate the importance of aromatic interactions between individual sheets during COF formation. Interactions between aromatic rings are controlled by a variety of factors including substituent effects that change the electron density or polarization of the π -cloud. Many explanations have been posited to explain the nature of aromatic stacking interactions,^{32,33} but empirically, electron deficient rings are known to preferentially adopt face-to-face arrangements. Since this co-facial orientation is representative of the structure of most 2D-COFs, we hypothesized that we could bias toward the formation of stacked COF sheets by incorporating electron withdrawing substituents onto the periphery of our COF monomers. We chose to use fluorine substitution for this study as it is not only electron withdrawing, but similar in steric bulk to hydrogen, thereby allowing a closer comparison between fluorinated and non-fluorinated monomers without introducing significant steric effects. We have synthesized two fluorine containing 1,3,5-triphenylbenzene derivatives to take advantage of this co-facial stacking preference, and were gratified to see that the addition a few fluorine atoms results in a drastic change not only in the crystallinity, but also the pore size and surface area of the resulting COFs.

3.3 Experimental

3.3.1 Materials and methods

Reagents were purchased from commercial suppliers (Sigma-Aldrich and Fisher Scientific) and used as received. ATR (attenuated total reflectance) FT-IR spectra were taken on a Cary 600 Series FT-IR spectrophotometer. The thermogravimetric analyses (TGA) were performed using a TA Instruments SDT Q600 Analyzer under nitrogen atmosphere with a heating rate of 10 °C

min⁻¹ from 30–950 °C. Low-pressure gas adsorption experiments (up to 760 torr) were carried out on a Micromeritics ASAP 2020 surface area analyzer. Ultrahigh-purity-grade N₂ gas (obtained from Airgas Corporation) were used in all adsorption measurements. N₂ (77 K) isotherms were measured using a liquid nitrogen bath. The pore volume of each material was estimated from the Dubinin-Raduskevich (DR) model with the assumption that the adsorbate is in the liquid state and that the adsorption involves a pore-filling process. Pore size distributions were determined using a density functional theory (DFT) cylindrical pores in an oxide surface model in the Micromeritics Software Package. Powder X-ray diffraction of all COFs were carried out on a Bruker D8 Advance diffractometer with a sealed tube radiation source (Cu K α , λ = 1.54184 Å), a low background sample holder, and Lynxeye XE detector. Scanning electron microscope (SEM) images were acquired with Zeiss-LEO model 1530 SEM instrument and energy dispersive X-ray spectroscopy (EDX) were acquired on a Zeiss SUPRA40 SEM instrument. The samples were prepared on 15 mm aluminum stubs using double-sided adhesive copper tapes. For EDX samples were imaged at a working distance of 10 mm and a voltage of 15 kV using a secondary electron detector. ¹H, ¹⁹F and ¹³C NMR spectra were carried out on a Bruker 500 MHz Advance Spectrometer. The ¹³C-NMR of TF-1 was carried out at 80 °C. MALDI-TOF measurements were carried out on a Shimadzu Biotech Axima Confidence instrument.

3.3.2 Monomer and COF synthesis

Monomers NF, TF-1, and TF-2 were synthesized through a Suzuki cross-coupling reaction (Scheme 3.1-3.3). All three COFs were prepared solvothermally in glass ampoules by polymerizing monomers NF, TF-1 or TF-2 with hydrazine (Figure 3.1, 3.2 and 3.6). Though

several solvent systems were tested, a mixture of *o*-dichlorobenzene(DCB)/*n*-butanol/6M aqueous acetic acid (1.9/0.1/0.1 by vol.) was found to be optimal.

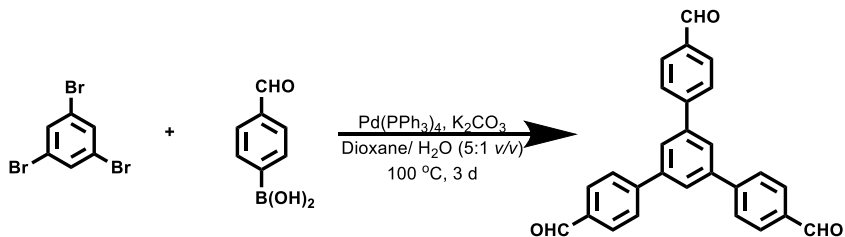


Figure 3.1. Synthesis of 1,3,5-*tris*(4-formylphenyl)benzene (NF)

The compound was synthesized as previously reported in literature.³⁴

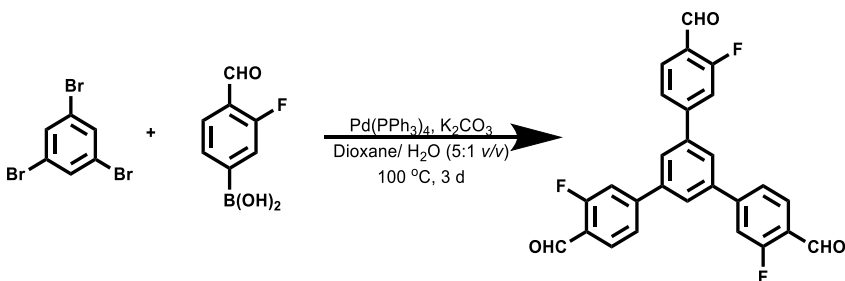


Figure 3.2. Synthesis of 1,3,5-*tris*(3-fluoro-4-formylphenyl)benzene (TF-1)

Dioxane (5 mL) and H₂O (1 mL) were mixed in a sealed tube equipped with a stir bar and then degassed with N₂ for about 15 minutes. Then, tribromobenzene (0.200 g, 0.635 mmol), (3-fluoro-4-formylphenyl) boronic acid (0.640 g, 3.81 mmol), potassium carbonate (0.526 g, 3.81 mmol) and palladium tetrakis(triphenyl phosphine) (0.0367 g, 0.0317 mmol) were added to it. The tube was sealed and then stirred at 100 °C for 72h. After that, the reaction mixture was cooled to rt, and the formed precipitate was washed with plenty of water and ethyl acetate to yield the pure product (0.150 g, 54%). ¹H NMR (500 MHz, DMSO, δ) 10.291 (s, 3H), 8.292 (s, 3H), 8.163 (d, *J* 12.5 Hz, 3H), 8.065 (d, *J* 8 Hz, 3H), 7.974 (t, *J* 7.5, 8 Hz, 3H) (Figure 3.3). ¹⁹F NMR (500 MHz, DMSO, δ): -120.28 (s, 3F) (Figure 3.4). ¹³C NMR (500 MHz, DMSO,

δ):187.61, 164.99, 162.95, 147.73, 139.80, 130.26, 126.94, 124.17, 115.70 (Figure 3.5). MALDI-TOF-MS for $C_{27}H_{15}F_3O_3$ (calculated: 444.10, found: 443.89 ($[M]^+$)).

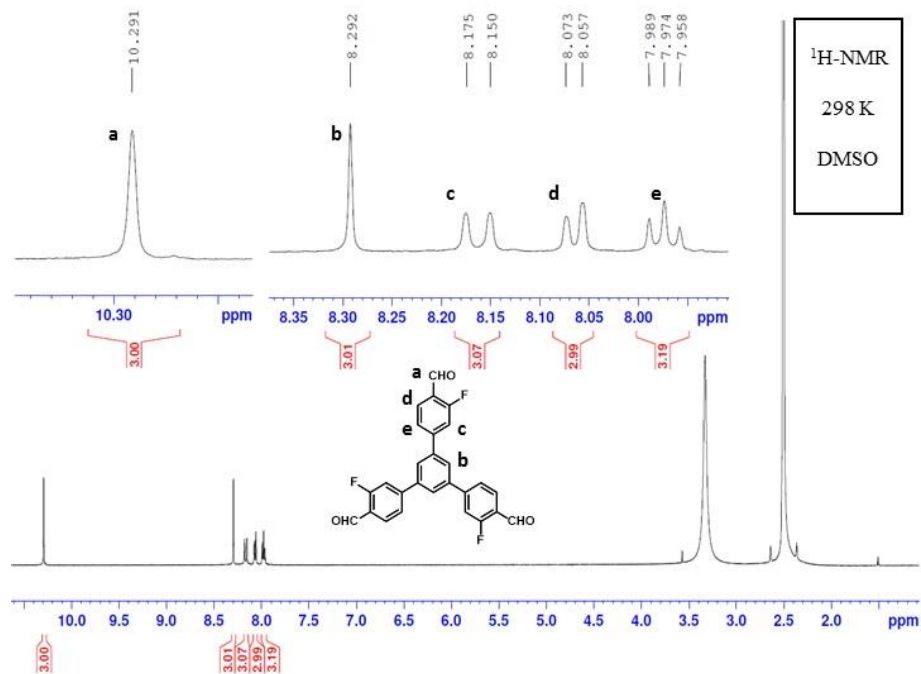


Figure 3.3. ^1H NMR (600 MHz) of 1,3,5-*tris*(3-fluoro-4-formylphenyl)benzene (TF-1) in DMSO-d_6

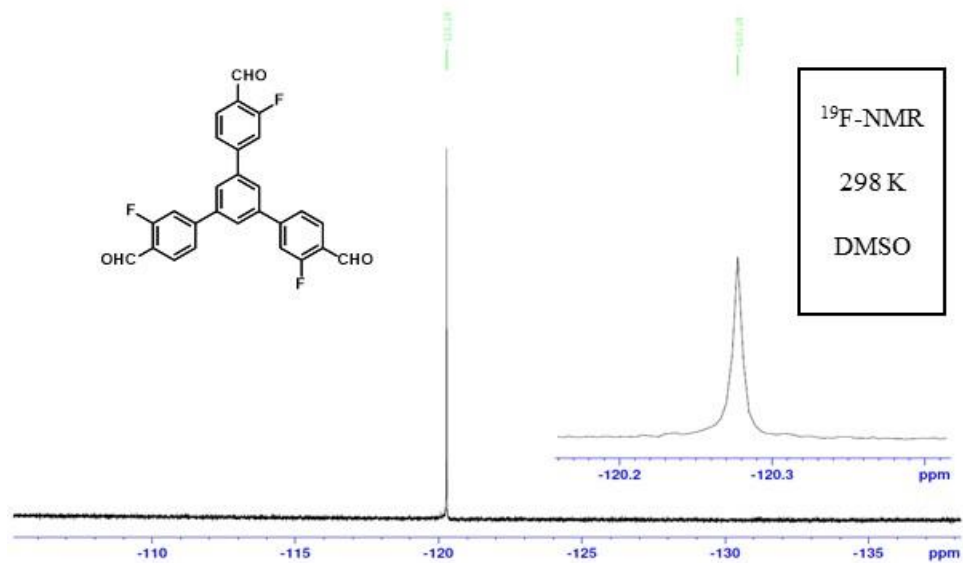


Figure 3.4. ^{19}F NMR (600 MHz) of 1,3,5-*tris*(3-fluoro-4-formylphenyl)benzene (TF-1) in DMSO-d_6

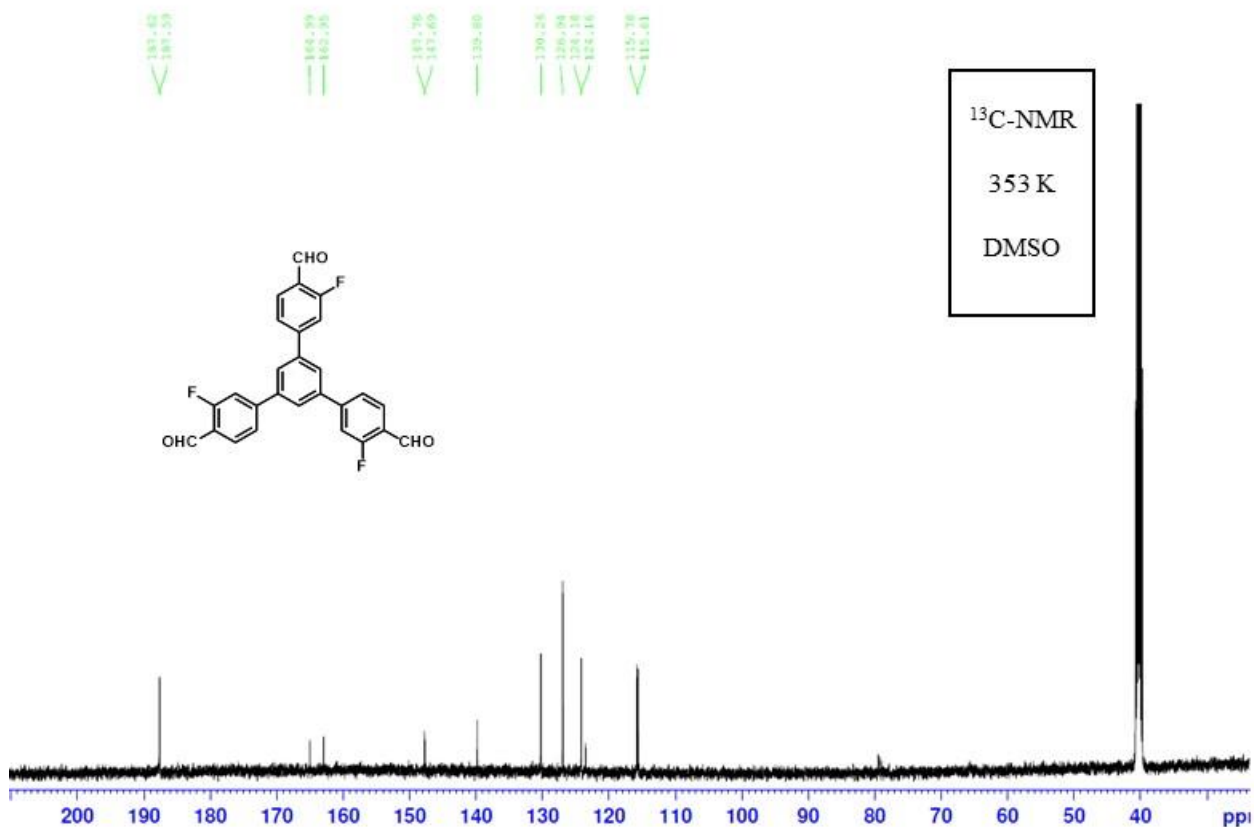


Figure 3.5. ^{13}C NMR (600 MHz) of 1,3,5-*tris*(3-fluoro-4-formylphenyl)benzene (TF-1) in DMSO-d_6

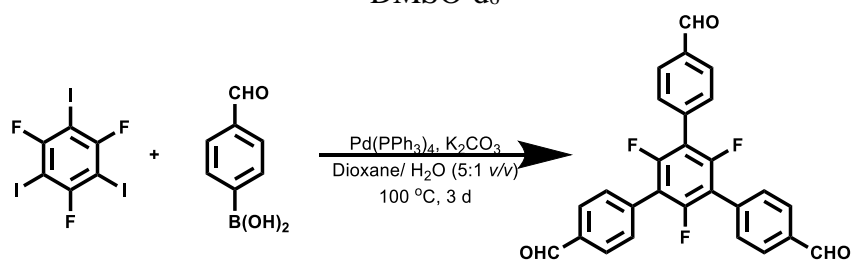


Figure 3.6. Synthesis of 1,3,5-trifluoro-2,4,6-*tris*(4-formylphenyl)benzene (TF-2)

Dioxane (5 mL) and H_2O (1 mL) were mixed in a sealed tube equipped with a stir bar and then degassed with N_2 for about 15 minutes. Then, 1,3,5-trifluoro-2,4,6-triiodobenzene (0.200 g, 0.392 mmol), 4-formylphenylboronic acid (0.354 g, 2.35 mmol), potassium carbonate (0.325 g, 2.35 mmol) and palladium *tetrakis*(triphenyl phosphine) (0.0227 g, 0.0196 mmol) were added to

it. The tube was sealed and then stirred at 100 °C for 72h. After that, the reaction mixture was cooled to r.t., and the formed precipitate was washed with plenty of water and ethyl acetate to yield the pure product (0.090 g, 52%). ^1H NMR (500 MHz, DMSO, δ) 10.089 (s, 3H), 8.072 (d, J 8.5 Hz, 6H), 7.858 (d, J 8 Hz, 6H) (Figure 3.7). ^{19}F NMR (500 MHz, DMSO, δ): -113.87 (s, 3F) (Figure 3.8). ^{13}C NMR (500 MHz, DMSO, δ): 192.82, 136.10, 133.68, 131.20, 129.56, 114.19 (Figure 3.9). MALDI-TOF-MS for $\text{C}_{27}\text{H}_{15}\text{F}_3\text{O}_3$ (calculated: 444.10), found: 444.02 ($[\text{M}]^+$).

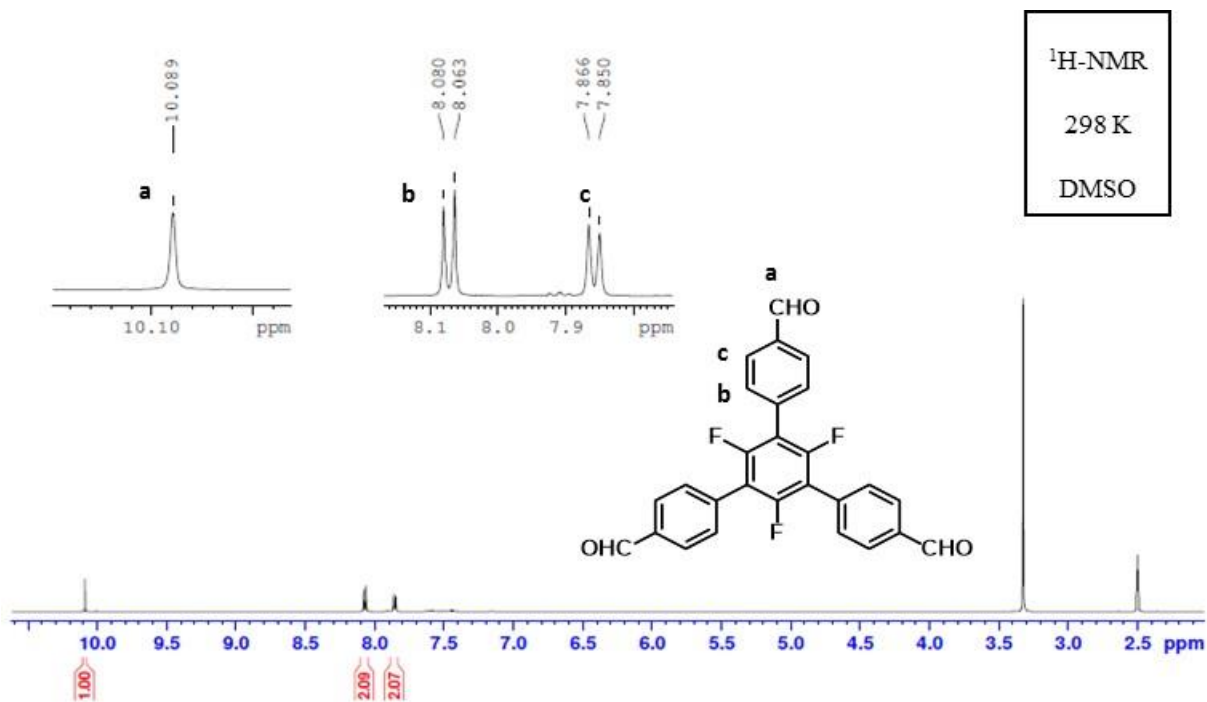


Figure 3.7. ^1H NMR (600 MHz) of 1,3,5-trifluoro-2,4,6-*tris*(4-formylphenyl)benzene (TF-2) in DMSO- d_6

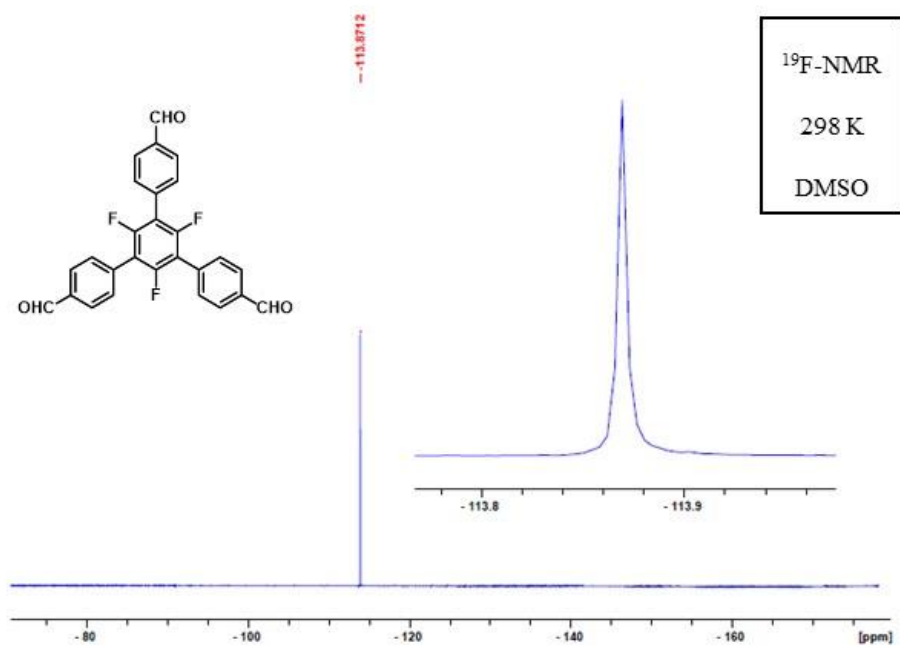


Figure 3.8. ^{19}F NMR (600 MHz) of 1,3,5-trifluoro-2,4,6-*tris*(4-formylphenyl)benzene (TF-2) in DMSO- d_6

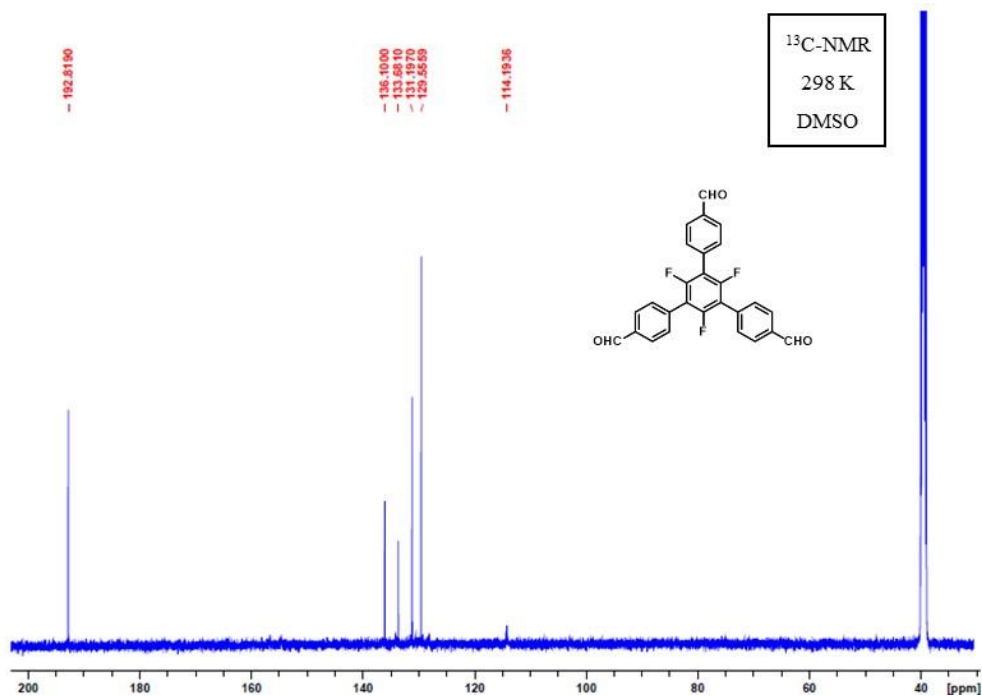


Figure 3.9. ^{13}C NMR (600 MHz) of 1,3,5-trifluoro-2,4,6-*tris*(4-formylphenyl)benzene (TF-2) in DMSO- d_6

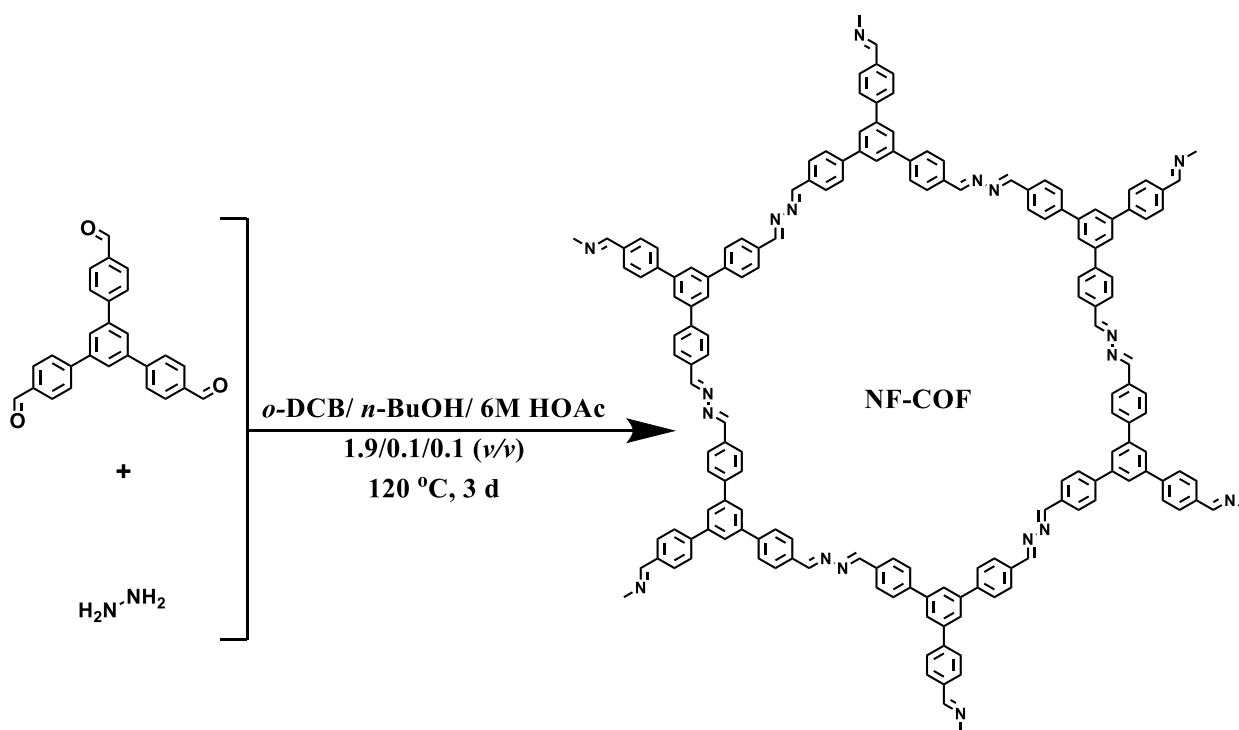


Figure 3.10. Synthesis of NF-COF

1,3,5-*tris*(4-formylphenyl)benzene (30.0 mg, 0.077 mmol) and hydrazine (3.60 μL , 0.115 mmol) were sonicated in a 4 mL ampoule with *o*-dichlorobenzene (1.9 mL) and *n*-butanol (0.1 mL) for about 10 mins. Then 6M acetic acid (0.1 mL) was added, the whole mixture was flash frozen in liquid N_2 and flame sealed. The ampoule was kept in an oven at 120 °C for 72 h. After that, it was cooled to rt, and the formed bright yellow solid was filtered. The filtered solid was soaked in neat THF (20 mL) for 2h and then dried under vacuum. Then it was degassed at 120 °C overnight to afford 24.7 mg (73% yield) of NF-COF (Figure 3.10).

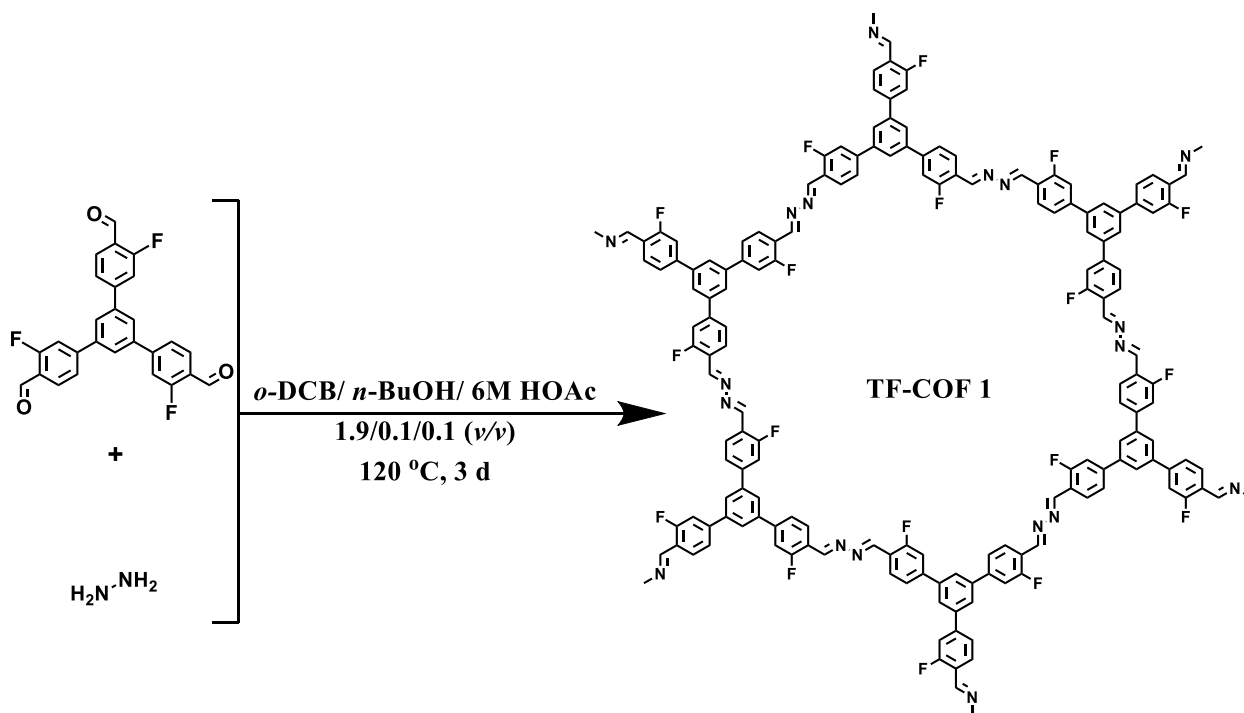


Figure 3.11. Synthesis of TF-COF 1

1,3,5-*tris*(3-fluoro-4-formylphenyl)benzene (25.0 mg, 0.056 mmol) and hydrazine (2.64 μL , 0.084 mmol) were sonicated in a 4 mL ampoule with *o*-dichlorobenzene (1.9 mL) and *n*-butanol (0.1 mL) for about 10 mins. Then 6M acetic acid (0.1 mL) was added, the whole mixture was flash frozen in liquid N_2 and flame sealed. The ampoule was kept in an oven at $120\text{ }^\circ\text{C}$ for 72h. After that, it was cooled to rt, and the formed bright solid was filtered. The filtered solid was soaked in neat THF (20 mL) for 2h and then dried under vacuum. Then it was degassed at $120\text{ }^\circ\text{C}$ overnight to afford 24.5 mg (89% yield) of TF-COF 1 (Figure 3.11).

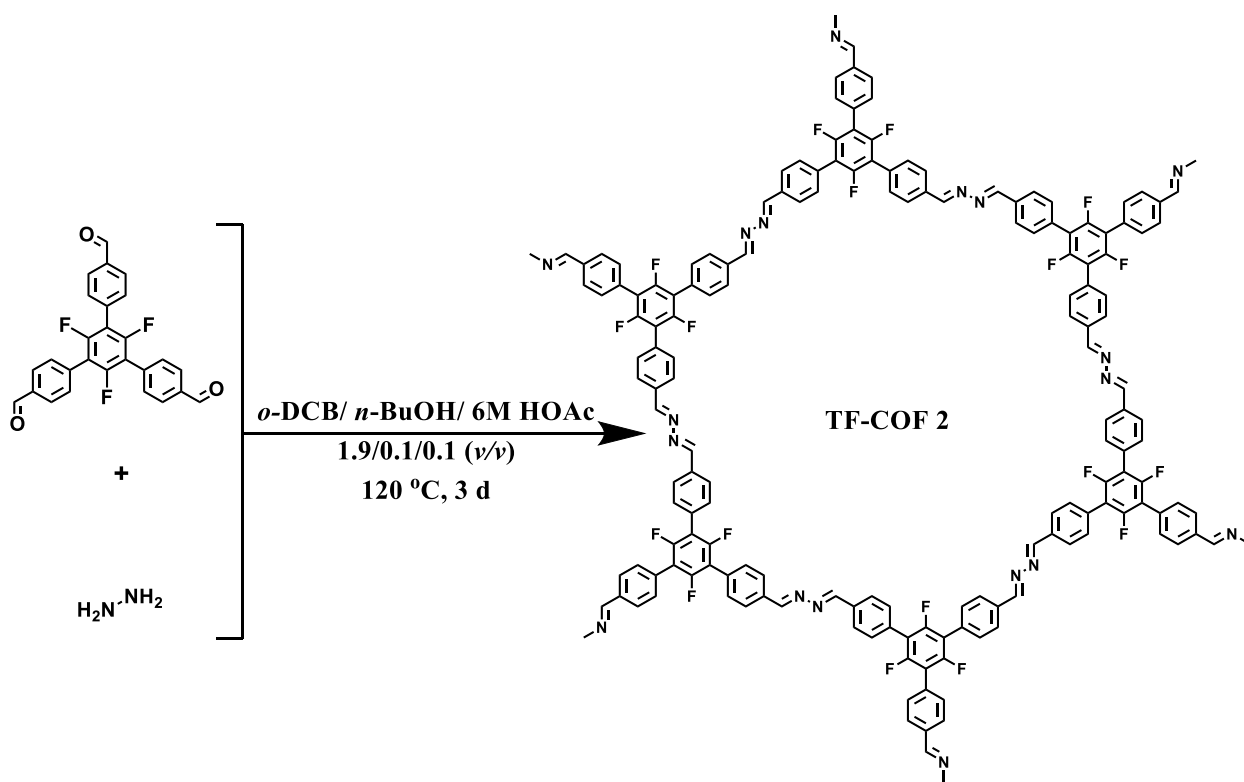


Figure 3.12. Synthesis of TF-COF 2

1,3,5-trifluoro-2,4,6-*tris*(4-formylphenyl)benzene (30.0 mg, 0.068 mmol) and hydrazine (3.17 μ L, 0.101 mmol) were sonicated in a 4 mL ampoule with *o*-dichlorobenzene (1.9 mL) and *n*-butanol (0.1 mL) for about 10 mins. Then 6M acetic acid (0.1 mL) was added, the whole mixture was flash frozen in liquid N₂ and flame sealed. The ampoule was kept in an oven at 120 °C for 72h. After that, it was cooled to rt, and the formed bright yellow solid was filtered. The filtered solid was soaked in neat THF (20 mL) for 2h and then dried under vacuum. Then it was degassed at 120 °C overnight to afford 26.5 mg (82% yield) of TF-COF 2 (Figure 3.12).

3.4 Results and discussion

3.4.1 Characterization of COFs

To help determine the 2D structure of each COF, powder X-ray diffraction (PXRD) measurements were performed. TF-COF 1 exhibited diffraction peaks at 3.67, 6.09, 9.28, 12.80 and 24.83°. TF-COF 2 exhibited diffraction peaks at 3.71, 6.19, 9.43, 12.41 and 23.70°. The peaks of both the COFs were assigned to the (100), (110), (120), (130), and (001) reflections, respectively. The only peaks clearly observed for NF-COF appeared at 3.67 and 6.09, indicating a lower level of crystalline order (Figure 3.13a). Computational models of each COF were created using Materials Studio in both staggered and eclipsed arrangements. The calculated PXRD patterns of the eclipsed TF-COFs (Figure 3.13b,c) match well with the experimental pattern. Significant enhancement in the resolution of the diffraction peaks was observed with both TF-COFs compared to NF-COF. Interestingly, the (001) reflection, attributed to the interlayer spacing between COF sheets, is much more prominent for both the TF-COFs than for NF-COF, indicating a higher degree of long range order. SEM images of each COF are shown in Figure 3.13d-f. Notably, the fluorinated COFs display crystallite morphology as opposed to the smooth, spherical agglomerates of NF-COF. Previous studies have attributed this to improved COF crystallinity owing to more organized interlayer stacking.³⁵

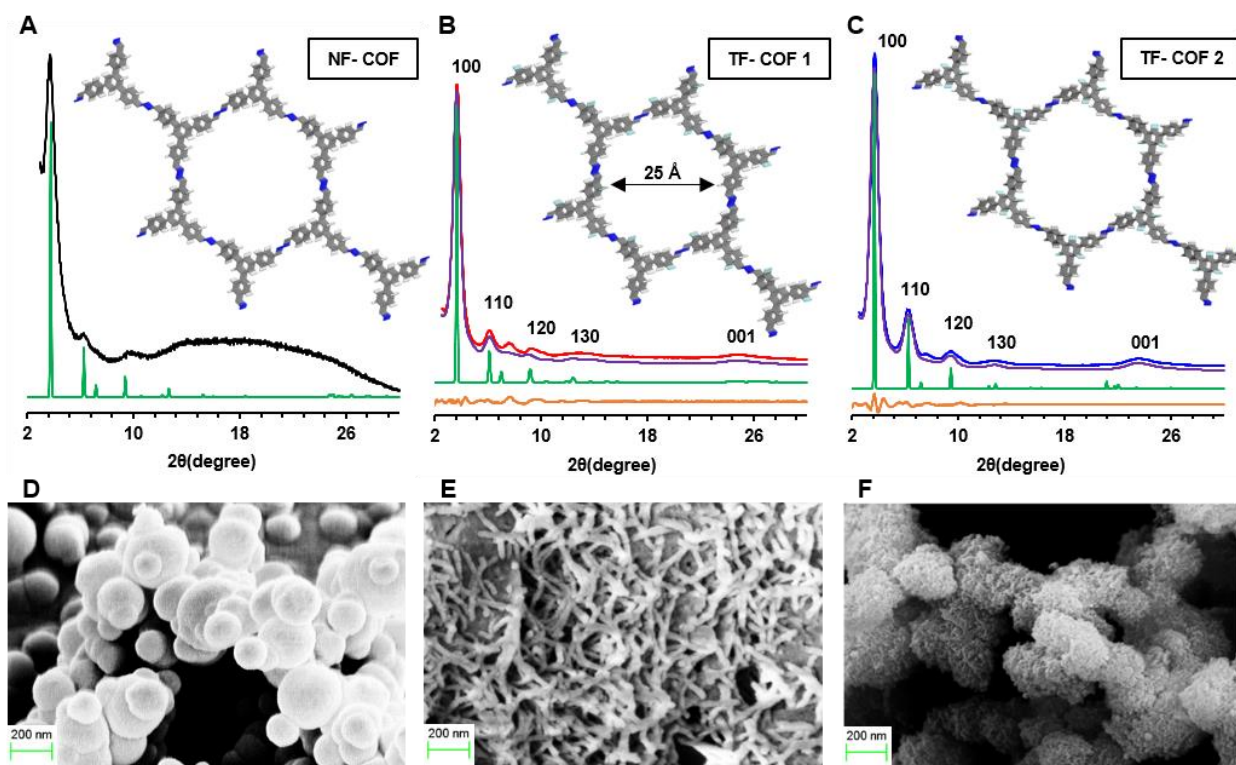


Figure 3.13. Experimental PXRDs of (A) NF-COF (black), (B) TF-COF 1 (red), (C) and TF-COF 2 (blue) with Pawley refined spectra, simulated eclipsed models and difference spectra (purple, green and orange respectively). Insets: Modeled eclipsed structures of COFs (C, grey; O, red; N, blue; F, light green. (H atoms are omitted for clarity). (D), (E) and (F) are SEM images of NF-COF, TF-COF 1 and TF-COF 2, respectively.

The surface area and pore size distributions of each COF were determined through nitrogen sorption measurements at 77 K (Figure 3.14). The NF-COF exhibits a type-I adsorption isotherm. However, both the fluorinated COFs exhibit type-IV isotherms, indicating the presence of mesopores (Figure 3.14e). The Brunauer-Emmett-Teller (BET) surface areas of TF-COF 1 and TF-COF 2 are 1820 and 2044 m^2/g , respectively, compared to only 760 m^2/g for NF-COF. To the best of our knowledge 2044 m^2/g is among the highest reported for 2D-COFs to date and COF surface areas over 2000 m^2/g are rare.¹⁸ The pore size distributions for each COF (Figure 3.14f) were obtained from the nitrogen isotherms using the density functional theory method

(DFT). The pore size distribution of NF-COF displays not only the expected pore size of 25 Å, but also has many other smaller pores. In combination with its type-I isotherm and poorly resolved diffraction pattern, it seems likely that the 2-D structure of NF-COF is poorly ordered and is not well represented by the hexagonal crystalline model often used to describe these COFs. TF-COFs 1-2, however, display much better defined pore structures. Both of these COFs have properties that are reminiscent of an eclipsed layer arrangement that demonstrate excellent agreement with the simulated pore diameters.

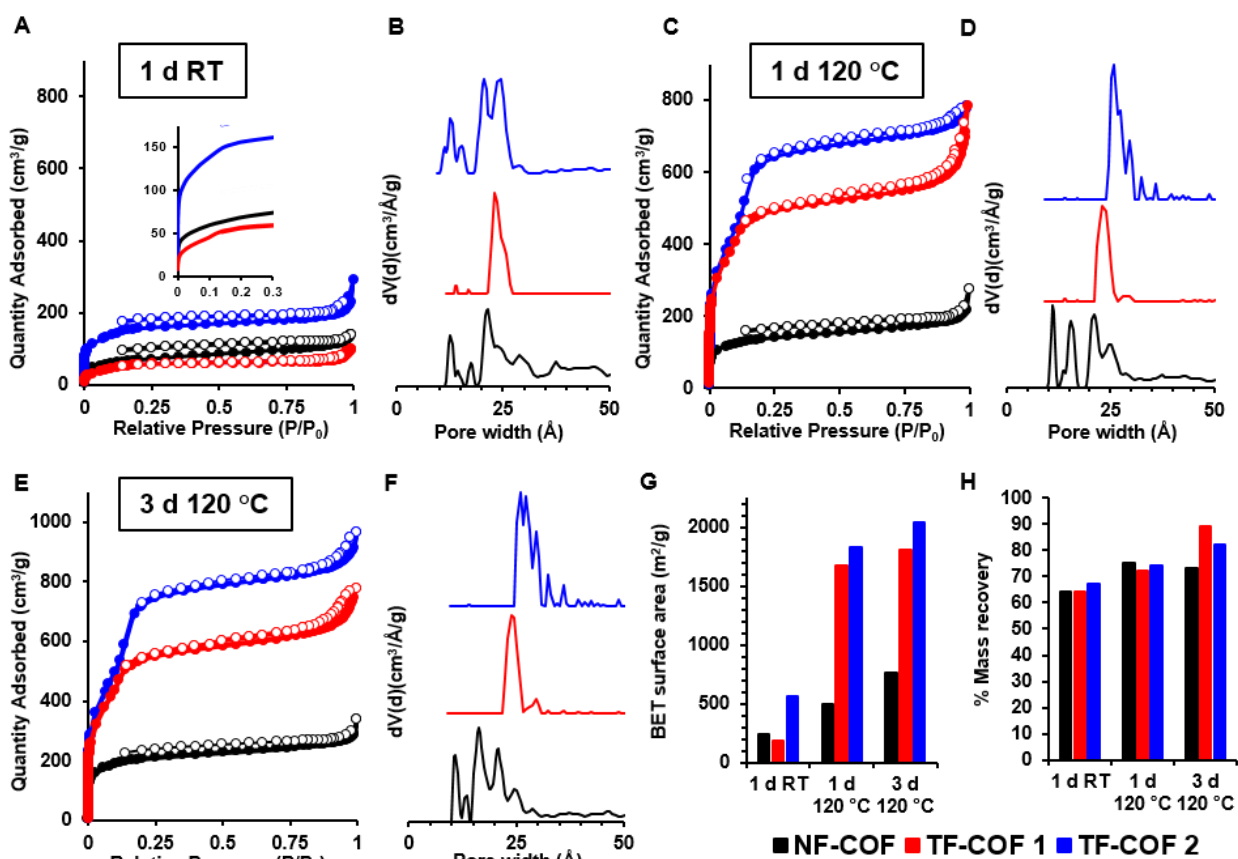


Figure 3.14. (A), (C) and (E) N₂ adsorption (solid circles) and desorption (open circles) isotherms (77 K) of 1 d RT, 1 d 120 °C and 3 d 120 °C COFs, respectively. (B), (D) and (F) PSD plots of 1 d RT, 1 d 120 °C and 3 d 120 °C COFs, respectively. (G) BET surface areas and (H) and mass recovery (%) of COFs.

A previous report on the synthesis of imine COFs found that the COF polymers initially formed porous materials that would equilibrate to more crystalline materials over time.²⁸ We performed several polymerizations of our COFs at different temperatures and reaction times to observe their formation behavior. Each COF was prepared with reaction times of 1d at either room temperature or 120 °C and 3d at 120 °C. After each experiment, the BET surface area, pore size distribution, and PXRD measurements (Figure S3.1) were carried out. These experiments revealed several interesting properties. Surprisingly, TF-COFs 1-2 display type-IV isotherms after only 1d at RT (Figure 3.14a) with a narrow pore size distribution (Figure 3.14b). As the temperature and reaction times increased, the surface areas for both fluorinated COFs increased significantly with the largest increase coming after heating to 120 °C for one day. However, NF-COF did not display the same improvement in crystallinity or display pore size distribution narrowing over time. The surface area for NF-COF does increase with increasing reaction time and temperature, but nowhere near as significantly as the TF-COFs 1-2, particularly after heating for only one day. Fourier transform infrared (FTIR) spectra of the COFs confirmed the formation of the azine linkage through disappearance of the carbonyl (1690 cm^{-1}) and the appearance of the azine (1622 cm^{-1}) stretches (Figure S3.2). These spectra reflect that the formation of the azine linkages form rapidly and are the major product (compared to the starting aldehydes) within 1d at 120 °C for all three COFs. In addition to this, the mass balances of each polymerization were recorded (Figure 3.14h) and it was found that more than 70% of the expected yield was recovered for each reaction regardless of the time or temperature. Longer reaction times at high temperatures resulted in somewhat higher yields (TF-COF 2 was ~90% for example), but overall the indication is that, consistent with previous work,²⁸ a kinetic product appears to form first,

followed by slow reorganization into a crystalline product with well-defined 2-D structure in the cases of TF-COFs 1-2. This work is novel in that, rather than modifying the reaction conditions, we have changed the chemical structure of the monomers. In other words, the electronic structure of the monomers can also favorably drive the conversion of the polymeric material from the non-crystalline kinetic product, to the thermodynamically favorable crystalline COF product. The presence of electron withdrawing fluorine substituents could serve to make the azine linkages more reactive and avoid the formation of kinetic traps. The fluorine atoms also could cause polarization in the aromatic rings which would lead to stronger cofacial interactions.³³ This effect should be especially pronounced in the case of TF-COF 2 as all three of the fluorine atoms are on the same ring, and indeed, TF-COF 2 has highest surface area observed in this study. A previous report on a related series of azine-linked COFs showed that crystallinity and surface area were improved by planarizing the monomers.¹³ In this case, we do not observe a correlation between torsion angle and surface area, and in fact, the highest surface area materials (TF-COF 2) has the largest torsion angle (Figure S3.20). We believe that these observations show that COF polymerization and crystallization can be controlled effectively through the careful design of both the steric and electronic structure of the monomers.

3.5 Conclusion

In conclusion, we have synthesized two novel fluorinated COFs that have significantly improved physical properties compared with an isostructural non-fluorinated variant. This work demonstrates that modifications to the electronic structure of COF monomers can result in an immense improvement in the structural properties of the COFs. We believe that these design

principles can be applied to other types of COFs and future work will be directed towards further elucidating these principles.

3.6 Acknowledgement

This research was supported with funds from The University of Texas at Dallas and the American Chemical Society Petroleum Research Fund (52906-DNI10).

3.7 Appendix – Supporting information

PXRD spectra of COFs prepared at different conditions

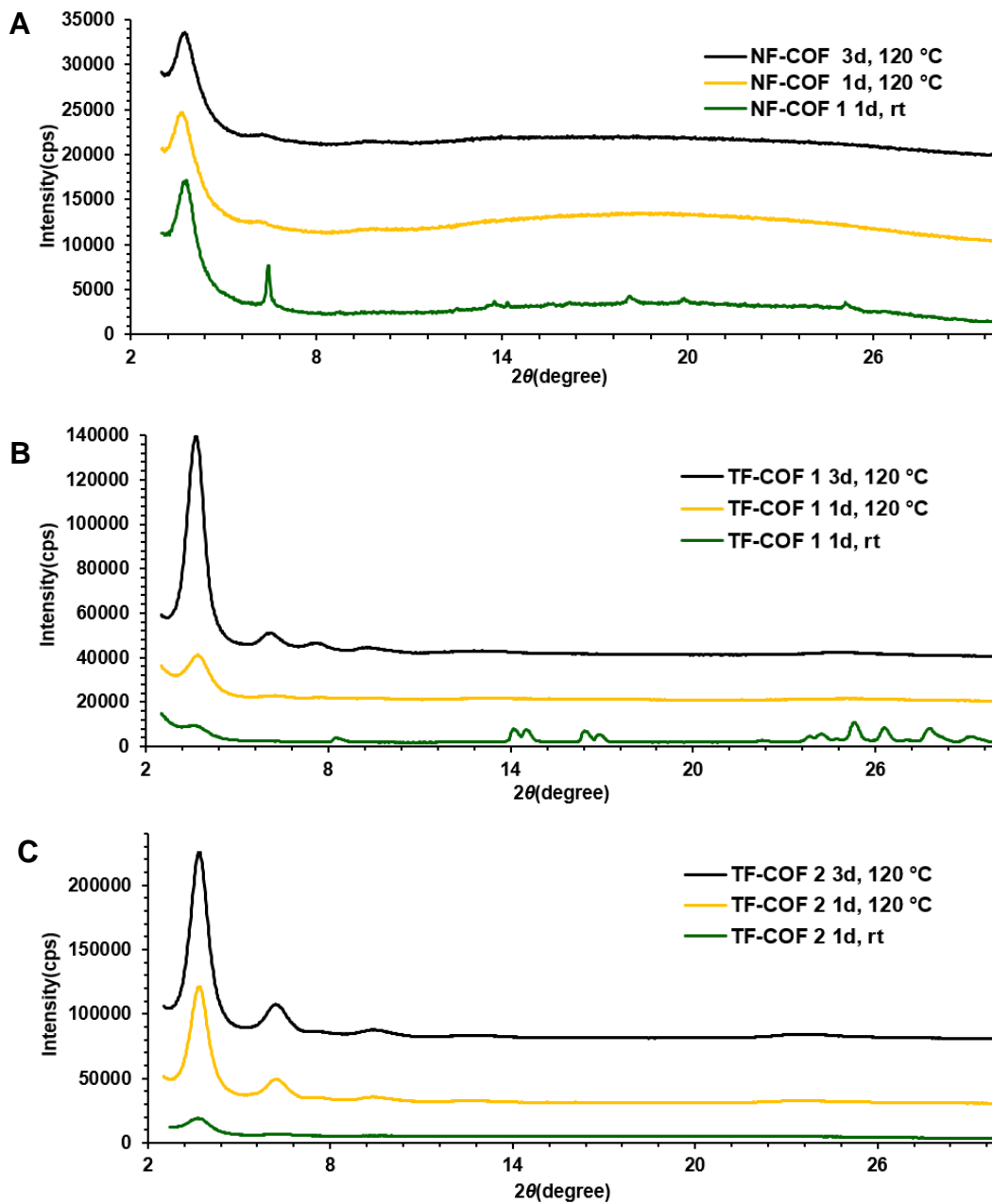


Figure S3.1. Experimental powder X-ray diffraction patterns of (A) NF-COF, (B) TF-COF 1 and (C) TF-COF 2 prepared at 3d, 120 °C (black), at 1d, 120 °C, (yellow), at 1d, r.t. (green)

FT-IR spectra of COFs prepared at different conditions

FT-IR spectroscopy of the NF-COF, TF-COF 1 and 2 exhibited a stretching vibration band at 1622 cm^{-1} which can be assigned to C=N bond based on previously reported azine COFs.^{10,14}

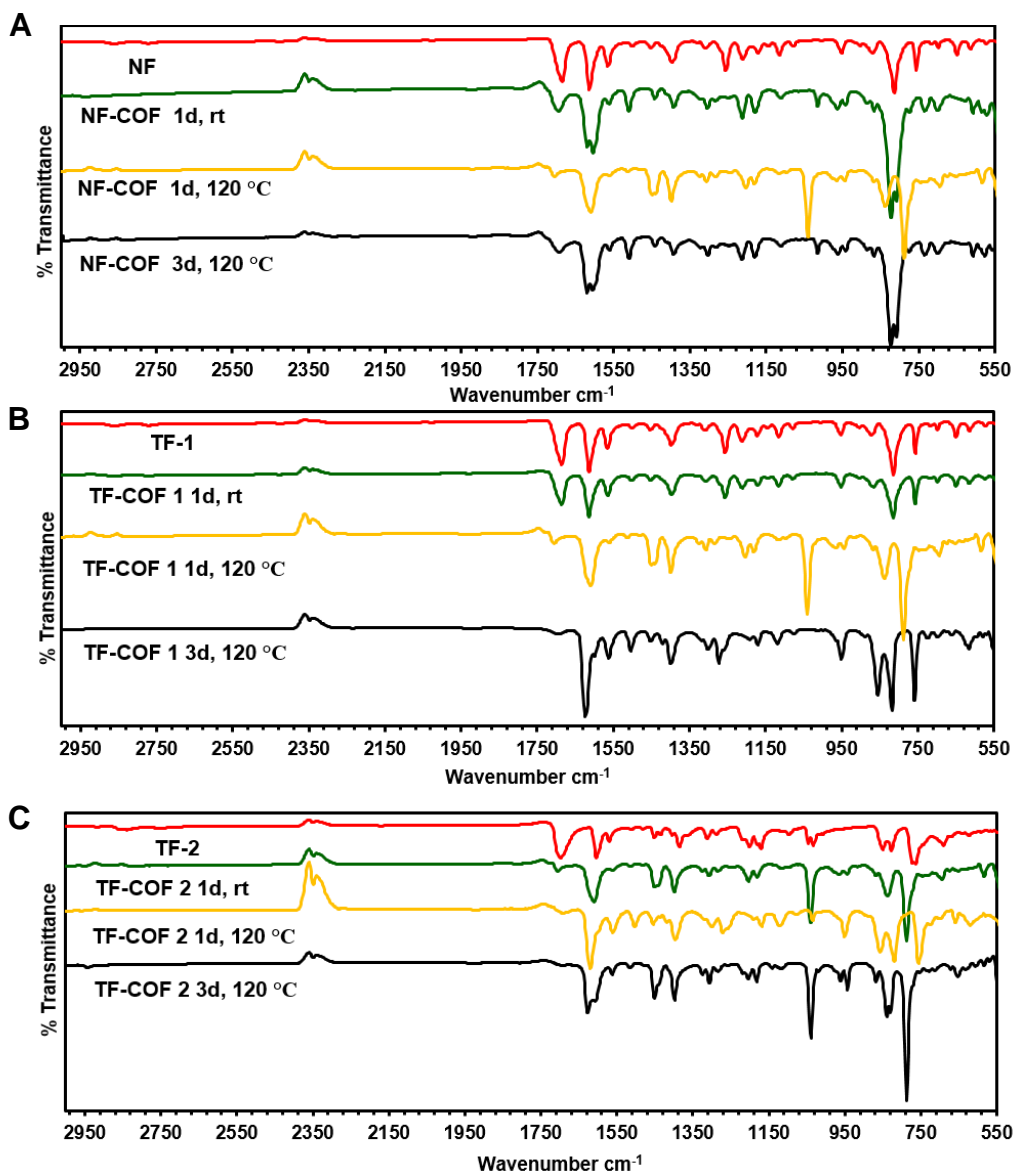


Figure S3.2. FT-IR spectra of (A) NF-COF, (B) TF-COF 1 and (C) TF-COF 2 synthesized at 1d, rt (green), at 1d, 120 °C (yellow) and at 3d, 120 °C (black) compared with the corresponding aldehyde (red)

Computational Modelling of NF-COF

Computational modelling of the structure of NF-COF was carried out using the Materials Studio (ver. 7.0) suite of programs. The initial lattice was created by starting with the space group P3. The constructed model was geometry optimized using the Forcite module (Smart algorithm). Then the calculated PXRD pattern was generated with the Reflex Plus module using Pseudo-Voigt function. The staggered arrangement for NF-COF was also constructed considering P6₃/m as the space group. Comparison of the observed and the simulated PXRD patterns is presented in Figure S3.3.

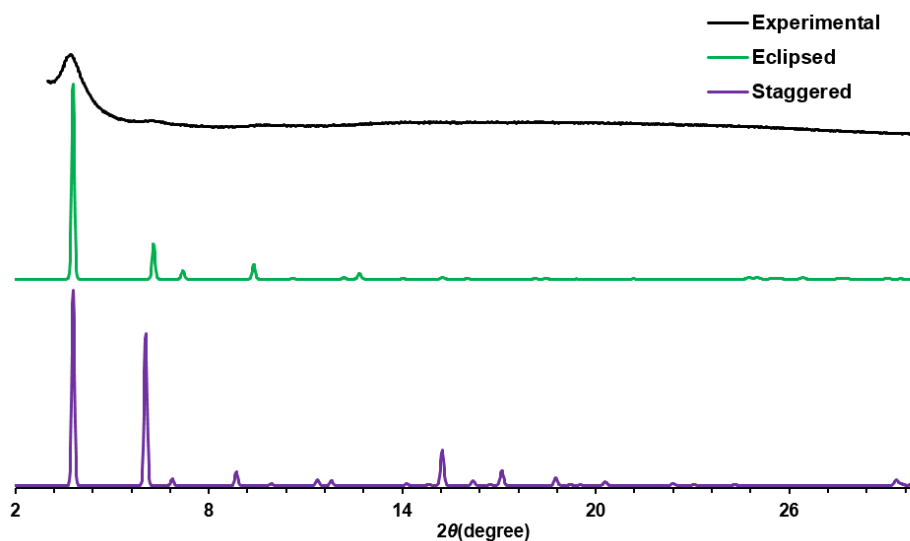


Figure S3.3. Experimental powder X-ray diffraction pattern of NF-COF (black), compared with simulated PXRD patterns of eclipsed layers of COF (green) considering P3 symmetry and staggered layers of COF (purple) considering P6₃/m symmetry.

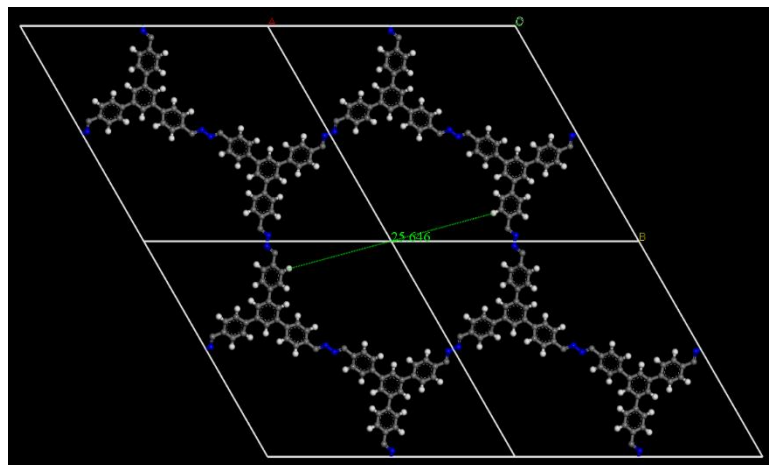


Figure S3.4. View of the simulated structure of the eclipsed NF-COF along c axis

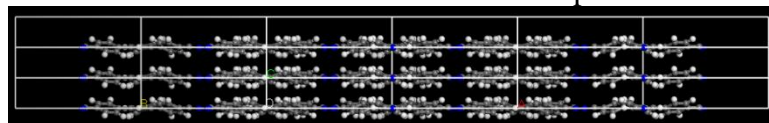


Figure S3.5. View of the simulated structure of the eclipsed NF-COF along a axis

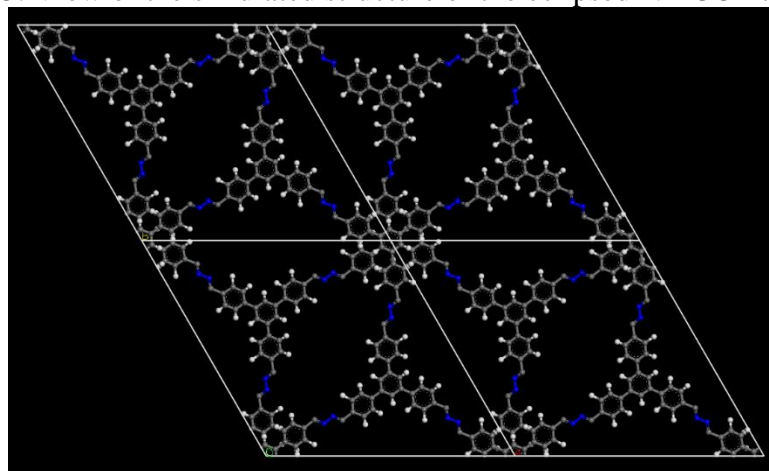


Figure S3.6. View of the simulated structure of the staggered NF-COF along c axis

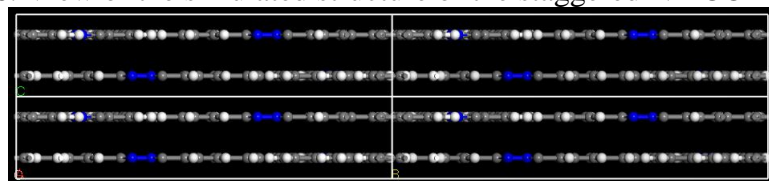


Figure S3.7. View of the simulated structure of the staggered NF-COF along a axis

Computational Modeling of TF-COF 1

Computational modeling of the structure of TF-COF 1 was carried out using the Materials Studio (ver. 7.0) suite of programs. The initial lattice was created by starting with the space group $P3$. The constructed model was geometry optimized using the Forcite module (Smart algorithm). Then the calculated PXRD pattern was generated with the Reflex Plus module using Pseudo-Voigt function. Finally, Pawley refinement was applied for profile fitting, producing the refined PXRD profile with the lattice parameters of $a = b = 29.522454 \text{ \AA}$ and $c = 3.637044 \text{ \AA}$. R_{wp} and R_p values converged to 5.46% and 3.07%, respectively. The staggered arrangement for TF-COF1 was also constructed considering $P6_3/m$ as the space group. Comparison of the observed and the simulated PXRD patterns (Figure S3.8) evident that the most preferred structure of TF-COF 1 is the eclipsed layer arrangement.

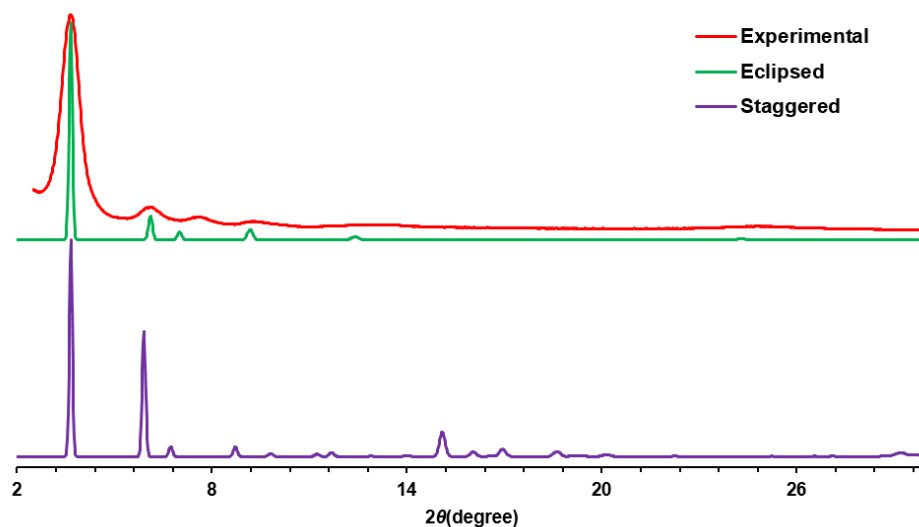


Figure S3.8. Experimental powder X-ray diffraction pattern of TF-COF 1 (red), compared with simulated PXRD patterns of eclipsed layers of COF (green) considering $P3$ symmetry and staggered layers of COF (purple) considering $P6_3/m$ symmetry.

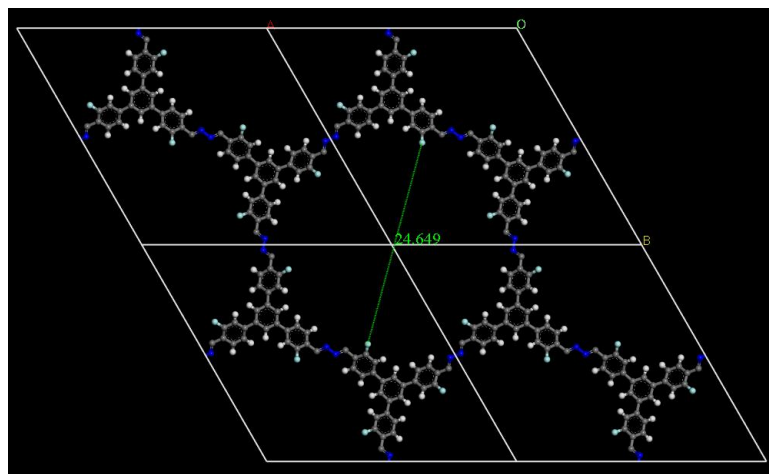


Figure S3.9. View of the simulated structure of the eclipsed TF-COF 1 along c axis

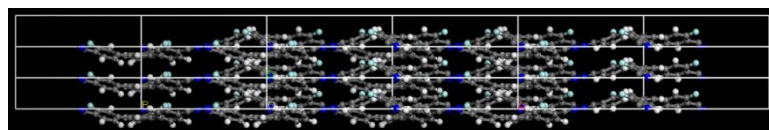


Figure S3.10. View of the simulated structure of the eclipsed TF-COF 1 along a axis

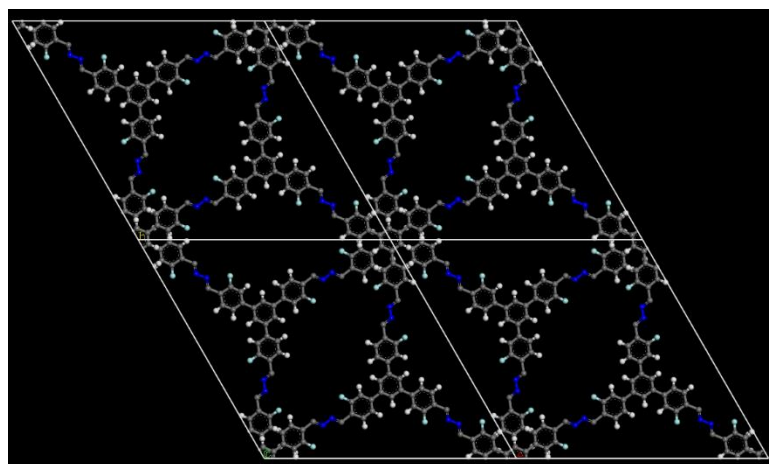


Figure S3.11. View of the simulated structure of the staggered TF-COF 1 along c axis

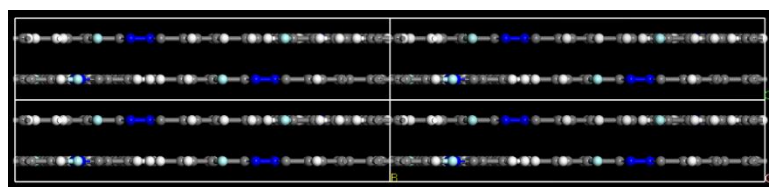


Figure S3.12. View of the simulated structure of the staggered TF-COF 1 along a axis

Computational Modeling of TF-COF 2

Computational modeling of the structure of TF-COF 2 was carried out using the Materials Studio (ver. 7.0) suite of programs. The initial lattice was created by starting with the space group $P3$. The constructed model was geometry optimized using the Forcite module (Smart algorithm). Then the calculated PXRD pattern was generated with the Reflex Plus module using Pseudo-Voigt function. Finally, Pawley refinement was applied for profile fitting, producing the refined PXRD profile with the lattice parameters of $a = b = 29.072739 \text{ \AA}$ and $c = 4.275722 \text{ \AA}$. R_{wp} and R_p values converged to 4.03% and 2.97%, respectively. The staggered arrangement for TF-COF2 was also constructed considering $P6_3/m$ as the space group. Comparison of the observed and the simulated PXRD patterns (Figure S3.13) evident that the most preferred structure of TF-COF 2 is the eclipsed layer arrangement.

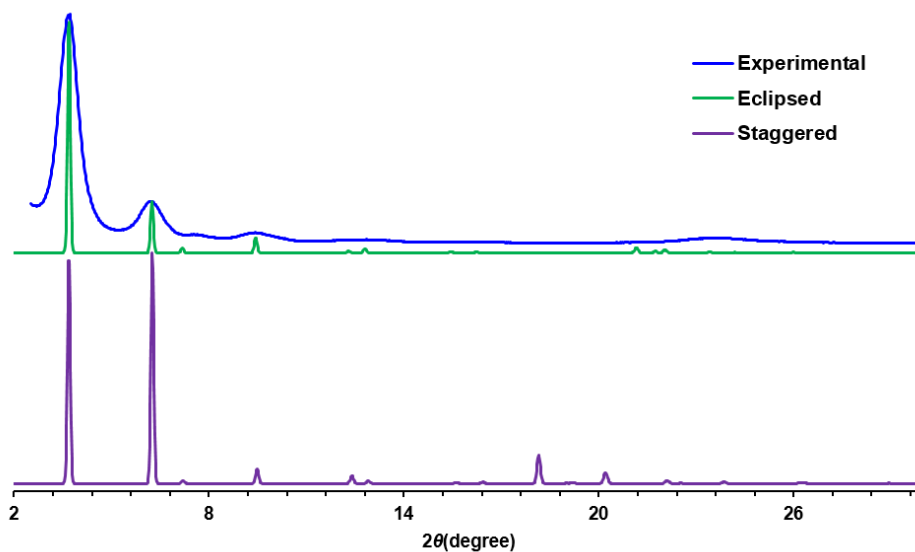


Figure S3.13. Experimental powder X-ray diffraction pattern of TF-COF 2 (blue), compared with simulated PXRD patterns of eclipsed layers of COF (green) considering $P3$ symmetry and staggered layers of COF (purple) considering $P6_3/m$ symmetry.

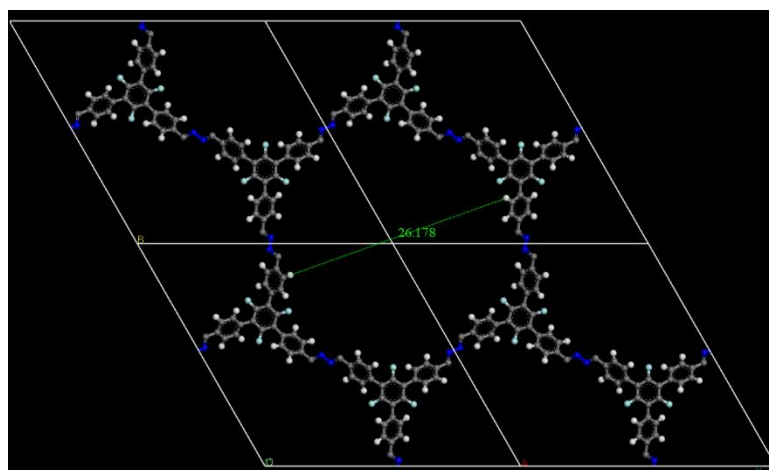


Figure S3.14. View of the simulated structure of the eclipsed TF-COF 2 along c axis

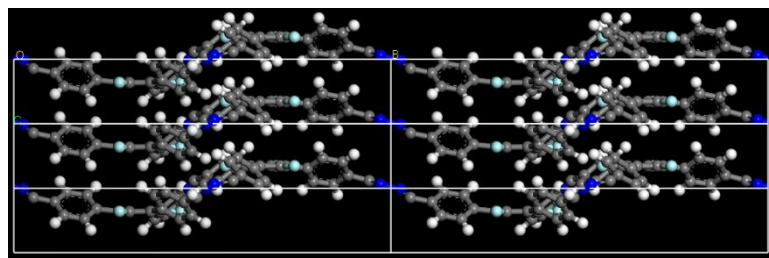


Figure S3.15. View of the simulated structure of the eclipsed TF-COF 2 along a axis

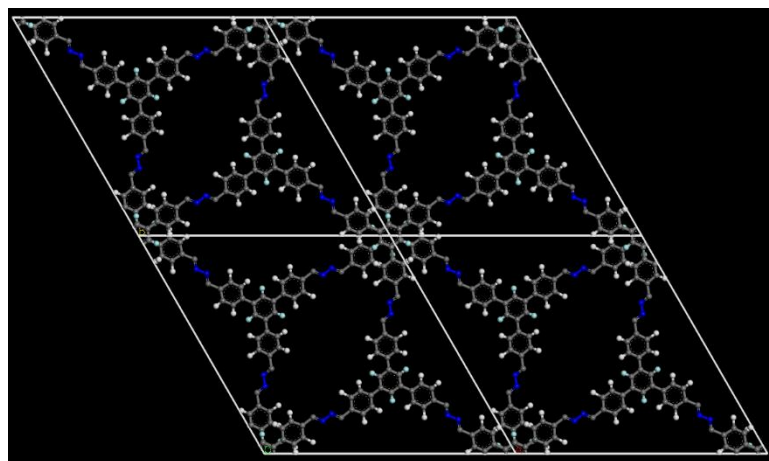


Figure S3.16. View of the simulated structure of the staggered TF-COF 2 along c axis

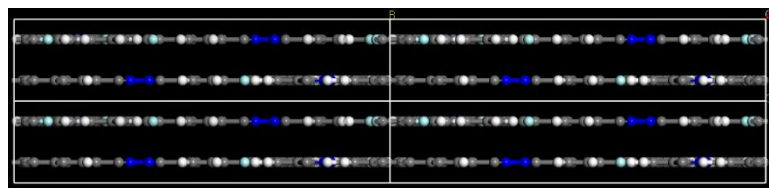


Figure S3.17. View of the simulated structure of the staggered TF-COF 2 along a axis

TGA curves of all COFs prepared at 120 °C for 3d

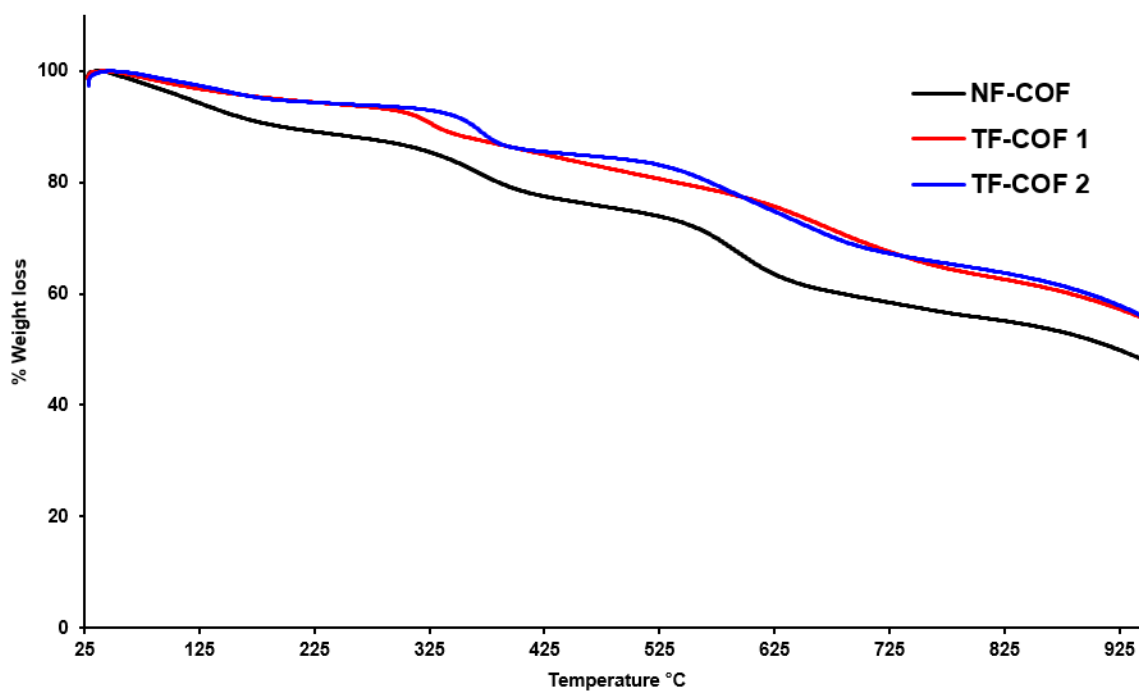


Figure S3.18. TGA curves of NF-COF 3d, 120 °C (black), TF-COF 1 3d, 120 °C (red) and TF-COF 2 3d, 120 °C (blue)

EDX data of TF-COF 1 and 2 prepared at 120 °C for 3d

Table S3.1. EDX data of TF-COF 1 3d, 120 °C and TF-COF 2 3d, 120 °C

Sample	Weight %		Atomic %	
	C%	F%	C%	F%
TF-COF 1	84.74	15.26	89.78	10.22
TF-COF 2	84.76	15.24	89.79	10.21

Scanning Electron Microscopy

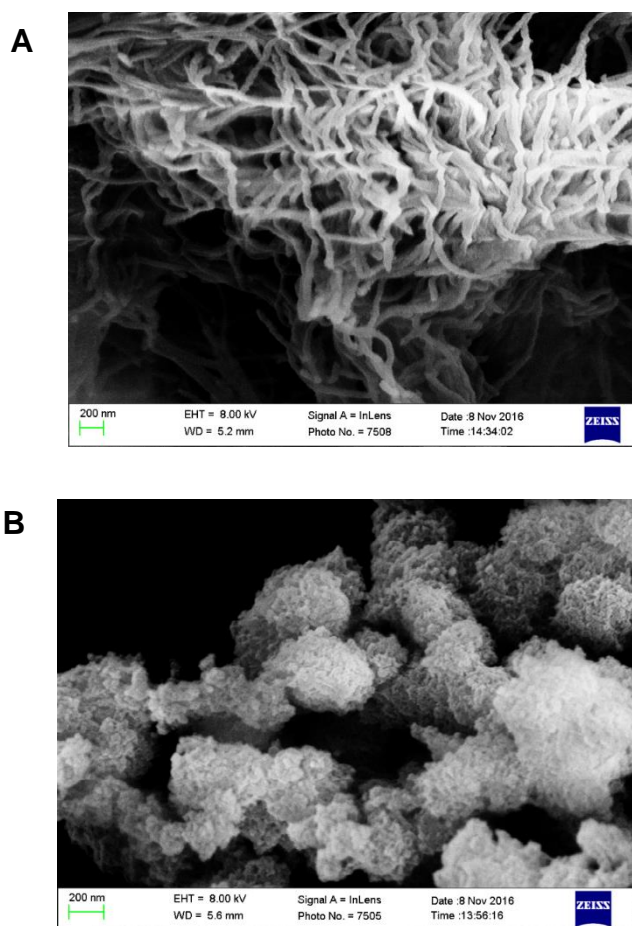


Figure S3.19. SEM images of (A) TF-COF 1 1d, 120 °C and (B) TF-COF 2 1d, 120 °C

Torsion angle measurements of the aldehyde monomers

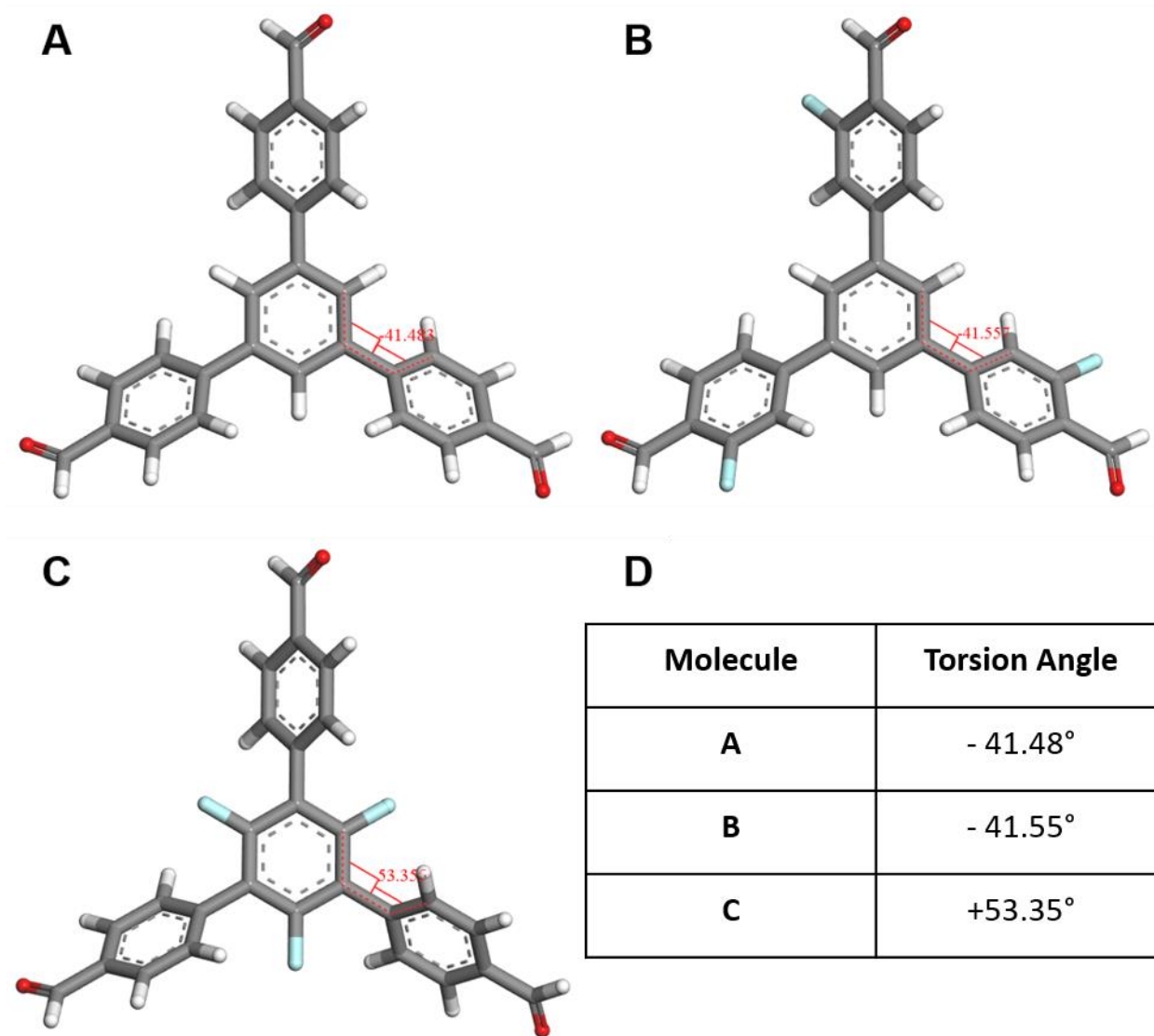


Figure S3.20. Geometry optimized structures of the aldehydes used in the COF synthesis (**A**) 1,3,5-*tris*(4-formylphenyl)benzene (**B**) 1,3,5-*tris*(3-fluoro-4-formylphenyl)benzene (**C**) 1,3,5-trifluoro-2,4,6-*tris*(4-formylphenyl)benzene (**D**) Calculated torsion angles of the precursor aldehydes. Calculation of the torsion angle of the aldehydes was carried out using Materials Studio Visualizer. Universal Force Field (UFF) was utilized for the geometry optimization of the aldehyde precursors.

3.8 References

1. Cote, A. P.; Benin, A. I.; Ockwig, N. W.; O'Keeffe, M.; Matzger, A. J.; Yaghi, O. M. *Science* **2005**, *310*, 1166.
2. El-Kaderi, H.; Hunt, J. R.; Mendoza-Cortes, J. L.; Cote, A. P.; Taylor, R. E.; O'Keeffe, M.; Yaghi, O. M. *Science* **2007**, *316*, 268.
3. Uribe-Romo, F.; Doonan, C. J.; Furukawa, H.; Oisaki, K.; Yaghi, O. M. *J. Am. Chem. Soc.* **2011**, *133*, 11478-11481.
4. Colson, J. W.; Woll, A. R.; Mukherjee, A.; Levendorf, M. P.; Spitler, E. L.; Shields, V. B.; Spencer, M. G.; Park, J.; Dichtel, W. R. *Science* **2011**, *332*, 228.
5. Jin, Y.; Yu, C.; Denman, R. J.; Zhang, W. *Chem. Soc. Rev.* **2013**, *42*, 6634-6654.
6. Uribe-Romo, F.; Hunt, J. R.; Furukawa, H.; Klock, C.; O'Keeffe, M.; Yaghi, O. M. *J. Am. Chem. Soc.* **2009**, *131*, 4570-4571.
7. Dalapati, S.; Addicoat, M.; Jin, S.; Sakurai, T.; Gao, J.; Xu, H.; Irle, S.; Seki, S.; Jiang, D. *Nat. Commun.* **2015**, *6*, 7786.
8. Stegbauer, L.; Schwinghammer, K.; Lotsch, B. V. *Chem. Sci.* **2014**, *5*, 2789-2793.
9. Kuhn, P.; Antonietti, M.; Thomas, A. *Angew. Chem. Inter. Ed.* **2008**, *47*, 3450-3453.
10. Dalapati, S.; Jin, S.; Gao, J.; Xu, Y.; Nagai, A.; Jiang, D. *J. Am. Chem. Soc.* **2013**, *135*, 17310-17313.
11. Li, Z.; Feng, X.; Zou, Y.; Zhang, Y.; Xia, H.; Liu, X.; Mu, Y. *Chem. Commun.* **2014**, *50*, 13825-13828.
12. Li, Z.; Zhi, Y.; Feng, X.; Ding, X.; Zou, Y.; Liu, X.; Mu, Y. *Chem. Eur. J.* **2015**, *21*, 12079-12084.
13. Vyas, V. S.; Haase, F.; Stegbauer, L.; Savasci, G.; Podjaski, F.; Ochsenfeld, C.; Lotsch, B. V. *Nat. Commun.* **2015**, *6*, 8508.
14. Alahakoon, S. B.; Thompson, C. M.; Nguyen, A. X.; Occhialini, G.; McCandless, G. T.; Smaldone, R. A. *Chem. Commun.* **2016**, *52*, 2843-2845.
15. Ganz, E.; Dornfeld, M. *J. Phys. Chem. C* **2012**, *116*, 3661-3666.
16. Rabbani, M. G.; Sekizkardes, A. K.; Kahveci, Z.; Reich, T. E.; Ding, R.; El-Kaderi, H. M. *Chem. Eur. J.* **2013**, *19*, 3324-3328.
17. Pachfule, P.; Kandambeth, S.; Diaz Diaz, D.; Banerjee, R. *Chem. Commun.* **2014**, *50*, 3169-3172.

18. Xu, H.; Gao, J.; Jiang, D. *Nat. Chem.* **2015**, *7*, 905-912.
19. Lin, S.; Diercks, C. S.; Zhang, Y.; Kornienko, N.; Nichols, E. M.; Zhao, Y.; Paris, A. R.; Kim, D.; Yang, P.; Yaghi, O. M.; Chang, C. J. *Science* **2015**, *349*, 1208.
20. Jin, S.; Furukawa, K.; Addicoat, M.; Chen, L.; Takahashi, S.; Irle, S.; Nakamura, T.; Jiang, D. *Chem. Sci.* **2013**, *4*, 4505-4511.
21. DeBlase, C. R.; Silberstein, K. E.; Truong, T.; Abruna, H. D.; Dichtel, W. R. *J. Am. Chem. Soc.* **2013**, *135*, 16821-16824.
22. Liu, X.; Guan, C.; Wang, D.; Wan, L. *Adv. Mater.* **2014**, *26*, 6912-6920.
23. Dogru, M.; Bein, T. *Chem. Commun.* **2014**, *50*, 5531-5546.
24. DeBlase, C. R.; Hernandez-Burgos, K.; Silberstein, K. E.; Rodriguez-Calero, G. G.; Bisbey, R. P.; Abruna, H. D.; Dichtel, W. R. *ACS Nano* **2015**, *9*, 3178-3183.
25. Duhovic, S.; Dinca, M. *Chem. Mater.* **2015**, *27*, 5487-5490.
26. Duncan, N. C.; Hay, B. P.; Hagaman, E. W.; Custelcean, R. *Tetrahedron* **2012**, *68*, 53-64.
27. Smith, B. J.; Dichtel, W. R. *J. Am. Chem. Soc.* **2014**, *136*, 8783-8789.
28. Smith, B. J.; Overholts, A. C.; Hwang, N.; Dichtel, W. R. *Chem. Commun.* **2016**, *52*, 3690-3693.
29. Salonen, L. M.; Medina, D. D.; Carbo-Argibay, E.; Goesten, M. G.; Mafra, L.; Guldris, N.; Rotter, J. M.; Stroppa, D. G.; Rodriguez-Abreu, C. *Chem. Commun.* **2016**, *52*, 7986-7989.
30. Chen, X.; Addicoat, M.; Irle, S.; Nagai, A.; Jiang, D. *J. Am. Chem. Soc.* **2013**, *135*, 546-549.
31. Ascherl, L.; Sick, T.; Margraf, J. T.; Lapidus, S. H.; Calik, M.; Hettstedt, C.; Karaghiosoff, K.; Doblinger, M.; Clark, T.; Chapman, K. W.; Auras, F.; Bein, T. *Nat. Chem.* **2016**, *8*, 310-316.
32. Hunter, C. A.; Sanders, J. K. M. *J. Am. Chem. Soc.* **1990**, *112*, 5525-5534.
33. Martinez, C. R.; Iverson, B. L. *Chem. Sci.* **2012**, *3*, 2191-2201.
34. Bunck, D. N.; Dichtel, W. R. *J. Am. Chem. Soc.* **2013**, *135*, 14952-14955.
35. Halder, A.; Kandambeth, S.; Biswal, B. P.; Kaur, G.; Roy, N. C.; Addicoat, M.; Salunke, J. K.; Banerjee, S.; Vanka, K.; Heine, T.; Verma, S.; Banerjee, R. *Angew. Chem. Int. Ed.* **2016**, *55*, 7806-7810.

CHAPTER 4
EXPERIMENTAL AND THEORETICAL INSIGHT INTO THE EFFECT OF
FLUORINE SUBSTITUENTS ON THE PROPERTIES OF AZINE LINKED
COVALENT ORGANIC FRAMEWORKS

Authors: Sampath B. Alahakoon,[†] Gino Occhialini,[†] Gregory T. McCandless,
Arosha A.K. Karunathilake, Steven O. Nielsen and Ronald A. Smaldone

Department of Chemistry and Biochemistry, BSB13

The University of Texas at Dallas

800 West Campbell Road

Richardson, Texas 75080-3021

[†] These authors contributed equally.

Alahakoon, S. B.; Occhialini, G.; McCandless, G. T.; Karunathilake, A. A. K.; Nielsen, S. O.; Smaldone, R. A. Experimental and Theoretical Insight Into the Effect of Fluorine Substituents on the Properties of Azine-Linked Covalent Organic Frameworks. *CrystEngComm.* **2017**, *19*, 4882-4885. Adapted with permission of The Royal Society of Chemistry.

4.1 Abstract

Herein we report a combined experimental and computational study on the effect of fluorine atom incorporation on the materials properties of azine-linked COFs. We found that increasing the ratio of fluorinated to non-fluorinated monomers led to substantial improvements in both crystallinity and porosity. Computational models suggest that this improvement might be explained by a substantial energetic stabilization in the face-to-face stacking interaction of the fluorinated COF monomers.

4.2 Introduction

Covalent organic frameworks (COFs)^{1,2} are a class of crystalline porous polymer networks that are synthesized with the aid of dynamic covalent bonds.³ The formation of boronate esters,^{1,2} spiroborates,⁴ imines,^{5,6} hydrazones,^{7,8} triazines,⁹ and azines^{10,11} have all been successfully utilized to form COFs. These highly porous materials with well-defined crystalline structures have attracted great attention over the past decade due to the broad spectrum of potential applications in gas storage,¹² solar and electrical energy storage,¹² and catalysis^{8,13}. Numerous studies¹⁴⁻²⁰ have demonstrated that the structure and properties of 2D-COFs are greatly influenced by the quality of the non-covalent interactions between the 2D layers. We have previously shown that the addition of electron withdrawing fluorine atoms greatly improves the COF properties even when using non-planar monomers.²¹ In an attempt to further elucidate the nature of this observation we have carried out a combined experimental and theoretical study that aims to clarify the role that aromatic stacking interactions have on the formation and structure of these COFs. In this report we have synthesized a series of mixed COFs using fluorinated (TF)

and non-fluorinated (NF) monomers with varied feed ratios. Furthermore, we have carried out a series of quantum mechanical calculations to determine the interaction energies between these monomers in the face-to-face orientation that would be expected in an eclipsed 2D-COF.

4.3 Experimental

4.3.1 Materials and methods

Reagents were purchased from commercial suppliers (Sigma-Aldrich and Fisher Scientific) and used as received. Low-pressure gas adsorption experiments (up to 760 torr) were carried out on a Micromeritics ASAP 2020 surface area analyzer. Ultrahigh-purity-grade N₂ gas (obtained from Airgas Corporation) were used in all adsorption measurements. N₂ (77 K) isotherms were measured using a liquid nitrogen bath. Pore size distributions were determined using a density functional theory (DFT) cylindrical pores in an oxide surface model in the Micromeritics Software Package. Powder X-ray diffraction of all COFs were carried out on a Bruker D8 Advance diffractometer with a sealed tube radiation source (Cu K α , $\lambda = 1.54184 \text{ \AA}$), a low background sample holder, and Lynxeye XE detector. Scanning electron microscope (SEM) images were acquired with Zeiss-LEO model 1530 SEM instrument. ¹H-NMR spectra were carried out on a Bruker 500 MHz Advance Spectrometer. ATR (attenuated total reflectance) FT-IR spectra were taken on a Cary 600 Series FT-IR spectrophotometer.

4.3.2 Monomer and mixed-linker COF synthesis

Monomers NF and TF were synthesized as reported previously.²¹ Mixed TF_x-COFs were synthesized by varying the monomer feed ratios of NF and TF (Figure 4.1). Each of these COFs were prepared solvothermally in glass ampoules using hydrazine as the co-monomer in a solvent system of *o*-dichlorobenzene(DCB)/*n*-butanol/6M aqueous acetic acid (1.9/0.1/0.1 v/v/v).

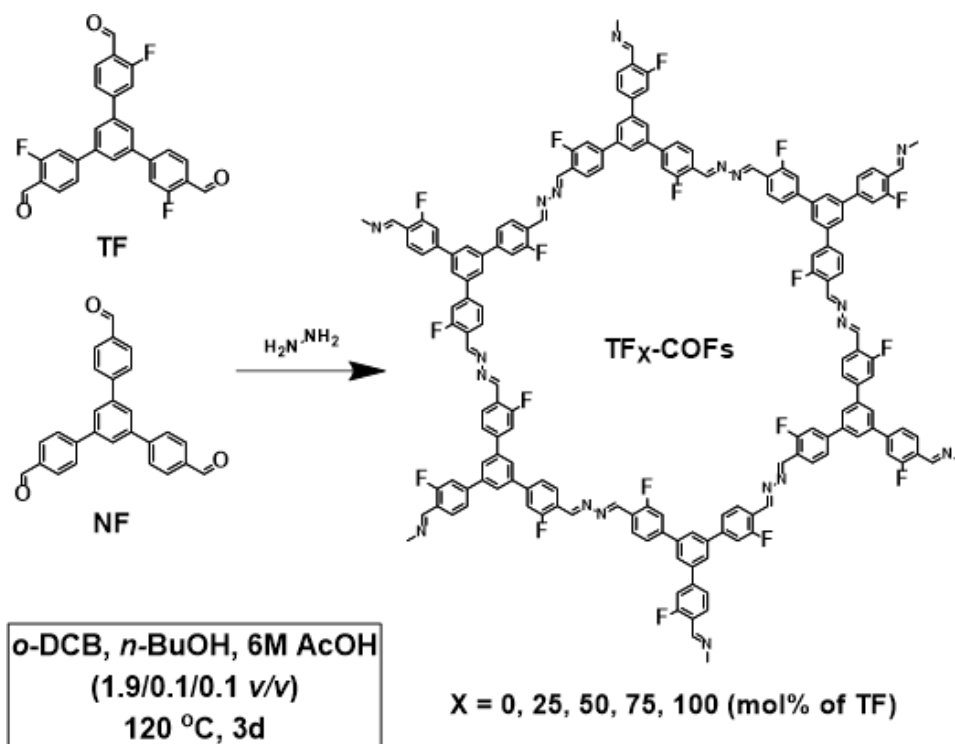


Figure 4.1. Synthesis of the TF_x-COF series by varying the mole % of the TF monomer with the remaining monomers represented by NF.

4.4 Results and discussion

4.4.1 Characterization of mixed-linker COFs

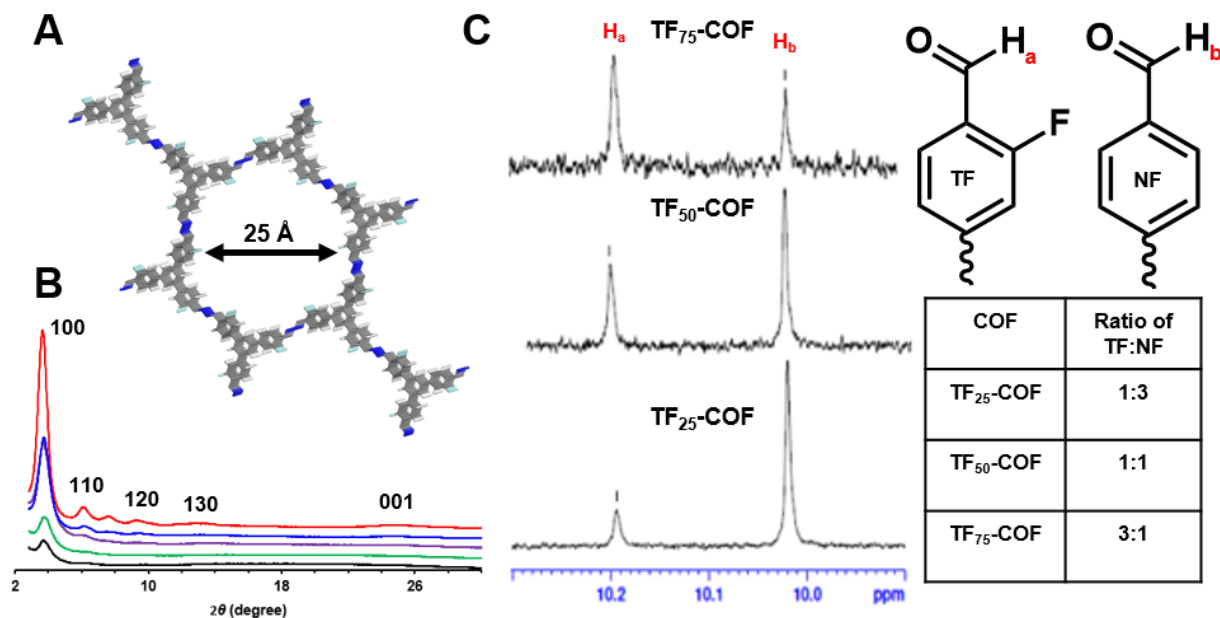


Figure 4.2. (A) Eclipsed layers of COFs. (B) PXRD spectra of the series of COFs. Black, Green, Purple, Blue and Red lines represent the TF₀-COF, TF₂₅-COF, TF₅₀-COF, TF₇₅-COF and TF₁₀₀-COF, respectively. (C) ¹H-NMR spectra of digested mixed COFs and the interaction of each aldehyde peaks in the mixed COFs.

Each of the mixed linker COFs was digested in acidified d₆-DMSO and ¹H-NMR studies were carried out to determine whether the final COF composition matched the monomer feed ratio. The incorporation of different ratios of the monomers in the COFs was confirmed by the integration ratios of NF (H_a-10.013 ppm) and TF (H_b-10.188 ppm) aldehyde peaks (Figure 4.2c). These experiments showed that the incorporation ratio (Figure 4.2c) of each monomer is consistent with the feed ratio (Figure 4.1).

The periodic arrangement of the COFs was analysed using powder X-ray diffraction (PXRD) analysis. Of the mixed COF series, only TF₅₀-COF, TF₇₅-COF, and TF₁₀₀-COF exhibited

observable diffraction peaks at 3.67, 6.09, 9.28, 12.80 and 24.83° which were assigned to the (100), (110), (120), (130), and (001) reflections, respectively. Poor crystallinity was observed in the TF₀-COF and TF₂₅-COF as they displayed only two diffraction peaks at 3.67 and 6.09 with low intensity (Figure 4.2b). The simulated PXRD patterns (generated in Materials Studio) of the eclipsed layers of COFs (Figure. S4.1) are in good agreement with the experimental patterns. Interestingly, the diffraction peak intensity of (001) reflection, which represents the interlayer spacing between COF sheets, improves significantly with increasing mole fraction of the TF monomer in the reaction. SEM images (Figure 4.3) of each mixed COF indicates a morphological change in the crystallites from smooth spherical agglomerates of TF₀-COF to long rod-like morphology in TF₁₀₀-COF with the variation of X mol% from 0-100. The change in morphology has been attributed to increased microscopic ordering in previous reports.²²

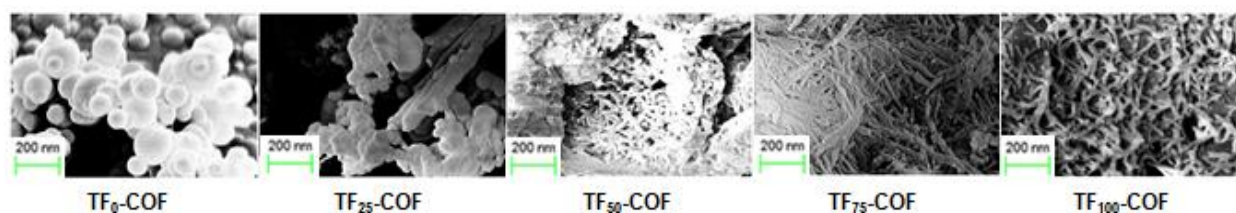


Figure 4.3. Morphological change in the SEM images with the variation of TF content in the COFs.

The surface area and pore size distributions of each COF were determined through nitrogen sorption measurements at 77 K (Figure 4.4a-b). The TF₀-COF and TF₂₅-COF exhibit type-I adsorption isotherms indicating microporous structures. However, when the TF content increases to X= 50 and 100 the shape of the isotherms changes to type IV indicating the formation of mesoporous materials (Figure 4.4a). The pore size distribution also indicates a consistent change from largely microporous to mesoporous character with increasing concentration of TF in the

COF (Figure 4.4b). The Brunauer-Emmett-Teller (BET) surface areas of mixed-linker COFs exhibited a linear increment from 710-1064 m²/g, when X varies from 25-75. However, TF₁₀₀-COF displayed a surface area of 1802 m²/g which is a 756 m²/g improvement compared to TF₇₅-COF (Figure 4.4c).

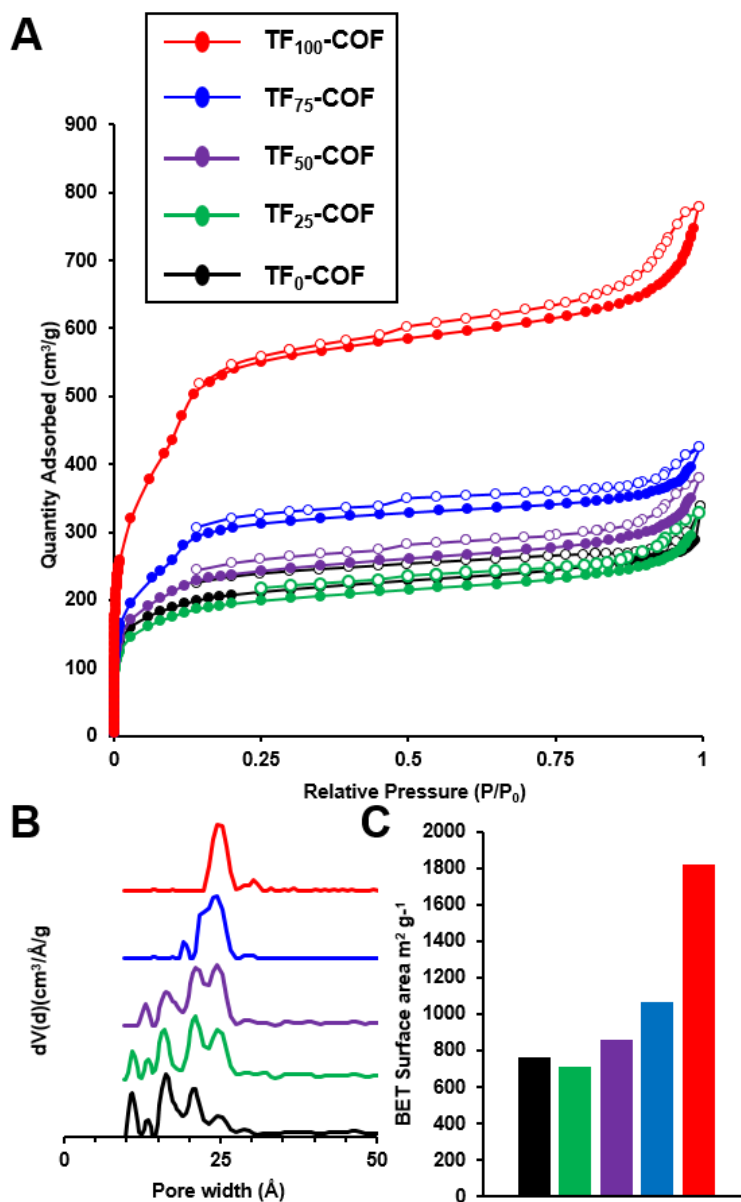


Figure 4.4. (A) Nitrogen isotherms (77 K), (B) NLDFT pore size distributions and (C) BET surface areas of the TF_x-COFs.

One potential explanation for these observations involves the polarization of the aromatic rings induced by the fluorine substituents. This polarization has been shown to improve the co-facial interactions²³ between aromatic rings that are present in eclipsed 2D COFs. To gain better insight into the role of the aromatic stacking interactions, we performed quantum mechanical computational studies to calculate the interaction energy of the face-to-face interaction of each monomer type. Quantum mechanical calculations were performed to measure the interaction energy between the monomers of an optimized dimer structure. Initial generation and preparation of the dimer structures was carried out in Avogadro,²⁴ in which the geometry was optimized using the MMFF94s²⁵ force field in order to get a good starting point for Hartree-Fock²⁶ optimization. Quantum calculations were then performed to minimize the dimer structures using GAMESS (US)^{27,28} via RHF with the 6-31G(d) basis set and Grimme's semi-empirical dispersion correction.^{29,30} After minimization of the dimer, single point energies were calculated for each individual monomer using the same dispersion corrected HF 6-31G(d) method. The stacking interaction energy was determined by subtracting the energies of the individual contributing monomers from the total energy of the minimized dimer structure. This procedure was used to calculate the energy of the stacking interactions between TF/TF, NF/TF, and NF/NF monomers (Figure 4.5). These calculations found stacking energies of -132, -128, and -100 kJ/mol, respectively, for these co-facial arrangements. The change from NF/NF to NF/TF caused a subsequent increase in associative interactions by 28 kJ/mol, while going from NF/TF to TF/TF an additional 4 kJ/mol of stabilization energy. These calculations suggest that there is a stronger preference for the TF-TF co-facial arrangement which could be a significant

driving force in converting the kinetic polymer products to the thermodynamically favoured COF.

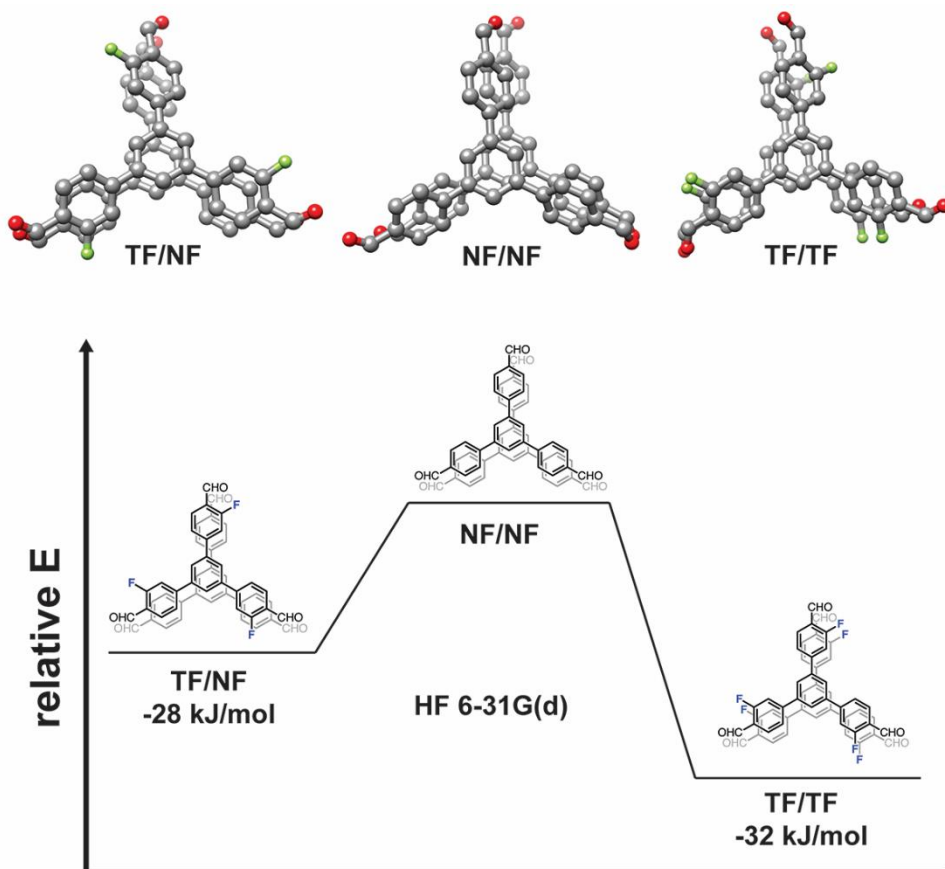


Figure 4.5. Computational models of the energy minimized stacked dimers (top, hydrogen atoms omitted for clarity). Interaction energies of the face-to-face stacking arrangements possible in each of the representative mixed COFs (bottom). The energies are measured relative to the highest energy NF/NF dimer.

One question we sought to answer with this study was whether COF formation could be improved using a mixture of electron rich and electron poor monomers rather than homogeneous mixtures. This does not appear to be true in this case. The behaviour observed with this particular monomer system appears to be consistent with other aromatic materials, such as *m*-phenylene ethynylene foldamers,³¹ which have been shown form more stable folded structures

using aromatic monomer units that contain electron poor units. We believe that this could be a potential design strategy for the synthesis of COFs using monomers that do not crystallize easily. To achieve mixed layer COFs that organize based on charge-transfer, or donor-acceptor interactions will likely require much larger polarization in the monomer units.

4.5 Conclusion

In conclusion, we have carried out experimental and computational studies on a class of mixed-linker azine COFs. These studies indicate that the quality of the aromatic stacking interactions between COF monomers plays an important role in the formation and final structural characteristics of azine COFs. Experimental studies demonstrate that increased incorporation of the more electron rich NF monomers disrupts the COF formation indicating that tuning the aromatic stacking interactions between the monomers is a key component to the design of highly ordered COFs. Computational studies support this hypothesis by showing that the interaction between electron poor TF rings is more favourable than those between the comparatively electron rich NF monomers, or even mixed dimers of NF and TF. Future work will include the use of other monomer systems to attempt to elucidate the optimal conditions to make COFs.

4.6 Acknowledgement

This research was supported with funds from The University of Texas at Dallas and the American Chemical Society Petroleum Research Fund (52906-DNI10).

4.7 Appendix – Supporting information

IR Spectra of TF_x-COFs

FT-IR spectroscopy of the TF_x-COF exhibited a stretching vibration band at 1622 cm⁻¹ which can be assigned to C=N bond based on previous literature.^{11,21}

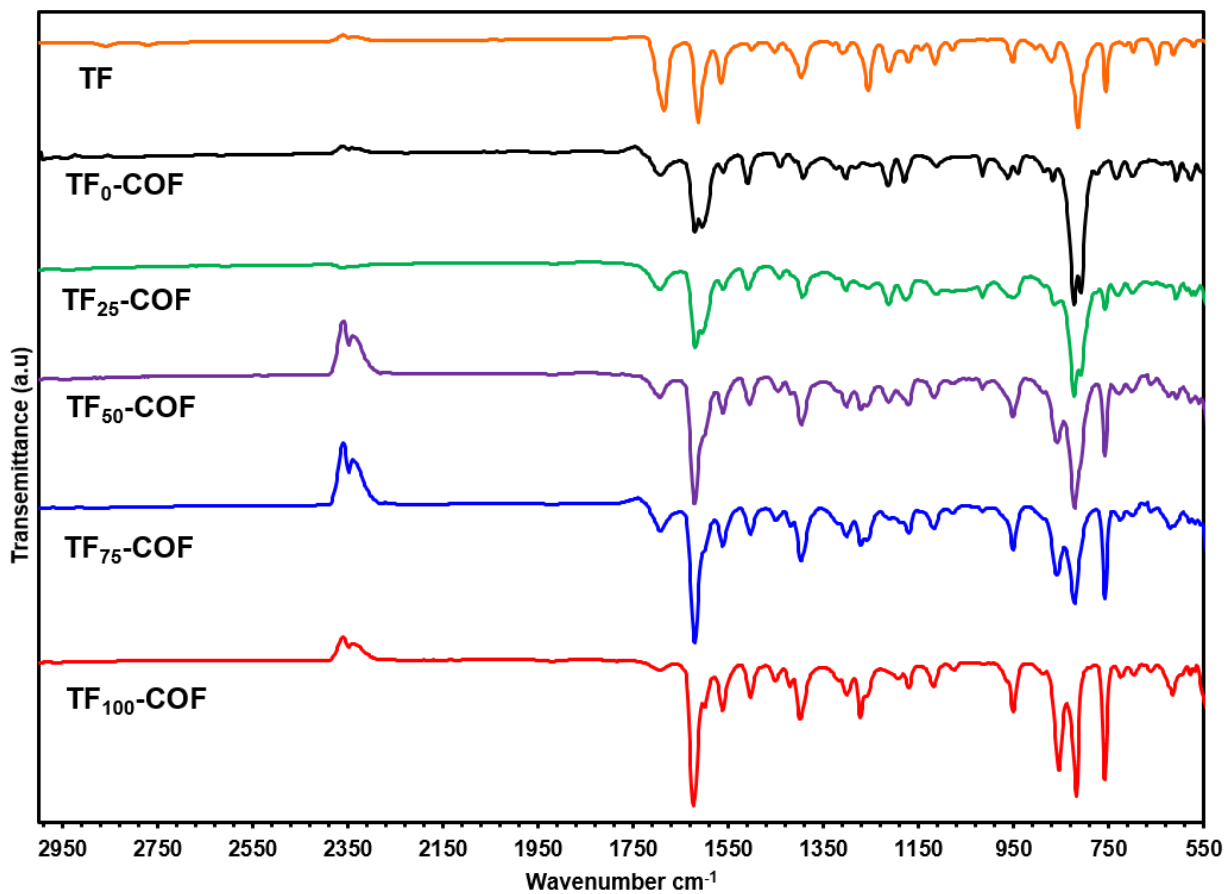


Figure S4.1. FT-IR spectra of TF₀-COF (black), TF₂₅-COF (green), TF₅₀-COF (purple), TF₇₅-COF (blue) and TF₁₀₀-COF (red) compared with TF aldehyde monomer (orange)

Computational Modelling of TF_x-COFs

Computational modelling of the structure of TF_x-COFs were carried out using the Materials Studio (ver. 7.0) suite of programs. For clarity the modelling of TF₁₀₀-COF is shown here.

The initial lattice was created by starting with the space group P3. The constructed model was geometry optimized using the Forcite module (Smart algorithm). Then the calculated PXRD pattern was generated with the Reflex Plus module using Pseudo-Voigt function. Finally, Pawley refinement was applied for profile fitting, producing the refined PXRD profile with the lattice parameters of $a = b = 29.522454 \text{ \AA}$ and $c = 3.637044 \text{ \AA}$. R_{wp} and R_p values converged to 5.46% and 3.07%, respectively. The staggered arrangement for TF₁₀₀-COF was also constructed considering P6₃/m as the space group. Comparison of the observed and the simulated PXRD patterns (Figure S4.2) evident that the most preferred structure of TF₁₀₀-COF is the eclipsed layer arrangement.

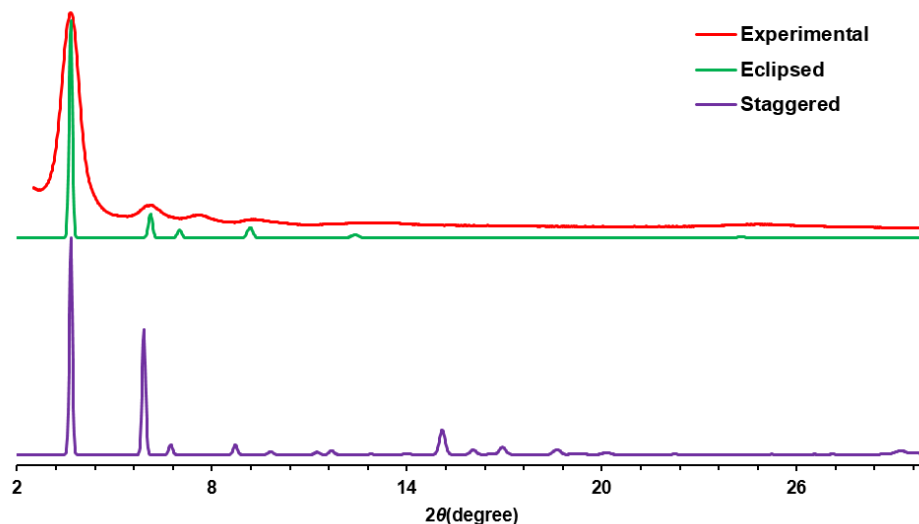


Figure S4.2. Experimental powder X-ray diffraction pattern of TF₁₀₀-COF (red), compared with simulated PXRD patterns of eclipsed layers of COF (green) considering P3 symmetry and staggered layers of COF (purple) considering P6₃/m symmetry.

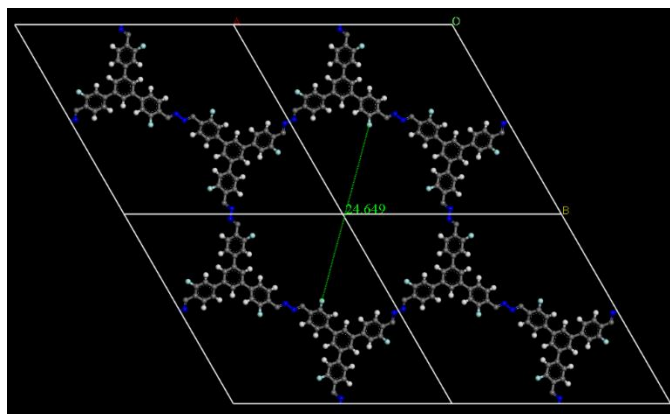


Figure S4.3. View of the simulated structure of the eclipsed TF₁₀₀-COF along *c* axis

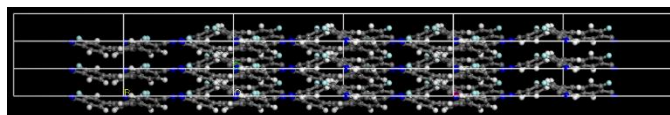


Figure S4.4. View of the simulated structure of the eclipsed TF₁₀₀-COF along *a* axis

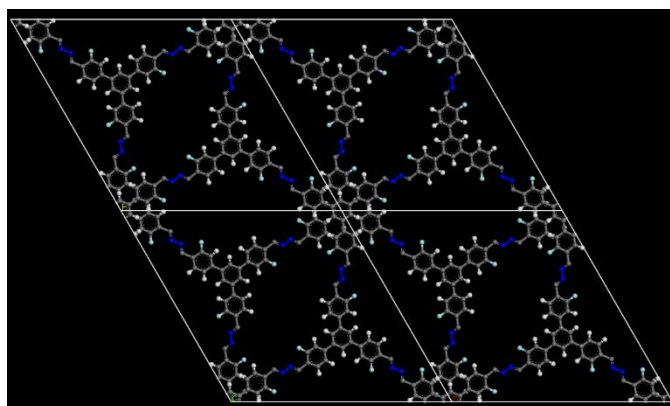


Figure S4.5. View of the simulated structure of the staggered TF₁₀₀-COF along *c* axis

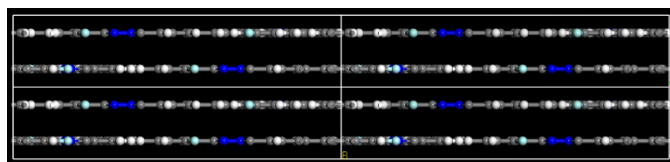


Figure S4.6. View of the simulated structure of the staggered TF₁₀₀-COF along *a* axis

Atom Coordinates for Dimer Calculations

Table S4.1. Atom Coordinates for TF/TF Dimer

ATOM	ATOMIC CHARGE	COORDINATES (BOHR)		
		X	Y	Z
C	6	1.098157566	-1.760657703	7.103574474
C	6	0.338865664	0.40020617	7.507578993
C	6	0.889248358	2.686623437	7.897032622
C	6	3.511621111	2.825801756	7.918613293
C	6	4.904009014	0.628239405	7.569732081
C	6	3.723988518	-1.682271869	7.149986144
C	6	5.240569212	-4.019711738	6.729522112
C	6	7.551647403	-3.937999986	5.45616805
C	6	-8.91083282	-6.11209194	5.018601997
C	6	8.034188934	-8.450060932	5.842635912
C	6	-5.76347529	-8.489953048	7.130692042
C	6	4.364492244	-6.343337709	7.588950594
H	1	2.640098383	-6.519516863	8.640583106
F	9	4.866006624	-10.68150607	7.958467614
C	6	9.430866514	-10.80586894	5.245236835
O	8	11.24883961	-10.84676261	3.915701219
H	1	8.685653071	-12.53525168	6.070933708
H	1	10.64858704	-6.050430181	3.974188239
H	1	8.242852478	-2.178891858	4.729643997
H	1	6.929908656	0.726845307	7.621794032
C	6	4.804231481	5.294823245	8.300243456
C	6	3.962169581	7.448940796	7.0302909
C	6	5.194006364	9.721676447	7.327639285
C	6	7.290581758	9.931965155	8.904842388
C	6	8.076953433	7.777450761	0.155160691
C	6	6.885556787	5.479033734	9.885969224
H	1	7.573171382	3.88769548	0.93792299
F	9	-10.0606177	7.908616642	1.686235583
C	6	8.630019538	12.38212718	9.186033615
O	8	8.065615077	14.22392972	8.022208071
H	1	10.18996944	12.41457377	0.527909142
H	1	4.584305171	11.37123716	6.3165036
H	1	-2.3979111	7.31497812	5.746902393

H	1	0.201671557	4.358123867	8.268552751
C	6	3.149530715	0.26441046	7.559867711
C	6	4.369726785	-1.703795848	8.820862966
C	6	6.969611799	-1.822281667	8.888741923
C	6	8.444164987	-0.007426623	7.686989578
C	6	7.191900267	1.916862453	6.444815995
C	6	4.597911198	2.096065168	6.366694723
H	1	3.75486664	3.6048035	5.306879697
F	9	8.527142855	3.66045593	5.216890945
C	6	11.25131515	-0.172891031	7.78291207
O	8	12.32981956	-1.690832328	9.042962461
H	1	12.28214178	1.189601407	6.641838826
H	1	7.914588176	-3.318037581	9.880281149
H	1	3.275103007	-3.107484312	9.795715911
H	1	0.151461538	-3.508106221	6.695450353
C	6	-1.75419484	-3.508106221	0.416193252
C	6	0.435336176	-0.405572992	0.153767004
C	6	1.786376874	1.804631627	0.591881077
C	6	4.408258298	1.848322091	0.434107854
C	6	5.678116367	-0.378058581	0.130769038
C	6	4.374205436	-2.618744479	0.549135475
C	6	5.769012187	-5.000951957	1.08882232
C	6	7.891571314	-5.027294737	2.651701301
C	6	9.244955272	-7.224403554	3.003398204
C	6	8.544679512	-9.459212404	1.812077147
C	6	6.410517468	-9.391843673	0.31482835
C	6	5.010136025	-7.233701006	0.055992581
H	1	3.445650777	-7.290543963	1.34571167
F	9	-5.70306075	-11.47394377	0.909959755
C	6	10.09550204	-11.78435016	2.122918175
O	8	-11.837168	-11.89737467	3.542007905
H	1	9.555304971	-13.39694783	0.970525473
H	1	10.88623898	-7.25070854	4.195059412
H	1	8.470167617	-3.331530225	3.603953123
H	1	-7.70594353	-0.369403636	0.244776207
C	6	5.826781111	4.248217404	0.844707517
C	6	4.983301916	-6.49795509	0.244360468
C	6	6.298116566	8.716550091	0.109811977
C	6	8.483546877	8.782973959	1.568453673

C	6	9.280973449	6.536184246	2.629194664
C	6	8.013307462	4.289602403	2.292143137
H	1	8.726301077	2.626208897	3.205542193
F	9	11.35407845	6.516814555	4.04845447
C	6	9.866259382	11.20203109	1.949233459
O	8	9.302629709	13.10118681	0.88613031
H	1	-11.4426877	11.15465566	3.270435383
H	1	5.665077258	-10.44177543	0.747877957
H	1	3.325653177	-6.489394631	1.415612635
H	1	0.797710031	3.497674933	1.120928764
C	6	2.377464265	-0.428835518	0.282400652
C	6	3.671567519	-2.459610654	1.359563362
C	6	6.267899848	-2.447629791	1.505147852
C	6	7.66814901	-0.430044943	0.565103659
C	6	6.352880826	-1.550236714	0.513230681
C	6	3.756642983	-1.589410734	0.669964554
H	1	2.856925543	-3.169070481	1.568340289
F	9	7.618921648	-3.508862111	1.438629497
C	6	10.46042703	-0.388281999	0.814112853
O	8	11.60830328	-1.916560097	2.006775615
H	1	11.43671616	-1.144720414	0.148929305
H	1	7.262027998	-3.979025937	2.387574299
H	1	2.632936321	-4.016007875	2.143308318
H	1	0.729982252	-4.304266677	0.834843147

Table S4.2. Atom Coordinates for TF/NF Dimer

ATOM	ATOMIC CHARGE	COORDINATES (BOHR)		
		X	Y	Z
C	6	3.455893092	19.98802861	12.67465676
C	6	2.80246364	17.82446243	13.9984854
C	6	2.845265933	17.75894563	16.62295575
C	6	3.439433579	19.96491727	17.92584623
C	6	3.443761051	19.98933253	9.86089256
C	6	4.361752141	17.91874086	8.534153739
C	6	4.366967785	17.9701792	5.934117547
F	9	5.310148923	15.98428506	4.712220723
O	8	2.261699651	21.51676025	0.555655029
C	6	3.456100962	19.99494501	4.559171815

C	6	3.440000496	20.01448478	1.745067463
C	6	1.093471046	15.31862908	20.3060695
C	6	0.591144084	13.05679715	21.49355441
F	9	0.496260942	13.14620009	23.73240728
C	6	1.177696133	10.74390482	20.40350377
C	6	2.337024129	10.80176823	18.05073822
C	6	2.886991083	13.04048882	16.83904592
O	8	0.649083082	7.931123279	23.41217431
C	6	0.624365466	8.259746628	21.59750824
C	6	4.086135606	22.14637915	14.02031174
C	6	4.015800005	22.18903027	16.64667181
C	6	2.526412468	22.06056669	8.513253369
C	6	2.525373118	22.04886929	5.90885191
C	6	4.553804993	24.59871436	18.0129815
C	6	5.706141004	24.65778719	20.38721433
C	6	6.23802328	26.92576074	21.55257055
C	6	5.624429252	29.21697791	20.41675075
C	6	4.459639948	29.11812634	18.08388402
C	6	3.914019363	26.88278837	16.87891914
F	9	3.863223529	31.26421256	16.91866008
O	8	7.57001554	31.8163527	23.46635275
C	6	6.309020285	31.65980779	21.60612539
C	6	2.251797487	15.34340339	17.94782375
C	6	10.51452988	19.96230944	12.67841732
C	6	9.875632423	17.80479039	14.02223926
C	6	9.945363312	17.75599766	16.64839147
C	6	10.52705877	19.979865	17.92733912
C	6	10.52979887	19.96820539	9.865220033
C	6	11.4523064	17.90432225	8.529410526
C	6	11.46672501	17.91626532	5.916694273
O	8	9.246164696	21.34834787	0.549437831
C	6	10.53807587	19.97782409	4.599611951
C	6	10.46208999	19.92220946	1.801910421
C	6	9.40854885	15.33979401	18.00852175
C	6	8.245649272	15.28270539	20.37646179
C	6	7.713086694	13.02253642	21.55954364
C	6	8.341118229	10.74834568	20.4067541
C	6	9.53117317	10.78009308	18.07796918
C	6	10.06364126	13.04536431	16.89604006

O	8	6.395758708	8.077255789	23.42691417
C	6	7.667960038	8.299827716	21.58446913
C	6	11.16933883	22.12198279	14.00576085
C	6	11.11837292	22.19042866	16.62973987
C	6	9.636468702	22.05310228	8.520642198
C	6	9.627870449	22.05879035	5.919528862
C	6	11.7109721	24.60787953	17.95817944
C	6	12.88318802	24.65342193	20.31886294
C	6	13.39284712	26.91120985	21.51800747
C	6	12.7640219	29.19050285	20.37818144
C	6	11.60800093	29.16468919	18.03250237
C	6	11.07031719	26.90331079	16.84484738
O	8	14.5612458	31.80711193	23.52854364
C	6	13.34628427	31.62715333	21.64611199
H	1	12.60018266	33.30832916	20.70340328
H	1	5.61036969	33.35249205	20.66439934
H	1	14.29530467	26.93645659	23.33533805
H	1	13.42909207	22.91683933	21.21799457
H	1	7.192032548	26.96967797	23.34113951
H	1	6.278142163	22.93235398	21.28455072
H	1	2.956041671	26.96141987	15.09424302
H	1	11.07712021	30.91380067	17.13784939
H	1	10.08741401	26.93405663	15.07018681
H	1	10.54213878	19.98141457	19.9564324
H	1	9.274151538	16.15483283	13.00772097
H	1	11.75946247	23.76500505	12.97684284
H	1	11.608908	18.44982946	0.90992196
H	1	4.570151123	18.56914675	0.815832503
H	1	12.18733422	16.29796068	9.530681841
H	1	12.1833847	16.30336529	4.905860945
H	1	8.876042964	23.64481848	9.524861485
H	1	8.875324869	23.63758083	4.889590404
H	1	1.779706141	23.6633	9.508836609
H	1	1.792121641	23.62679049	4.866535747
H	1	5.14113183	16.30633216	9.485026061
H	1	2.214002967	16.18121341	12.96832018
H	1	4.678054477	23.79852879	13.00515094
H	1	3.433310866	19.9605331	19.95452377
H	1	0.533488544	17.02928464	21.24067128

H	1	2.862708104	9.04324592	17.17570061
H	1	3.873333563	12.99216852	15.06918525
H	1	1.476329531	6.661340799	20.60084786
H	1	8.403082344	6.626399765	20.61254526
H	1	10.04328891	9.031416235	17.17184556
H	1	11.03144553	13.02083567	15.11215762
H	1	7.679959798	17.01522507	21.26841246
H	1	6.761137228	12.99364251	23.35181646

Table S4.3. Atom Coordinates for NF/NF Dimer

ATOM	ATOMIC CHARGE	COORDINATES (BOHR)		
		X	Y	Z
C	6	0.659949007	-1.981396595	8.039536859
C	6	0.722725704	0.23455279	8.325887038
C	6	0.564574536	2.517587447	8.502614212
C	6	3.187457515	2.595330774	8.423396899
C	6	4.526970884	0.355627534	8.141071836
C	6	3.283890232	-1.947249247	7.933485436
C	6	-4.72782986	-4.330855121	7.534942225
C	6	6.690064634	-4.428705133	5.776193146
C	6	7.989383531	-6.647867052	5.35189297
C	6	7.356873346	-8.822752692	6.683601771
C	6	5.432074044	-8.730685241	8.462098487
C	6	4.125914338	-6.506761213	8.88483019
H	1	2.657786218	-6.449672591	10.28717695
H	1	-4.93775952	-10.40067389	9.51386328
C	6	8.654245825	-11.24642076	6.149489618
O	8	-10.1213346	-11.56187272	4.469825571
H	1	8.150501569	-12.81073593	7.406195194
H	1	9.457889596	-6.735304674	3.956103561
H	1	7.146244487	-2.777235798	4.687918847
H	1	6.556687773	0.409881567	8.081772234
C	6	4.578749377	5.035533942	8.625446401
C	6	4.027799765	7.027815359	6.992288511
C	6	5.407488708	9.236016868	7.080463125
C	6	7.347273538	9.507570492	8.833089493
C	6	7.856497999	7.56056691	10.51127955

C	6	6.496651179	5.331465032	10.39816056
H	1	6.910104328	3.826506153	11.6978574
H	1	9.326307975	7.774937426	11.90211788
C	6	8.916180744	11.8261509	8.867652581
O	8	8.846582136	13.42499136	7.285082655
H	1	10.21759724	11.98847836	10.46732453
H	1	5.031697799	10.74373475	5.775512845
H	1	2.575091809	6.802956864	5.591472431
H	1	0.47868649	4.239467973	8.773695405
C	6	3.534430104	0.140841278	8.433922672
C	6	4.749467222	-1.663639171	9.924519634
C	6	7.348993188	-1.816272339	9.979321688
C	6	8.796674473	-0.16786436	8.533511232
C	6	7.603406998	1.651261465	7.078951345
C	6	4.993222977	1.813078702	7.031689298
H	1	4.087704079	3.172207427	5.823587474
H	1	8.710295098	2.908704035	5.928353882
C	6	11.59773972	-0.368364287	8.540238656
O	8	12.7468065	-1.78212499	9.861402786
H	1	12.577128	0.891818385	7.234060054
H	1	8.282669004	-3.203822542	11.12914436
H	1	3.64452554	-2.933213781	11.06222917
H	1	0.325561993	-3.743736154	7.820593206
C	6	2.161033948	-2.414824148	0.932825439
C	6	0.808708236	-0.228505666	-0.40572417
C	6	2.110540469	2.023745355	-0.0517218
C	6	4.731628209	2.111693202	0.196682681
C	6	6.043910627	-0.103462498	0.711368451
C	6	4.782839783	-2.377747724	-1.1013701
C	6	6.224417253	-4.729077079	1.678492417
C	6	8.260521416	-4.684120498	-3.35590769
C	6	-9.64765588	-6.838067973	3.824540838
C	6	9.038710577	-9.090224508	2.614662671
C	6	7.001888319	-9.157385369	0.972849836
C	6	5.594420403	-6.999545059	0.519806927
H	1	4.064970675	-7.059165913	0.814301825
H	1	-6.54650215	-10.88119342	0.00296687
C	6	10.56816031	-11.39946966	3.062603319
O	8	12.28960619	-11.50941392	4.506958686

H	1	10.01278874	-13.05201614	1.954997123
H	1	11.20828609	-6.803353707	5.121762139
H	1	8.733160782	-2.960633705	4.320045889
H	1	8.072210221	-0.052420999	0.827832263
C	6	6.095651324	4.550705843	0.189709592
C	6	5.368673737	6.689724483	-1.1710254
C	6	6.589436725	8.965181339	0.832254222
C	6	8.559022533	9.163526979	0.895730118
C	6	9.293955867	7.046674825	2.249151871
C	6	8.078276241	4.755514345	1.899306899
H	1	8.628640038	3.145845749	3.00984217
H	1	-10.8006155	7.188536555	3.609225459
C	6	9.868810512	11.62355337	1.261051946
O	8	9.431433432	13.45830723	0.037227602
H	1	11.30390622	11.65964714	2.743088449
H	1	6.044288572	10.60070139	-1.90253833
H	1	3.856061467	6.548996589	2.521159029
H	1	1.076236745	3.710439182	0.412640567
C	6	2.005396115	-0.278507816	0.206471461
C	6	3.201668255	-1.909190165	1.481280613
C	6	5.792047947	-1.874116851	1.75695384
C	6	7.245511793	-0.22861905	0.315244089
C	6	6.073522633	1.351928869	1.413741806
C	6	3.472522681	1.343519588	1.661900623
H	1	2.577642939	2.588300994	2.995121204
H	1	7.188139712	2.611865877	2.558934652
C	6	10.0199508	-0.089459628	0.654922336
O	8	11.15845401	-1.095757614	2.317200903
H	1	11.01789619	1.062706307	0.744608731
H	1	6.700968353	-3.069179566	3.122129688
H	1	2.080871771	-3.145259934	2.638964547
H	1	1.159346894	-4.147268242	1.282557028

4.8 References

1. Cote, A. P.; Benin, A. I.; Ockwig, N. W.; O'Keeffe, M.; Matzger, A. J.; Yaghi, O. M. *Science* **2005**, *310*, 1166.
2. El-Kaderi, H.; Hunt, J. R.; Mendoza-Cortes, J. L.; Cote, A. P.; Taylor, R. E.; O'Keeffe, M.; Yaghi, O. M. *Science* **2007**, *316*, 268.
3. Jin, Y.; Yu, C.; Denman, R. J.; Zhang, W. *Chem. Soc. Rev.* **2013**, *42*, 6634-6654.
4. Du, Y.; Yang, H.; Whiteley, J. M.; Wan, S.; Jin, Y.; Lee, S.; Zhang, W. *Angew. Chem. Int. Ed.* **2016**, *55*, 1737-1741.
5. Uribe-Romo, F.; Hunt, J. R.; Furukawa, H.; Klock, C.; O'Keeffe, M.; Yaghi, O. M. *J. Am. Chem. Soc.* **2009**, *131*, 4570-4571.
6. Dalapati, S.; Addicoat, M.; Jin, S.; Sakurai, T.; Gao, J.; Xu, H.; Irle, S.; Seki, S.; Jiang, D. *Nat. Commun.* **2015**, *6*, 7786.
7. Uribe-Romo, F.; Doonan, C. J.; Furukawa, H.; Oisaki, K.; Yaghi, O. M. *J. Am. Chem. Soc.* **2011**, *133*, 11478-11481.
8. Stegbauer, L.; Schwinghammer, K.; Lotsch, B. V. *Chem. Sci.* **2014**, *5*, 2789-2793.
9. Kuhn, P.; Antonietti, M.; Thomas, A. *Angew. Chem. Int. Ed.* **2008**, *47*, 3450-3453.
10. Dalapati, S.; Jin, S.; Gao, J.; Xu, Y.; Nagai, A.; Jiang, D. *J. Am. Chem. Soc.* **2013**, *135*, 17310-17313.
11. Alahakoon, S. B.; Thompson, C. M.; Nguyen, A. X.; Occhialini, G.; McCandless, G. T.; Smaldone, R. A. *Chem. Commun.* **2016**, *52*, 2843-2845.
12. Alahakoon, S. B.; Thompson, C. M.; Occhialini, G.; Smaldone, R. A. *ChemSusChem* **2017**, *10*, 2116-2129.
13. Pachfule, P.; Kandambeth, S.; Diaz Diaz, D.; Banerjee, R. *Chem. Commun.* **2014**, *50*, 3169-3172.
14. Smith, B. J.; Overholts, A. C.; Hwang, N.; Dichtel, W. R. *Chem. Commun.* **2016**, *52*, 3690-3693.
15. Smith, B. J.; Dichtel, W. R. *J. Am. Chem. Soc.* **2014**, *136*, 8783-8789.
16. Salonen, L. M.; Medina, D. D.; Carbo-Argibay, E.; Goesten, M. G.; Mafra, L.; Guldris, N.; Rotter, J. M.; Stroppa, D. G.; Rodriguez-Abreu, C. *Chem. Commun.* **2016**, *52*, 7986-7989.
17. Vyas, V. S.; Haase, F.; Stegbauer, L.; Savasci, G.; Podjaski, F.; Ochsenfeld, C.; Lotsch, B. V. *Nat. Commun.* **2015**, *6*, 8508.

18. Jin, S.; Furukawa, K.; Addicoat, M.; Chen, L.; Takahashi, S.; Irle, S.; Nakamura, T.; Jiang, D. *Chem. Sci.* **2013**, *4*, 4505-4511.
19. Chen, X.; Addicoat, M.; Irle, S.; Nagai, A.; Jiang, D. *J. Am. Chem. Soc.* **2013**, *135*, 546-549.
20. Ascherl, L.; Sick, T.; Margraf, J. T.; Lapidus, S. H.; Calik, M.; Hettstedt, C.; Karaghiosoff, K.; Doblinger, M.; Clark, T.; Chapman, K. W.; Auras, F.; Bein, T. *Nat Chem* **2016**, *8*, 310-316.
21. Alahakoon, S. B.; McCandless, G. T.; Karunathilake, A. A. K.; Thompson, C. M.; Smaldone, R. A. *Chem. Eur. J.* **2017**, *23*, 4255-4259
22. Halder, A.; Kandambeth, S.; Biswal, B. P.; Kaur, G.; Roy, N. C.; Addicoat, M.; Salunke, J. K.; Banerjee, S.; Vanka, K.; Heine, T.; Verma, S.; Banerjee, R. *Angew. Chem. Int. Ed.* **2016**, *55*, 7806-7810.
23. Martinez, C. R.; Iverson, B. L. *Chem. Sci.* **2012**, *3*, 2191-2201.
24. Hanwell, M. D.; Curtis, D. E.; Lonie, D. C.; Vandermeersch, T.; Zurek, E.; Hutchison, G. R. *J. Cheminf.* **2012**, *4*, 17.
25. Halgren, T. A. *J. Comput. Chem.* **1996**, *17*, 490-519.
26. Roothaan, C. C. J. *Rev. Mod. Phys.* **1951**, *23*, 69-89.
27. Schmidt, M. W.; Baldridge, K. K.; Boatz, J. A.; Elbert, S. T.; Gordon, M. S.; Jensen, J. H.; Koseki, S.; Matsunaga, N.; Nguyen, K. A.; Su, S.; Windus, T. L.; Dupuis, M.; Montgomery, J. A. *J. Comput. Chem.* **1993**, *14*, 1347-1363.
28. Gordon, M. S.; Schmidt, M. W. Chapter 41 - Advances in electronic structure theory: GAMESS a decade later A2 - Dykstra, Clifford E. In *Theory and Applications of Computational Chemistry*; Frenking, G., Kim, K. S. and Scuseria, G. E., Eds.; Elsevier: Amsterdam, 2005; pp 1167-1189.
29. Peverati, R.; Baldridge, K. K. *J. Chem. Theory Comput.* **2008**, *4*, 2030-2048.
30. Grimme, S.; Antony, J.; Ehrlich, S.; Krieg, H. *J. Chem. Phys.* **2010**, *132*, 154104.
31. Hill, D. J.; Mio, M. J.; Prince, R. B.; Hughes, T. S.; Moore, J. S. *Chem. Rev.* **2001**, *101*, 3893-4012.

BIOGRAPHICAL SKETCH

Sampath Bandara Alahakoon was born in Kandy, Sri Lanka in 1988. He obtained his primary education from the Kingswood Collage Kandy, Sri Lanka. Then he obtained his Bachelor's degree in Chemistry in 2013 from The University of Peradeniya, Sri Lanka. After that, he entered The University of Texas at Dallas in Fall 2013 to pursue his Doctor of Philosophy in Chemistry. In Spring 2013 he started working on the dissertation titled "Enhanced Structural Organization and Sorption Properties of 2D-Covalent Organic Frameworks Through Rational Monomer Design" under the supervision of Dr. Ronald A. Smaldone.

CURRICULUM VITAE

Sampath B. Alahakoon

Office: 800 W. Campbell, BE 26, Richardson, TX, 75080

E-mail: sba130030@utdallas.edu

EDUCATION

Candidate for Doctor of Philosophy in Chemistry - GPA: 3.8 **2013 Aug - 2018 Aug (expected)**

University of Texas at Dallas, Texas, USA

Advisor: Prof. Ronald A. Smaldone

Dissertation title: Enhanced Structural Organization and Sorption Properties of 2D-Covalent Organic Frameworks Through Rational Monomer Design

Bachelor of Science in Chemistry (Honors) - GPA: 3.7 **2008 – 2012**

University of Peradeniya, Peradeniya, Sri Lanka

Advisor: Prof. Anura Wickramasinghe (Department of Chemistry)

Co-advisor: Prof. Sanath Rajapaksha (Department of Molecular Biology and Biotechnology)

Thesis title: A Preliminary Study on Antimicrobial Activity of *Schumacheria castaneifolia* & *Schumacheria alnifolia*

AWARDS

Outstanding Poster Award –PMSE (Polymeric Materials Science and Engineering) Division

Aug 2017

American Chemical Society 254th National Meeting, Washington DC

Ph. D. Small Research Grant

Aug 2016, 2017

The Office of Vice President for Research, University of Texas at Dallas

Best Oral Presentation–2ndplace

Apr 2017

American Chemical Society 50th Annual Meeting-in-Miniature, Fort Worth Texas

Graduate Studies Scholarship

2013 Aug - 2018 Aug

School of Natural Science and Mathematics, University of Texas at Dallas

RESEARCH/PROFESSIONAL EXPERIENCE

Research Assistant, University of Texas at Dallas, Texas, USA

2013 Aug – present

- Design and synthesize aromatic monomers with varying geometry and electronic structure to understand the structure function relationships in 2D-polymer formation
- Demonstrate the significance of monomer planarity, non-covalent aromatic stacking and hydrogen bonding in 2D-polymer synthesis
- Develop efficient and cost-effective strategies to improve crystallinity and surface area of 2D-polymers by controlling the electron densities of the aromatic monomers in polymer synthesis
- Design experiments to understand the mechanism of formation of 2D-polymers in molecular level

- Perform the extensive characterization of aromatic monomers and polymers experimentally and computational modeling

Collaboration with Adaptive 3D Technologies, Dallas, Texas, USA

Feb 2017 – Jul 2017

- Developed a cost effective, column free synthetic route for the large scale synthesis (yield >90%) of photobases used in 3D printing

Research Assistant, University of Peradeniya, Sri Lanka

2011 – 2012

- Conducted an extensive set of experiments to extract and isolate natural products of endemic plants of Sri Lanka
- Designed and conducted microbial assays to identify the antimicrobial activity of isolated natural products to develop future antimicrobial agents

Dipped Products PLC, Kottawa, Sri Lanka (Hayleys Subsidiary)

May 2011 – Jul 2011

- Formulated a laboratory technique to analyze the shelf-life of latex compounds used in glove manufacturing

Volunteer technologist in Regional Food Testing Laboratory, Kandy, Sri Lanka

2008 – 2012

- Conducted chemical analysis of polluted water (COD- chemical oxygen demand and BOD- biological oxygen demand) and microbial analysis of food

PUBLICATIONS

1. Bandara, R. M. C. J.; **Alahakoon, A. M. C. S. B.**; Bandara, B. M. R.; Wickramasinghe, A.; Karunaratne, D, N.; Karunaratne, V.; Rajapakse, R. G. S. C.; Wijesundara, D. S. A. “Total Polyphenol Content and Antimicrobial Activity of Schumacheria castaneifolia and S. alnifolia” *Proc. Peradeniya Univ. Res. Sess. (PURSE)*, **2012**, *17*, 177.
2. **Alahakoon, S. B.**; Thompson, C. M.; Nguyen, A. X.; Occhialini, G.; McCandless, G. T.; Smaldone, R. A. “An Azine Linked Hexaphenylbenzene-Based Covalent Organic Framework” *Chem. Commun.* **2016**, *52*, 2843-2845.
3. **Alahakoon, S. B.**; McCandless, G. T.; Karunathilake, A. K.; Thompson, C. M.; Smaldone, R. A. “Enhanced Structural Organization in Covalent Organic Frameworks Through Fluorination” *Chem. Eur. J.* **2017**, *23*, 4255-4259.
4. **Alahakoon, S. B.**; McCandless, G. T.; Karunathilake, A. K.; Thompson, C. M.; Smaldone, R. A. “Enhanced Structural Organization in Covalent Organic Frameworks Through Fluorination” *Chem. Eur. J.* **2017**, *23*, 4255. (**Frontispiece**)
5. **Alahakoon, S. B.**; Thompson, C. M.; Occhialini, G.; Smaldone, R. A. “Design Principles for Covalent Organic Frameworks in Energy Storage Applications” *ChemSusChem*, **2017**, *10(10)*, 2116-2129 (**Invited Review**)

6. **Alahakoon, S. B.**; Occhialini, G.; McCandless, G. T.; Karunathilake, A. K.; Nielsen, S. O.; Smaldone, R. A. "Experimental and Theoretical Insight into the Effect of Fluorine Substituents on the Properties of Azine Linked Covalent Organic Frameworks" *CrystEngComm*, **2017**, *19*, 4882-4885 (**Invited article for a special issue on covalent organic frameworks**)
7. Lin, Y.; Jiang, X.; Kim, S.; **Alahakoon, S. B.**; Hou, X.; Zhang, Z.; Thompson, C. M.; Smaldone, R. A.; Ke, C. "An Elastic Hydrogen-bonded Covalent Organic Framework for Effective Iodine Capture in Water", *J. Am. Chem. Soc.*, **2017**, *139*, 7172–7175
8. Thompson, C. M.; Occhialini, G.; McCandless, G. T.; **Alahakoon, S. B.**; Cameron, V. V.; Nielsen, S. O.; Smaldone, R. A. "Computational and Experimental Studies on the Effects of Monomer Planarity on Covalent Organic Framework Formation" *J. Am. Chem. Soc.*, **2017**, *139* (30), 10506-10513
9. **Alahakoon, S. B.**; Occhialini, G.; McCandless, G. T.; Smaldone, R. A. "Improved Structural Organization in Hydrazone Covalent Organic Frameworks Through Inter Layer Hydrogen Bonding", *collaboration with U.S. Army Research Laboratory, manuscript in preparation*

PRESENTATIONS

1. **Alahakoon A.M.C.S.B.**; A study of Latex compound properties and development of a test method to define shelf life; Industrial training oral presentation; University of Peradeniya, Sri Lanka, February 29, 2012
2. **Alahakoon A.M.C.S.B.**; Rathnayake R.M.D.; Hettiarachchi C.V.; Beauty of Chemistry-chemistry of cosmetics; Final year seminar oral presentation; University of Peradeniya, Sri Lanka, May 2, 2012
3. **Alahakoon A.M.C.S.B.**; Wickramasinghe A.; Rajapakse S.; A preliminary study on antimicrobial activity of *Schumacheria castaneifolia* & *Schumacheria alnifolia*; Final year poster presentation; University of Peradeniya, Sri Lanka, January, 2013.
4. Bandara R.M.C.J.; **Alahakoon A.M.C.S.B.**; Bandara B.M.R.; Wickramasinghe A.; Karunaratne N.; Karunaratne V.; Rajapakse R.G.S.C.; Wijesundara D.S.A.; Total polyphenol content and antimicrobial activity of *Schumacheria castaneifolia* and *Schumacheria alnifolia*; University of Peradeniya Research Sessions (PURSE), Sri Lanka, July 4th, 2013.
5. **Alahakoon S.B.**; Smaldone R.A.; Synthesis of a Series of Novel Indoline Dyes to Enhance the Power Conversion Efficiency in Dye-Sensitized Solar Cells (DSSCs); Qualifying exam oral presentation; UT Dallas, TX, USA, January 9, 2015
6. **Alahakoon, S. B.**; Smaldone R.A.; Novel Hexaphenylbenzene-based Zn and Co Metal Organic Frameworks (MOFs); 48th Annual Meeting-in-Miniature, Dallas-Fort Worth Section of the American Chemical Society; UT Arlington, TX, USA; April, 2015.
7. Smaldone R.A.; Thompson C.M.; McCandless G.T.; **Alahakoon, S. B.**; Porous covalent organic frameworks made from polycyclic aromatic hydrocarbons; 250th ACS National Meeting and Exposition; Boston, MA, USA; August 16-20, 2015.

8. **Alahakoon, S. B.**; McCandless, G. T.; Thompson, C. M.; Smaldone R.A.; Novel hydrazone covalent organic frameworks (COFs) for CO₂ adsorption; 49th Annual Meeting-in-Miniature, Dallas-Fort Worth Section of the American Chemical Society; Texas Women's University, TX, USA; April, 2016.
9. **Alahakoon, S. B.**; McCandless, G. T.; Thompson, C. M.; Smaldone R.A.; Rational Design of Azine-linked 2D-Covalent Organic Frameworks (COFs); 2016 Texas Soft Matter Meeting; UT Dallas, TX, USA; August 12, 2016.
10. **Alahakoon, S. B.**; Smaldone R.A.; Azine-linked tetraphenylmethane (TPM) based covalent organic frameworks (COFs) for gas storage applications; 252nd ACS National Meeting and Exposition; Philadelphia, PA, USA; August 21-25, 2016.
11. **Alahakoon, S. B.**; McCandless, G. T.; Thompson, C. M.; Smaldone R.A.; Rational design of highly crystalline azine-linked 2D-covalent organic frameworks (COFs) with high surface area utilizing non-planar aldehyde precursors; 72nd Southwest Regional Meeting of the American Chemical Society; Galveston, TX, USA; November 10-13, 201
12. **Alahakoon, S. B.**; McCandless, G. T.; Karunathilake, A. K.; Thompson, C. M.; Smaldone R.A.; Improved Structural Arrangement in 2D Azine-linked Covalent Organic Frameworks upon Fluorination, 50th Annual Meeting-in-Miniature, Dallas-Fort Worth Section of the American Chemical Society; Texas Christian University, TX, USA; April, 2017.
13. **Alahakoon, S. B.**; McCandless, G. T.; Karunathilake, A. K.; Thompson, C. M.; Smaldone R.A.; Fluorinated non-planar precursors for enhanced structural arrangement in two-dimensional (2D) azine-linked covalent organic frameworks ;254th ACS National Meeting and Exposition; Washington DC, USA; August 20-24, 2017.

TECHNICAL SKILLS

- **Chemical methods:** multi-step organic synthesis including (microwave, photochemical, metal catalyzed synthesis under inert conditions), polymers synthesis, compound purification (column chromatography, recrystallization), and single crystal growth
- **Instrumentation:** NMR, porosity analyzer, FT-IR, UV-Vis, MALDI-TOF, SEM, PXRD, HPLC, TGA, DSC, GPC, and a certified clean room user
- **Software:** MS Office, Chemdraw, Avogadro, Materials Studio, Mercury, Chimera and Bruker TopSpin, SciFinder, and Refworks

TEACHING AND MENTORING EXPERIENCE

University of Texas at Dallas, Texas, USA

2013 Aug – present

Teaching General Chemistry I and II

- Conducted prelab lectures and lab classes
- Graded prelab, post lab assignments and quizzes
- Proctored and graded exams
- Provided support for the students in their lab work during the office hours

- Lead TA for laboratory preparations (solution preparation, maintaining the chemical/equipment stock and waste management)

Mentoring in the research lab

- Mentored undergraduates, junior graduate students and high school students to reach their project goals

University of Peradeniya, Peradeniya, Sri Lanka

Mar 2013 – Jun 2013

Teaching Advanced Physical Chemistry and Physical Chemistry

- Conducted prelab lectures and lab classes
- Graded post labs, quizzes and exams
- Conducted tutorial classes on principles of General and Organic Chemistry
- Proctored and graded exams
- Lead the solvent preparations, standardizing instruments and waste management

Volunteer Chemistry teacher, Kandy, Sri Lanka

2009 - 2012

- Conducted General, Organic, Inorganic and Physical Chemistry classes for high school students
- Carried out problem sets and model paper discussions aiming university entrance exam in Sri Lanka
- Conducted science classes for grade 10 and 11 students

AFFILIATIONS

Member, American Chemical Society

Since 2013

Member, Sri Lankan Student Association, University of Texas at Dallas

Since 2013